Dissipative Closures for Statistical Moments, Fluid Moments, and Subgrid Scales in Plasma Turbulence

Stephen Andrew Smith

A Dissertation
Presented to the Faculty
of Princeton University
in Candidacy for the Degree
of Doctor of Philosophy

Recommended for Acceptance
By the Department of
Applied and Computational Mathematics

November 1997

Abstract

Closures are necessary in the study physical systems with large numbers of degrees of freedom when it is only possible to compute a small number of modes. The modes that are to be computed, the resolved modes, are coupled to unresolved modes that must be estimated. This thesis focuses on dissipative closures models for two problems that arises in the study of plasma turbulence: the fluid moment closure problem and the subgrid scale closure problem.

The fluid moment closures of Hammett and Perkins (1990) were originally applied to a one-dimensional kinetic equation, the Vlasov equation. These closures are generalized in this thesis and applied to the stochastic oscillator problem, a standard paradigm problem for statistical closures. The linear theory of the Hammett–Perkins closures is shown to converge with increasing numbers of moments.

A novel parameterized hyperviscosity is proposed for two-dimensional drift-wave turbulence. The magnitude and exponent of the hyperviscosity are expressed as functions of the large scale advection velocity. Traditionally hyperviscosities are applied to simulations with a fixed exponent that must be arbitrarily chosen. Expressing the exponent as a function of the simulation parameters eliminates this ambiguity. These functions are parameterized by comparing the hyperviscous dissipation to the subgrid dissipation calculated from direct numerical simulations. Tests of the parameterization demonstrate that it performs better than using no additional damping term or than using a standard hyperviscosity.

Heuristic arguments are presented to extend this hyperviscosity model to three-dimensional (3D) drift-wave turbulence where eddies are highly elongated along the field line. Preliminary results indicate that this generalized 3D hyperviscosity is capable of reducing the resolution requirements for 3D gyrofluid turbulence simulations.

Acknowledgments

My thesis advisor Greg Hammett has been a great role model as I attempt to enter the world of science. Greg's clear, physically motivated pictures of the process that we study taught me not only about plasma turbulence, but also the importance of communicating scientific ideas in an understandable fashion. I have watched Greg work during difficult times for Fusion, on a project that has generated a significant amount of controversy. Greg has demonstrated that it is possible to engage in fairly heated scientific debates in a professional and respectful manner.

Prof. Steve Orszag provided very useful guidance in our investigations into subgrid models for drift-wave turbulence. I learned a great deal about neutral fluid turbulence from a course and seminar that he taught. Many aspects of this thesis have benefited from countless discussions with Dr. John Krommes. He has taught me a great deal about plasma turbulence, closure theory, and how to write scientific prose.

Fellow graduate students (now research scientists) Bill Dorland and Mike Beer explained many of the details of the gyrofluid model to me. Mike and Bill made working in gyrofluids a pleasurable experience socially as well as scientifically. I'd like to thank Mike for going over my thesis.

Dr. Alexei Chekhlov graciously provided a 2D Navier-Stokes pseudospectral code that was modified for use in this study. Dr. John Bowman suggested the transformation from the stochastic oscillator problem to the Vlasov equation that is used in this thesis.

I'd like to thank my parents, David and Lindsay Smith, and my sister Karen Aiken for their support and encouragement and their patience with someone who's still in college eleven years after finishing high school. Thanks to Barbara Sarfaty for all her help the past six years, and for making me feel at home at the Plasma Physics Lab. Pat Mueller was very helpful with my arrival and short stay in Fine Hall. I can't imagine better program administrators than those two. John Wright deserves special recognition for suffering as my roommate for the past three years. Many friends made the six years in Princeton a fun experience, Hans, Ryn, Charlie, Mark, Kim, Katie and Keith Herrmann, Hilary Oliver, Jon Menard, Theresa Luhm, Richard Levien, Andrea Fraser, Alex Patelis, Phil Snyder, Bob Heeter, Joy Siegel, the friendly people at Lockhart and 2D (especially Steph and Pete), Tobin Munsat, Not-So-Big Steve and Beth, Mehmet Artun, David Coster, Peter Liu, Ed and Andrea Chao, Ernest Lo, OA people, wall people, the South Americans, Tadashi, Nadia and friends, and Cold Fusion the hockey team. For five years I didn't have a car here and got a lot of rides from a lot of people. Bill, Mike, Ernest, Joel Walker, Cait Crawford, Jon and John, were a significant help in this respect.

Most of the computations were carried out on a Cray YMP at the National Energy Research Supercomputer Center, Lawrence Livermore National Laboratory. This work was supported by the United States Department of Energy Contract Nos. DE-AC02-76CH03073, DE-FG02-93ER54204, and by a graduate fellowship from the Natural Sciences and Engineering Research Council of Canada.

To Mom, Dad, Karen and Carolyn.

Contents

List of Figures

List of Tables

Chapter 1

Introduction

Moment closure problems appear in a wide range of applications. In statistical theories of turbulence, for example, equations for second-order statistics (energy) are coupled to equations for third-order statistics (transfers), which are coupled to higher-order statistics *ad infinitum*. A number of theories exist that attempt to close the system by estimating the third-order correlations as a function of the second-order terms. In fluid mechanics the equations for momentum, a first-order velocity moment of the particle distribution, contain terms involving second-order velocity moments (the pressure tensor). For common fluids, the high collision rate and short mean free path enable one to derive simple models for the pressure tensor that work very well. Viscosity is essentially a closure for some second-order particle-velocity moments (off-diagonal components of the pressure tensor) as functions of gradients of the first-order particle velocity moment (fluid momentum). In many plasma turbulence problems, the long mean free path has led to the need to consider new approaches to the fluid moment closure problem. Ion-temperature-gradient-driven (ITG) instabilities in collisionless plasmas, for example, experience strong collisionless damping from the interaction of resonant particles with waves (ion Landau damping). The correct choice of fluid moment closure can enable fluid equations to model these kinetic effects (Hammett and Perkins 1990; Chang and Callen 1992).

A simple illustration of the moment closure problem is given by the stochastic oscillator problem (Kraichnan 1961; Kubo 1963; Kraichnan 1968), a simple model that has served as a useful paradigm for studying statistical moment closures. The oscillator problem considers an ensemble of phases $y(t)$ that evolve according to

$$\frac{\partial y}{\partial t} + iby = 0, \qquad y|_{t=0} = 1, \tag{1.1}$$

where b is a constant-in-time random variable that sets the frequency at which each phase oscillates. The phases of different realizations in the stochastic oscillator or different velocity components of a given perturbation will eventually become decorrelated, causing the ensemble average $\langle y\rangle$ to decay in time. (Averages of the form $\langle b^n y\rangle$ will be called *moments* of y.) For this simple problem, the exact time behavior of this average is easy to compute directly by integrating the evolution equation (1.1) in time and then taking averages. Instead, if one takes the ensemble average of Eq. (1.1) first, one obtains the evolution equation

$$\frac{\partial\langle y\rangle}{\partial t} + i\langle by\rangle = 0, \qquad \langle y\rangle|_{t=0} = 1. \tag{1.2}$$

The initial condition for and time derivative of the moment $\langle y\rangle$ are given by this equation. This equation contains the unknown moment $\langle by\rangle$, however, so it cannot be integrated alone to give the time behavior of the moment $\langle y\rangle$. After multiplying the evolution equation (1.1) by b^n and taking the ensemble average, one obtains the moment hierarchy

$$\begin{aligned} \frac{\partial\langle by\rangle}{\partial t} + i\left\langle b^2 y\right\rangle = 0, &\qquad \langle by\rangle|_{t=0} = \langle b\rangle, \\ \frac{\partial\left\langle b^2 y\right\rangle}{\partial t} + i\left\langle b^3 y\right\rangle = 0, &\qquad \left\langle b^2 y\right\rangle\Big|_{t=0} = \left\langle b^2\right\rangle, \\ \vdots \qquad\qquad &\qquad\qquad \vdots \end{aligned} \tag{1.3}$$

Because the evolution equation for a given moment contains the next higher-order moment, no finite set of these equations can be integrated. Determining an appropriate estimate for the unresolved moment in terms of resolved moments is the moment closure problem.

The stochastic oscillator problem may appear overly simplified. However, the oscillator is a good model problem for the physical process of phase mixing, which is a fundamental process in many systems. With the substitutions $y(t) \to f(v, z, t)$ and $ib \to v\partial/\partial z$, the stochastic oscillator becomes the propagator of the Vlasov equation in plasma physics. (This transformation was pointed out to us by Dr. John Bowman and will be used in this thesis to map closures for the stochastic oscillator to fluid moment closures of the Vlasov equation.) With the substitutions $y(t) \to v(x, t)$ and $ib \to v \cdot \nabla$, the stochastic oscillator equation becomes the Euler equation describing fluid turbulence in the absence of dissipation. (The fluid advection term is nonlinear in the advected term, unlike the stochastic oscillator. There are limits, however, in which phase-mixing processes are important, such as the coherent straining of short-wavelength modes by long-wavelength modes.)

There are many approaches to obtaining closures for unresolved terms in moment hierarchies. This thesis focuses on a set of simple closures that model the phase-mixing decay process by linear dissipative terms that introduce damping proportional to the spread of frequencies. For fluid moments of the Vlasov equation, the spread of frequencies for a given wave number k is proportional to $|k|v_t$, where v_t is the average thermal velocity. The subgrid-scale closure problem for drift-wave turbulence considered in Chapter 6 can also be understood in terms of phase mixing. The phases of different points on an eddy with wave number $\mathbf{k}$ become decorrelated at a rate proportional to $|\Delta\mathbf{V}\cdot\mathbf{k}|$ where $\Delta\mathbf{V}$ is the difference in the advecting velocity at the two points. An estimate for the velocity difference is given by $\Delta\mathbf{V} \sim \Delta\mathbf{x}\cdot\boldsymbol{\nabla}\mathbf{V}$ where $\Delta\mathbf{x}$ is the distance between the two points. For isotropic turbulence, a rough scaling of the damping rate that should be introduced by the subgrid-scale closure is therefore given by the average magnitude of the shear tensor $\boldsymbol{\nabla}\mathbf{V}$, since $|\Delta\mathbf{x}| \sim 1/|\mathbf{k}|$. Extending the results to three-dimensional (3D) ITG turbulence, one must be slightly more careful to account for the elongated nature of the eddies. (The perpendicular wave number is much larger than the parallel wave number, so the eddy turnover rate is enhanced over the basic shearing rate $\nabla_{||}\mathbf{V}_{\perp}$ by a factor of $|\mathbf{k}_{\perp}|/k_{||}$.)

1.1 Closures in One Dimension

Statistical moment closures for the stochastic oscillator problem are considered first. The procedure of Hammett and Perkins (1990) for deriving fluid moment closures is generalized and applied to the stochastic oscillator moment hierarchy. The n closure coefficients for the n-moment system are computed using conditions obtained by matching the response function for the closed moment system to the exact response function q times in the $\omega \to 0$ limit and $n-q$ times in the $\omega \to \infty$ limit. Results concerning the form of this closure are easily expressed for closures written in terms of polynomial moments where the polynomials are orthogonal with respect to the underlying distribution. Numerical evidence is presented indicating that the response function for the closed moment system converges to the true response for a Gaussian distribution of frequencies. The convergence rate is faster for larger q. A closure for n moments is shown to match the linear response for background distributions that can be written as a polynomial of order $n-q$ in the frequency b multiplied by the original background distribution. Therefore, a series of closures for which the number of moments n increases and q and $n-q$ increase will exhibit linear theory that simultaneously converges for a wide class of frequency distributions.

Transformations are presented to show that the stochastic oscillator problem is equivalent to the linearized Vlasov equation, so results concerning convergence of the response function carry over to Landau-fluid closures. There is a transformation from fluid moments to Hermite polynomial moments, which in turn are equivalent to coefficients in the Hermite series traditionally used in simulations of the Vlasov equation (Armstrong et al. 1970).

A simple nonlinear problem in one dimension, the electron plasma echo, is used to test the higher-order behavior of moment systems with closure. The number of moments retained turns out to be the primary factor in determining how well the second-order response is modeled. The precise form of the linear closure seems to be relatively unimportant for higher-order effects.

1.2 Subgrid-Scale Closures in Two Dimensions

A simple one-field two-dimensional (2D) drift-wave model is used to study the transfer of fluctuation energy to unresolved scales. This model equation contains the so-called "$i\delta$" term (Terry and Horton 1982; Liang et al. 1993), which produces linear drive, and a simple model for Landau damping, which provides the dominant source of dissipation. While this model cannot accurately reproduce the linear physics of ITG modes captured by more comprehensive fluid models, it does share the basic $\mathbf{E}\times\mathbf{B}$ advection nonlinearity responsible for the transfer of fluctuation energy to small scales. The advantages of studying the simplified 2D model are that simulations can be performed at high enough resolution to ensure convergence, and that a large number of simulations can be performed to parameterize the results.

Numerical simulations of drift-wave turbulence can be very expensive computationally. Typically one would like to obtain the saturated turbulent state for a large number of choices of parameters in order to study the scalings of macroscopic quantities such as the heat or particle flux. Performing the simulations at reduced spatial resolution saves a substantial amount of computation time. At sufficiently low resolutions, however, the absence of nonlinear coupling to smaller scales mode causes the simulations to fail to saturate or to yield wildly inaccurate results. It is possible to recover accurate results at low resolutions, through the use of simple dissipative terms that model the fluctuation energy transfer to smaller scales. A novel parameterized hyperviscosity proposed by Smith and Hammett (1997) is presented and applied to the simplified 2D model considered here.

The transfer of energy to small scales was calculated in direct numerical simulations for a wide range of parameters and cutoff wave numbers. The resulting subgrid damping rate was well parameterized by a hyperviscous dissipation term with magnitude that scaled with the mean rate of shear in the flow and exponent that scaled with the cutoff wavenumber. Traditionally hyperviscosities are applied to simulations with a fixed exponent that must be arbitrarily chosen. Expressing the exponent as a function of the simulation parameters eliminates this ambiguity.

The parameterization can be used as a nonlinear damping term in numerical simulations of drift waves. (The parameterization assigns a linear damping rate to each Fourier mode, but the magnitude of the damping rate is a function of the mean flow, so the damping is nonlinear.) Tests of the parameterization demonstrate that it performs better than using no additional damping term or than using a standard hyperviscosity.

The parameterized hyperviscosity contains no reference to the linear physics of the simple 2D drift-wave model studied here. The damping rate is a function of the large scale $\mathbf{E}\times\mathbf{B}$ flow only. One would therefore expect this nonlinear damping term to be applicable to more general fluid models that contain more accurate models of the linear physics.

1.3 Extension to Three Dimensions

Heuristic arguments are given to extend this hyperviscosity model to 3D drift-wave turbulence where eddies are highly elongated along the field line. Due to the computational cost of 3D turbulence simulations, a comprehensive study of the performance of this hyperviscosity has yet to be performed. Some preliminary results are presented, however, that demonstrate that this generalized 3D hyperviscosity is capable of reducing the resolution requirements for 3D gyrofluid turbulence simulations.

Chapter 2

Moment Closures in One Dimension

To connect theory of kinetic fluid-moment closures to statistical closure theories, the main results of this chapter will be explained in terms of the stochastic oscillator problem (Kraichnan 1961; Kubo 1963; Kraichnan 1968), which is precisely analogous to the linearized Vlasov equation. Several common statistical closures are reviewed here, including simple truncation, cumulant discard, and Padé approximations.

One would like to evolve a finite set of equations for the first n statistical or fluid moments, denoted by $g_0(t), g_1(t), \ldots, g_{n-1}(t)$. The equation for $g_{n-1}(t)$ contains the next higher moment $g_n(t)$, which must somehow be approximated. Early simulations of the Vlasov equation (Armstrong et al. 1970) solved this problem by truncation [analogous to setting $g_n(t) = 0$] and noting that the simulations are only rigorously correct as long as the effect of the missing term is small. This time limit turns out to be a very severe restriction, however, since for a purely collisionless plasma the number of moments necessary to simulate a given time t is proportional to t^2. Even in highly collisionless plasma, though, one expects that the fluctuations transfered to finer and finer scales will eventually be wiped out by the small collisionality. It is reasonable, therefore, to propose a dissipative closure at a moderate number of moments that models the collisionless transfer to small scales. In fact, a closure of the form $g_n(t) = C_0 g_0(t) + \cdots + C_{n-1} g_{n-1}(t)$ was proposed by Knorr (1973) for series solutions of the Vlasov equation that guaranteed dissipative behavior. The size of the damping, which is determined by the coefficients, was left undetermined, however.

The linear response for the one-dimensional Vlasov equation is easily calculated and can be expressed in terms of the plasma dispersion function $Z(\zeta)$. Using the exact response, it is possible to construct a closed set of fluid equations that exactly reproduces the linear theory of the Vlasov equation (Chang and Callen 1992). Such a closure is frequency dependent, however, so implementation in numerical simulations would require the calculation of time-history integrals.

The novel idea of Hammett and Perkins (1990) was to construct linear single-time closures that have a very low computational cost. The resulting "Landau-fluid" equations are optimized to approximate the exact linear theory of the Vlasov equation by choosing appropriate closure coefficients. For n moment equations, matching in the "adiabatic" limit $\omega \to 0$ limit to $\mathcal{O}(\omega^q)$ and in the fluid limit $\omega \to \infty$ to $\mathcal{O}(\omega^{-(2n+1-q)})$, where $q \leq n$ is an integer, gives n conditions that uniquely determine all the coefficients. This procedure yields a set of equations with a linear response that matches the exact response somewhat uniformly over a wide range of frequencies. The choice of limits in which the matching is performed is somewhat arbitrary, but the limits $\omega \to \infty$ and $\omega \to 0$ are natural choices. Simply adding more moment equations improves the short-time response of the system and hence improves the matching in the high-frequency limit, $\omega \to \infty$. Matching purely in the high-frequency limit, however, yields a system of equations that fails to capture the long-time decay due to collisionless dissipation from Landau damping. Obtaining some conditions at low frequencies introduces dissipation into the closure that models Landau damping. (Hence, the Hammett–Perkins closure is often referred to as the Landau-fluid closure.) One might ask why the low-frequency matching is not performed at some other natural frequency, such as the mode frequency. The mode frequency for a given wavenumber is a complicated function of the background gradients and plasma parameters. Matching at $\omega \to 0$ yields simple expressions for the closure coefficients and gives a response that matches the exact response simultaneously at all frequencies. In the saturated turbulent state, fluctuations are not locked to the mode frequency, but instead are driven at over a broad band of frequencies by the nonlinear coupling to other modes. It is therefore appropriate to attempt to model the linear response simultaneously at all frequencies; the matching technique of Hammett–Perkins that is generalized here meets this objective.

In Section 2.7.1 it is demonstrated that for moment systems closed with this two-point closure the response function converges to the exact response function with increasing numbers of moments for the standard Gaussian (Maxwellian) background. Convergence is demonstrated for any fixed q, the number of times the response is matched in the $\omega \to 0$ limit, but the convergence is faster for larger q. Similar results were observed for three, four and five moment equations in the application of Landau-fluid closures to resistive g modes by Hedrick and Leboeuf (1992). Recently, a novel renormalization-group like approach to the Hermite series formulation was proposed by Parker and Carati (1995) to generate closures corresponding to the $q = 1$ case.

Orthogonal polynomial moments provide the natural basis for expressing results about linear closures for the stochastic oscillator and the Vlasov equation. The major results obtained in Section 2.6.1 concerning the behavior of the error of the approximate response function are expressed in terms of setting the first $n - q$ closure coefficients to 0. When the closure condition is not expressed in terms of orthogonal polynomials, the $n - q$ conditions for these results become general linear combinations of the closure coefficients with no simple form. The Vlasov equation is typically modeled by assuming a Maxwellian background. For a Maxwellian, the orthogonal moments are the Hermite moments defined in Section 3.3. The Hermite moments correspond precisely to the Hermite series expansions of the Vlasov equation considered in the past. It has often been observed for statistical closures that cumulants have nice properties (Kubo 1963). Cumulants are shown to be linearly equivalent to Hermite moments for linear closures about a Maxwellian background.

2.1 The Plasma Dispersion Function

The Laplace transform in time is a natural tool in the study of plasma instabilities, since the assumption of a fixed (in time) background distribution leads to differential equations with constant (in time) coefficients. The convention used here is to define the Laplace transform of a function of time, $f(t)$, by

$$\widehat{f}(\omega) = \int_0^\infty \exp(i\omega t) f(t)\, dt, \tag{2.1}$$

for ω with positive imaginary part, and by analytic continuation for ω in the lower-half complex plane. The inverse transform is given by

$$f(t) = \frac{1}{2\pi} \int_{-\infty+i\delta}^{\infty+i\delta} \exp(-i\omega t) \widehat{f}(\omega)\, d\omega, \tag{2.2}$$

where the $i\delta$ in the limits indicates that the contour is to be taken in the complex plane above any singularities of $\widehat{f}(\omega)$. At the risk of some ambiguity, the hats will be dropped throughout this thesis and $f(\omega)$ should be interpreted as the Laplace transform of $f(t)$.

Named by Fried and Conte (1961), the plasma dispersion function $Z(\zeta)$ can be written simply as the Laplace transform of a Gaussian time response:

$$Z(\zeta) = i \int_0^\infty \exp(i\zeta t) \exp(-t^2/4)\, dt. \tag{2.3}$$

The 'Z function' has the series and asymptotic expansions (Brook 1987)

$$Z(\zeta) \sim i \sum_{j=0}^{\infty} \frac{(2i)^j \Gamma((j+1)/2)}{\Gamma(j+1)} \zeta^j \qquad (\zeta \to 0), \tag{2.4}$$

$$Z(\zeta) \sim -\sum_{j=0}^{\infty} \frac{(2j)!}{j! 2^{2j}} \frac{1}{\zeta^{2j+1}} \qquad (|\zeta| \to \infty,\ \mathrm{Im}(\zeta) \geq 0). \tag{2.5}$$

Plotted for reference in Fig. 2.1, the Z function is useful for expressing the frequency response of systems involving Gaussian distributions.

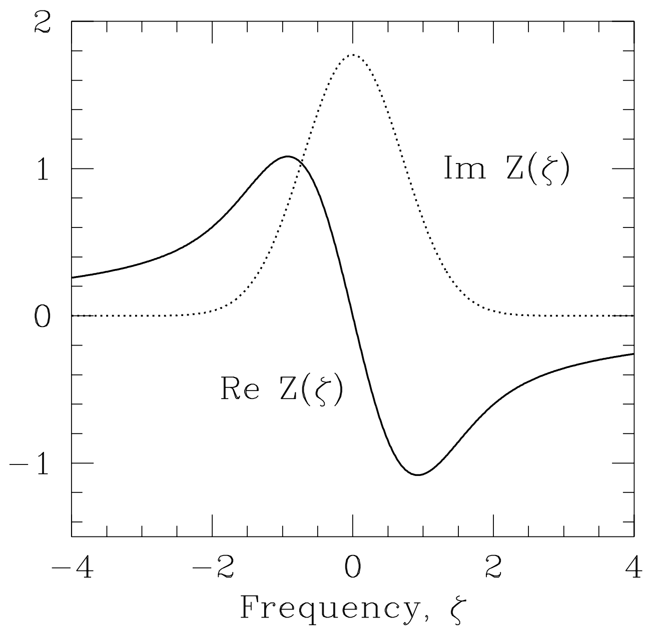

Figure 2.1: The plasma dispersion function.

2.2 The Stochastic Oscillator Problem

The random-oscillator problem is defined by the ensemble of initial-value problems,

$$\left(\frac{d}{dt} + \nu\right) y(t) + iby(t) = 0, \qquad y(0) = 1, \tag{2.6}$$

where b is a real-valued random variable with probability density function (PDF) $\rho(b)$. This oscillator equation has the simply computed exact solution

$$y(t) = \exp\big(-(ib + \nu)t\big) \qquad (t \geq 0), \tag{2.7}$$

and yet is sufficiently interesting to illustrate the behavior of several standard approximation schemes for turbulence (Kraichnan 1961). In the limit of no damping, $\nu \to 0$, the behavior of statistical moments of the oscillator equation is directly analogous to the behavior of fluid moments due to phase mixing.

A particular class of statistical moments is defined by

$$g_n(t) = \langle b^n y(t) \rangle \,, \tag{2.8}$$

where $\langle \cdot \rangle$ is an average over the ensemble of possible values of b. [The average can be written as $\langle f \rangle = \int_{-\infty}^{\infty} f \rho(b)\, db$.] One is typically interested in the time behavior of the lowest-order moments, $g_0(t)$ in particular. By taking moments of the oscillator solution (2.7), one directly obtains the exact time response

$$\begin{aligned} g_n(t) &= \langle b^n \exp(-(ib+\nu)t)\rangle \\ &= \int_{-\infty}^{\infty} b^n \exp(-(ib+\nu)t)\rho(b)\,db. \end{aligned} \tag{2.9}$$

The ensemble of amplitudes $y(t)$ have frequencies b with distribution $\rho(b)$. Initially $y(0) = 1$, so all realizations are "in-phase". As time progresses, the phases change at different frequencies and become decorrelated from one another. This *phase mixing* leads to a decay of the moments, since realizations that are out of phase ($\Delta bt \approx \pi$) will cancel one another. The spread in the frequencies (given by the standard deviation $\sqrt{\langle b^2\rangle - \langle b\rangle^2}$) is a good estimate of the rate of damping due to phase mixing. The dissipative closures introduced later in this chapter introduce a damping rate that scales with this frequency spread.

Several of the standard closure techniques will be applied to the case where b has a Gaussian distribution with PDF

$$\rho_G(b) = (2\pi)^{-1/2}\exp(-b^2/2). \tag{2.10}$$

In this case, the response of the lowest moment is just

$$g_0(t) = \exp(-t^2/2 - \nu t) \qquad (t \geq 0), \tag{2.11}$$

which is plotted against several approximation in Fig. 2.2. The decay is faster than exponential, so simple exponential damping at the same rate can only roughly model the true decay. However, as we will find, combining several moment equations with a dissipative closure of the right magnitude enables one capture both the short-time behavior $g_0(t) = 1 - \nu t + (\nu^2 - 1)t^2/2 + \cdots$ and the decay for large times.

2.3 Review of Closure Techniques

Taking moments of the oscillator equation (2.6) directly [operating on both sides by $\int_{-\infty}^{\infty} \cdot b^n \rho(b)\,db$], an infinite hierarchy of moment equations. The nth moment equation

$$\left(\frac{d}{dt} + \nu\right) g_n(t) + i g_{n+1}(t) = 0, \qquad g_n(0) = \langle b^n\rangle, \tag{2.12}$$

couples the nth moment to the $(n+1)$st moment. A finite subset of equations in this hierarchy cannot be solved directly, since the evolution of higher-order moments is required. A moment closure that expresses the nth moment $g_n(t)$ in terms of the first n moments $g_0(t), g_1(t), \ldots, g_{n-1}(t)$ can be used with the first n moment equations to form a closed finite system that approximates the infinite-dimensional moment system.

Definition 1
The n-moment system with closure for the stochastic oscillator problem is the system of equations

$$
\begin{aligned}
\left(\frac{d}{dt}+\nu\right) g_0(t) &= -ig_1(t), & g_0(0) &= \langle 1 \rangle, \\
\left(\frac{d}{dt}+\nu\right) g_1(t) &= -ig_2(t), & g_1(0) &= \langle b \rangle, \\
&\vdots & &\vdots \\
\left(\frac{d}{dt}+\nu\right) g_{n-1}(t) &= -ig_n(t), & g_{n-1}(0) &= \left\langle b^{n-1} \right\rangle, \\
g_n(t) &= F(g_0, g_1, \ldots, g_{n-1}, t).
\end{aligned}
\tag{2.13}
$$

In general, the closure function $F(\cdot)$ can be nonlinear and can depend on the time histories of the resolved moments $g_0(t), g_1(t), \ldots, g_{n-1}(t)$. The solution of the closed moment system (2.13) will be denoted $g_0^{\mathrm{a}}(t), g_1^{\mathrm{a}}(t), \ldots, g_n^{\mathrm{a}}(t)$ in order to differentiate it from the exact solution (2.9).

A natural criterion for evaluating the performance of a given moment closure $F(\cdot)$ is the ability of the response $g_0^{\mathrm{a}}(t)$ for the lowest moment of the closed system to reproduce the exact response $g_0(t)$ from Eq. (2.9). For convergence of the two-point approximation closures considered in Section 2.7, the transformed approximate response $g_0^{\mathrm{a}}(\omega)$ will be compared to the transformed exact response $g_0(\omega)$.

The definition of a closure function used here is sufficiently general that one can trivially reproduce the exact response. When the frequencies have a Gaussian PDF, for example, the exact solution for the first moment is known, so the first moment closure

$$
g_1(t) = F(g_0, t) \equiv -it\exp(-t^2/2 - \nu t) \tag{2.14}
$$

and the zeroth moment equation form a system that exactly reproduces the response $g_0(t)$. This closure for the first moment uses no information about the state of the zeroth moment, and obviously leads to incorrect results for problems where the frequencies have a different non-Gaussian PDF (or even a Gaussian PDF with different variance). One would like to apply statistical closures to more complex problems, so the stochastic oscillator problem should be regarded as a simple test case only. In order to be generally applicable, a closure should be derived using as little information about the specific problem as is possible. The types of closure functions considered, the criterion used to evaluate convergence of a closure scheme, and the nature of convergence considered will all depend on the desired application.

For the statistical moment closure problem considered by Kraichnan (1968), the desired application of the closures is to statistical moment hierarchies arising in the study of fluid turbulence. For the statistical turbulence problem, the probability distributions of most field quantities are likely non-Gaussian, and one does not know ahead of time what form the probability distributions will take. In this case, it is unreasonable to use information about the probability distribution in the derivation of the closure. An expansion based on the form of the equations was derived by Kraichnan (1968). The result is a sequence of Padé approximations to the first moment of the form $g_1(\omega) = F_i(g_0(\omega))$, where $i \geq 0$ takes on integral values. (When this expression is transformed back to the time domain, it will contain time-history integrals when the function is nonlinear.)

The results obtained in this chapter will be applied to the derivation of fluid moment closures for the study of plasma instabilities. In contrast to the turbulence problem, the underlying distribution is assumed to be known. Information about the exact response will be used to construct linear closures for the nth moment of the form $g_n(t) = F_{n,q}(g_0(t), g_1(t), \ldots, g_{n-1}(t))$ for integers $0 < q \leq n < \infty$. The fluid moment closures are to be used in numerical simulations that follow the time evolution of plasma turbulence, so closures that involve time-history integrals are prohibitively expensive to compute. The linear closure function costs very little to compute, but has a limited number of degrees of freedom (n) that can be adjusted to fit the response. Convergence in this case is considered for a set of closures with increasing numbers of moments, $n \to \infty$, as opposed to the statistical turbulence closures that consider successively higher-order nonlinear closures for the first moment.

Note that the closure techniques derived in this chapter do not directly carry over to statistical moment closures for turbulence, since the form of the background distribution is used in deriving the closures. However, the nature of the convergence of the response for these linear closures with increasing numbers of moments may provide some insight for those attempting to extend nonlinear turbulence closures to arbitrary numbers of moments.

2.3.1 Realizability and the Approximate Distribution

An estimate for a finite set of statistical moments is called *realizable* if an ensemble of realizations with non-negative probability exists that has those moments (Kraichnan 1980). (By definition the true moments of a probability distribution are realizable.) Realizability constraints can lead to some interesting closures for turbulence models (Kraichnan 1985). For the problem at hand, the closed moment system (2.13), only single-time moments $\langle b^n y(t) \rangle$ that are first order in $y(t)$ are considered. A particular ensemble is constructed here that has a useful physical interpretation.

For the closed moment system (2.13) of the stochastic oscillator, it is possible to construct an ensemble of realizations that satisfy the stochastic oscillator evolution equation (2.6), but with a modified distribution of frequencies. From the exact solution (2.7) Kraichnan (1961) noted that, for $\nu = 0$, the PDF of b is related to the transform of the zeroth moment response by $\pi\rho(b) = \mathrm{Re}\big(g_0(\omega)|_{\omega=b}\big)$. If the Laplace transform of an approximate solution $g_0^{\mathrm{a}}(t)$ exists for a given closed moment system, then we can define the *approximate distribution*

$$\rho^{\mathrm{a}}(b) = \frac{1}{\pi}\mathrm{Re}(\,g_0^{\mathrm{a}}(\omega)|_{\omega=b}). \tag{2.15}$$

[The approximate distribution for a given closure is called the *spectral density* in the discussion by Kraichnan (1968).] The approximate distribution for an n-moment system with closure has the same moments to order n as the exact distribution $\rho(b)$. The one-time joint PDF for b and $y(t) = y_r + iy_i$ given by

$$P(b, y_r, y_i) = \rho^{\mathrm{a}}(b)\delta(y_r - \cos(bt))\delta(y_i + \sin(bt)) \tag{2.16}$$

describes an ensemble of realizations with moments that satisfy the closed moment system (2.13). A requirement that the approximate distribution be non-negative, $\rho^{\mathrm{a}}(b) \geq 0$, can be viewed as a kind of realizability condition. (A closed moment system may yield an approximate distribution that fails this criterion and still be realizable, however.)

In the analogy between the stochastic oscillator problem and the linearized Vlasov equation, the PDF $\rho(b)$ corresponds to the background distribution. For a given fluid approximation, Hammett and Perkins (1990) define the *equivalent background distribution* f_0 in a manner analogous to the definition of the approximate distribution here. Requiring that the background distribution be non-negative leads to the condition on the approximate distribution, $\rho^{\mathrm{a}}(b) \geq 0$. (This condition is desirable even if one has no philosophical qualms with a negative distribution of particles. A background distribution of particles that goes negative for some velocities can lead to spurious bump-on-tail instabilities.)

2.3.2 Taylor-Series Approximation

The simplest possible closure for the n-moment system (2.13) would evolve the first n equations and set the nth moment to zero, $g_n(t) = 0$, where it arises in the $(n-1)$st equation. [The closure function is simply $F(g_0, \ldots, g_{n-1}) = 0$.] The solution of the truncated system,

$$g_0^{\mathrm{a}}(t) = \sum_{j=0}^{n-1}(-i)^j \left\langle b^j \right\rangle \frac{t^j}{j!}, \tag{2.17}$$

is a Taylor-series approximation to the true response (2.9). This series converges to the correct answer for any fixed time t as $n \to \infty$. For a fixed number of moment equations, however, the approximate solution behaves horribly for large t, blowing up instead of decaying to zero. The truncated system has no approximate distribution, since the Laplace transform of the response does not exist.

2.3.3 Cumulant-Discard Approximation

Another commonly used approximation scheme is found by assuming that the nth cumulant average is zero, $\langle b^n y(t)\rangle_c = 0$. Cumulant averages for two variables b and y are defined by identifying coefficients of powers of λ and γ in the series expansion of the equation

$$\langle \exp(\lambda b + \gamma y)\rangle = \exp\left(\sum_{j+k\geq 1}^{\infty} \frac{\lambda^j}{j!}\frac{\gamma^k}{k!}\left\langle b^j y^k\right\rangle_c\right) \tag{2.18}$$

(Kubo 1963). One is interested in moments and cumulants that are first order in y such as $g_n = \langle b^n y\rangle$. The first derivative of the cumulant definition (2.18) with respect to γ evaluated at $\gamma = 0$ is the expression

$$\langle y \exp(\lambda b)\rangle = \left(\sum_{j=0}^{\infty} \frac{\lambda^j}{j!}\left\langle b^j y\right\rangle_c\right) \exp\left(\sum_{j=1}^{\infty} \frac{\lambda^j}{j!}\left\langle b^j\right\rangle_c\right), \tag{2.19}$$

which relates the moments and cumulants that are first order in y. Using this definition, one can obtain closure approximations for an arbitrary number of moments,

$$\begin{aligned}
g_1(t) =& \langle b\rangle g_0(t),\\
g_2(t) =& 2\langle b\rangle g_1(t) + \left(\left\langle b^2\right\rangle - 2\langle b\rangle^2\right) g_0(t),\\
g_3(t) =& 3\langle b\rangle g_2(t) + \left(3\left\langle b^2\right\rangle - 6\langle b\rangle^2\right) g_1(t) + \left(\left\langle b^3\right\rangle - 6\left\langle b^2\right\rangle\langle b\rangle + 6\langle b\rangle^3\right) g_0(t),\\
g_4(t) =& 4\langle b\rangle g_3(t) + \left(6\left\langle b^2\right\rangle - 12\langle b\rangle^2\right) g_2(t) + \left(4\left\langle b^3\right\rangle - 24\left\langle b^2\right\rangle\langle b\rangle + 24\langle b\rangle^3\right) g_1(t),\\
&+ \left(\left\langle b^4\right\rangle - 8\left\langle b^3\right\rangle\langle b\rangle + 36\left\langle b^2\right\rangle\langle b\rangle^2 - 6\left\langle b^2\right\rangle^2 - 24\langle b\rangle^4\right) g_0(t),\\
&\vdots
\end{aligned} \tag{2.20}$$

For centered Gaussian distributions, the only nonzero cumulant is the second-order cumulant, so cumulant expansions work very well when the actual PDF is nearly Gaussian. Kraichnan (1961) illustrated the behavior of the cumulant discard closure on the stochastic oscillator problem by considering the fourth-cumulant closure, which takes the form

$$g_4(t) = 6g_2(t) - 3g_0(t), \tag{2.21}$$

when the frequency b has a Gaussian distribution (2.10). For the closed system containing this closure and the first three moment equations (2.12), the lowest moment evolves as

$$g_0^{\mathrm{a}}(t) = \frac{1}{6}\left[(3-\sqrt{6})\cos(t\sqrt{3+\sqrt{6}}) + (3+\sqrt{6})\cos(t\sqrt{3-\sqrt{6}})\right]. \tag{2.22}$$

Unlike the simple closure that yields a power series, this approximation gives a solution that at least remains bounded for $t \to \infty$. Also, the error from the exact solution (2.11) as $t \to 0$ is $\mathcal{O}(t^8)$ for the fourth-cumulant closure instead of the $\mathcal{O}(t^4)$ error that one obtains from the simple fourth moment closure $g_4(t) = 0$. This closed system has a non-negative approximate distribution that can be written as the sum of delta functions,

$$\begin{aligned}\rho^{\mathrm{a}}(b) =& \frac{3-\sqrt{6}}{12}\left[\delta(b-\sqrt{3+\sqrt{6}}) + \delta(b+\sqrt{3+\sqrt{6}})\right] \\ &+ \frac{3+\sqrt{6}}{12}\left[\delta(b-\sqrt{3-\sqrt{6}}) + \delta(b+\sqrt{3-\sqrt{6}})\right],\end{aligned} \tag{2.23}$$

which is quite unlike the true continuous Gaussian distribution.

Several results of the cumulant closure approach in the aforementioned case—realizability, bounded solutions, and higher-order accuracy as $t \to 0$—arise because a Gaussian distribution of frequencies was assumed. For a Gaussian distribution (2.10) of frequencies, the first-order cumulant equation (2.19) becomes

$$\begin{aligned}\sum_{j=0}^{\infty} \frac{\lambda^j}{j!}\left\langle b^j y\right\rangle_c &= \langle y \exp(\lambda b)\rangle \exp(-\lambda^2/2) \\ &= \left\langle y \exp(2(\lambda/\sqrt{2})(b/\sqrt{2}) - (\lambda/\sqrt{2})^2)\right\rangle \\ &= \sum_{j=0}^{\infty} \frac{\lambda^j}{j!} 2^{-j/2}\left\langle H_j(b/\sqrt{2})y\right\rangle,\end{aligned} \tag{2.24}$$

where H_j is the jth Hermite polynomial defined in Table 2.1. (The exponential generating function for Hermite polynomials,

$$\exp(2xt - t^2) = \sum_{j=0}^{\infty} \frac{t^j}{j!} H_j(x), \tag{2.25}$$

is used to obtain this result.) Therefore, the cumulant averages can be written as

$$\langle b^n y\rangle_c = 2^{-n/2}\left\langle H_n(b/\sqrt{2})y\right\rangle. \tag{2.26}$$

The Hermite polynomials $H_n(x/\sqrt{2})$ are also the orthogonal polynomials with respect to the weight function given by the Gaussian distribution. For a Gaussian distribution, therefore, the nth cumulant-discard closure is equivalent to setting the nth orthogonal-polynomial moment to zero. Realizability and bounded solutions for systems closed by truncation in orthogonal-polynomial moments follows from the connection to the physical mass–spring system demonstrated in Section 2.7.2. The higher-order accuracy as $t \to 0$ for orthogonal polynomial moment truncation is a simple corollary of the asymptotic behavior of this form of closure demonstrated in

Result 4. However, note that for non-Gaussian distributions the cumulant moments will be different in general from the orthogonal polynomial moments. Thus, the cumulant-discard approach should not be expected to produce bounded solutions in general.

One can easily construct examples where the cumulant-discard procedure fails. Consider a distribution with large kurtosis ($\langle b^4\rangle/\langle b^2\rangle^2$),

$$\rho(b) = \frac{1}{187\sqrt{2\pi}}\left[\frac{81}{7}\exp(-9x^2/98) + 320\exp(-2x^2)\right], \tag{2.27}$$

which has moments, $\langle b\rangle = 0$, $\langle b^2\rangle = 1$, $\langle b^3\rangle = 0$, $\langle b^4\rangle = 13$, and so on. Using the fourth-cumulant closure for this example [$g_4(t) = 6g_2(t) + 7g_0(t)$ in this case] gives the approximate response

$$g_0^{\mathrm{a}}(t) = \frac{1}{4}\cos(\sqrt{7}t) + \frac{3}{4}\cosh(t). \tag{2.28}$$

The approximation in this case blows up exponentially as $t \to \infty$, and only matches the true solution as $t \to 0$ to $\mathcal{O}(t^4)$.

2.3.4 Padé Approximations

Padé approximation refers to the use of ratios of polynomials to approximate functions. They are a standard tool in analysis that can often give uniformly excellent approximations to functions even in situations where series approximations are divergent. The monographs of Baker (1975) and Baker and Graves-Morris (1996) provide an excellent overview of Padé theory and are the source of the basic results and notation used in this thesis.

Definition 2
Suppose a function $f(z)$ has a power series $f(z) = c_0 + c_1z + c_2z^2 + \cdots$. The L, M Padé Approximant *to f is a ratio of polynomials*

$$[L/M]_f(z) = \frac{Q^{[L/M]}(z)}{P^{[L/M]}(z)} \tag{2.29}$$

such that $Q^{[L/M]}(z)$ is a polynomial of degree at most L, $P^{[L/M]}(z)$ is a polynomial of degree at most M, and the first $L+M+1$ coefficients in the series for $[L/M] - f(z)$ are zero. Padé approximants to an asymptotic series $f(w) = c_0 + c_1w^{-1} + c_2w^{-2} + \cdots$ are obtained by taking $z = 1/w$ in the defining equation (2.29).

One expects to be able to fulfill the $L+M+1$ conditions required to match the series since $Q^{[L/M]}(z)$ has $L+1$ coefficients, $P^{[L/M]}(z)$ has $M+1$ coefficients, and one degree of freedom is lost since the ratio is taken. It is possible with this definition for the Padé approximation to fail to exist in some cases.

Kraichnan (1968) obtains interesting Padé approximations to the response function by considering the Laplace transform of the moment equations (2.12),

$$
\begin{aligned}
(-i\omega+\nu)g_0(\omega)+ig_1(\omega) &= 1,\\
(-i\omega+\nu)g_1(\omega)+ig_2(\omega) &= \langle b\rangle\,,\\
(-i\omega+\nu)g_2(\omega)+ig_3(\omega) &= \left\langle b^2\right\rangle, \\
&\vdots
\end{aligned}
\tag{2.30}
$$

Upon expanding in inverse powers of $\omega+i\nu$, one easily obtains the asymptotic series solution

$$
g_0(\omega)=i\sum_{j=0}^{\infty}\frac{\langle b^j\rangle}{(\omega+i\nu)^{j+1}},
\tag{2.31}
$$

which can be divergent for distributions of interest.

For example, consider the Gaussian case with the distribution in Eq. (2.10). The exact response is

$$
g_0(\omega)=-iZ((\omega+i\nu)/\sqrt{2})/\sqrt{2},
\tag{2.32}
$$

and the asymptotic series (2.31) is divergent for all choices of ω and ν in this case. The N,N Padé approximations to g_0,

$$
\begin{aligned}
[1/1]_g(\omega) &= i\frac{(\omega+i\nu)^{-1}}{1},\\
[2/2]_g(\omega) &= i\frac{(\omega+i\nu)^{-1}}{1-(\omega+i\nu)^{-2}},\\
[3/3]_g(\omega) &= i\frac{(\omega+i\nu)^{-1}-(\omega+i\nu)^{-3}}{1-3(\omega+i\nu)^{-2}},\\
&\vdots
\end{aligned}
\tag{2.33}
$$

are equivalent to the solutions obtained using the cumulant-discard closure (2.20) for the Nth moment. The diagonal Padé series $[0/0]\,,[1/1]\,,[2/2]\,,\ldots$ corresponds to convergents of a Jacobi-type continued fraction. In this case the continued fraction expansion

$$
g_0(\omega)=\cfrac{i}{\omega+i\nu-\cfrac{1}{\omega+i\nu-\cfrac{2}{\omega+i\nu-\cfrac{3}{\omega+i\nu-\cdots}}}}
\tag{2.34}
$$

converges for $\nu > 0$, but diverges for $\nu = 0$ (Kraichnan 1968; Wall 1967). The Padé series is therefore an improvement over the asymptotic series. Many physical problems of interest, however, are analogous to the low-dissipation limit $\nu \to 0$, where even the Padé series converges increasingly poorly.

The Padé and asymptotic series are derived in the high-frequency $\omega \to \infty$ limit. This limit is matched naturally for the closed moment system (2.13) as increasing numbers of moments are taken. The cumulant discard approximation and the Padé approximation discussed here match the exact response extremely well in the high-frequency limit, but fail to capture the long-time decay due to phase mixing. The Landau-fluid closures achieve highly accurate response functions by generalizing to two-point Padé approximations that are constructed by matching in the low-frequency limit $\omega \to 0$ as well as the high-frequency limit $\omega \to \infty$.

2.3.5 Random-Coupling Model

An alternate approach suggested by Kraichnan (1968) is to consider expansion in powers of the response $g_0(\omega)$ itself. For the Gaussian case, there is evidence that the continued fraction expansion

$$ig_1(\omega) = \cfrac{g_0(\omega)^2}{1 + \cfrac{g_0(\omega)^2}{1 + \cfrac{3g_0(\omega)^2}{1 + \cfrac{11g_0(\omega)^2}{1 + \cdots}}}} \tag{2.35}$$

converges even in the limit $\nu = 0$, and therefore provides more robust closure approximations. The lowest-order approximation,

$$ig_1(\omega) = g_0(\omega)^2, \tag{2.36}$$

is equivalent to the random-coupling approximation of Kraichnan (1961). This closure has a corresponding non-negative approximate distribution

$$\rho^{\mathrm{a}}(b) = \frac{1}{\pi}\sqrt{1 - (b/2)^2} \qquad (-2 \le b \le 2), \tag{2.37}$$

and gives the time response

$$g_0(t) = J_1(2t)/t, \tag{2.38}$$

where J_n denotes the standard Bessel function of the first kind. One obtains a response that decays to zero as $t \to \infty$ with this approximation at the expense of introducing a nonlinear closure.

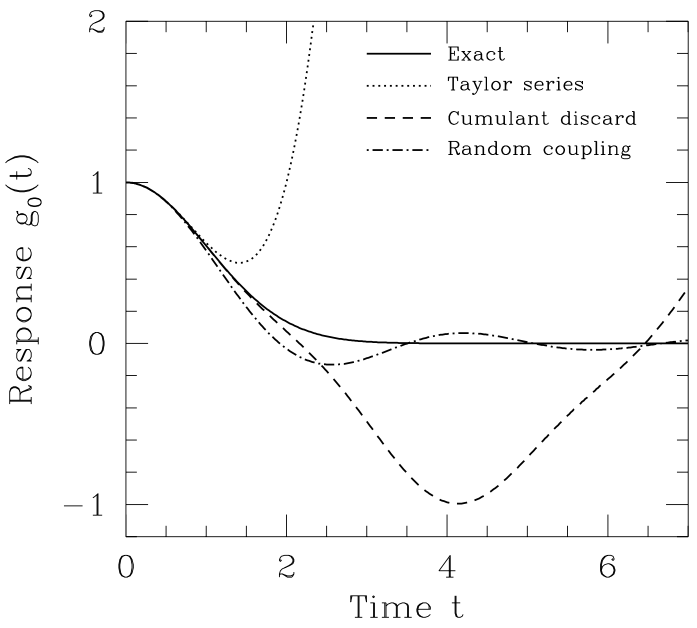

Figure 2.2: Response functions obtained from several approximation schemes for the stochastic oscillator with Gaussian-distributed b and $\nu = 0$. Results are displayed for the fourth-order Taylor-series approximation (2.17), the fourth-cumulant discard closure (2.21), and the random-coupling approximation (2.36). The random-coupling approximation matches the exact response to $\mathcal{O}(t^3)$ as $t \to 0$.

2.3.6 Hammett–Perkins Closure

Consider a generalization of the cumulant-discard closure to a linear closure with arbitrary coefficients. The simplest such closure is the a linear closure for the first moment,

$$g_1(\omega) = A_0 g_0(\omega). \tag{2.39}$$

[For constant A_0, the closure is the same in the time domain; $g_1(t) = A_0 g_0(t)$.] In reality, the first moment $g_1(\omega)$ is not simply a multiple of $g_0(\omega)$, so this closure cannot be exact. The advantage to constant linear closures of this form is that they are easily implemented in numerical simulations. [Replacing A_0 with $\omega + \sqrt{2}/Z(\omega/\sqrt{2})$ in Eq. (2.39) results in a closure that matches the response exactly. However, implementing such a closure in a numerical simulation would require expensive computations of time-history integrals.] Using the Laplace transformed stochastic oscillator

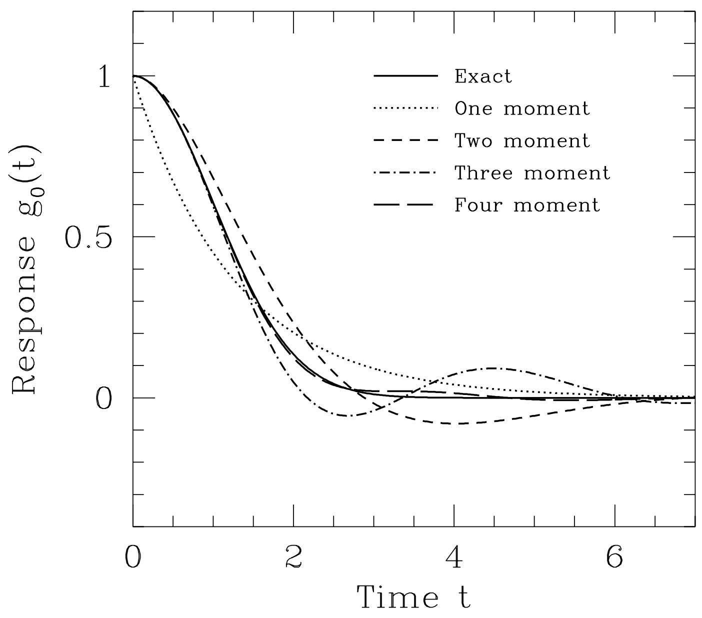

Figure 2.3: Response functions obtained using one, two, three, and four moment Hammett–Perkins closures compared to the exact time response for the stochastic oscillator with Gaussian-distributed b and $\nu = 0$.

equations (2.31) in the limit $\nu = 0$, one easily finds the response for this closure,

$$g_0^{\mathrm{a}}(\omega) = i\frac{1}{\omega - A_0}. \tag{2.40}$$

We would like to choose the closure coefficient A_0 so that this approximate response is a good estimate of the exact response (2.32). Hammett and Perkins (1990) considered linear closures of this form where the coefficients are chosen by matching the exact response in the $\omega = 0$ limit as well as $\omega \to \infty$. (The structure of moment equations causes the response to match in the high-frequency limit as more moment equations are added, and the low-frequency limit gives conditions that cause the coefficients to capture the physics of Landau damping.) The resulting closures yield linear responses that match the exact response well simultaneously at all frequencies. For the first moment closure here, taking $A_0 = -i\sqrt{2/\pi}$ matches the exact response (2.32) at $\omega = 0$. [Alternately, one could derive this closure by considering the low frequency limit of the exact closure coefficient $\omega + \sqrt{2}/Z(\omega/\sqrt{2})$.]

To illustrate the method more generally, consider the fourth-moment closure

$$g_4(\omega) = A_3 g_3(\omega) + A_2 g_2(\omega) + A_1 g_1(\omega) + A_0 g_0(\omega). \tag{2.41}$$

For the Gaussian case with $\nu = 0$, this closure results in a Padé approximation to the exact response,

$$g_0^{\mathrm{a}}(\omega) = i\frac{\omega^3 + \omega - A_3(\omega^2+1) - A_2\omega - A_1}{\omega^4 - A_3\omega^3 - A_2\omega^2 - A_1\omega - A_0}. \tag{2.42}$$

The coefficients (A_0, A_1, A_2, A_3) can now be chosen to try to approximate the true response (2.32). Matching the asymptotic series (2.31) to $\mathcal{O}(\omega^{-8})$ gives conditions on the coefficients that yields $A_0 = -3, A_1 = 0, A_2 = 6, A_3 = 0$, which is just the fourth-cumulant closure (2.21). [Note that the form of Eq. (2.42) already matches the asymptotic series to $\mathcal{O}(\omega^{-4})$ for any choice of coefficients, so matching to $\mathcal{O}(\omega^{-8})$ gives four conditions.] If one obtains two conditions by matching the response to $\mathcal{O}(\omega^6)$ at $\omega \to \infty$ and two conditions from matching to $\mathcal{O}(\omega)$ at $\omega = 0$, one finds the closure approximation

$$g_4(\omega) = (6+2\beta_1)g_2(\omega) - (3+2\beta_1)g_0(\omega) - \sqrt{2}D_1 i\left[g_3(\omega) - 3g_1(\omega)\right], \tag{2.43}$$

where $D_1 = 2\sqrt{\pi}/(3\pi - 8)$ and $\beta_1 = (32 - 9\pi)/(6\pi - 16)$, which corresponds to the four-moment Landau-fluid closure. This closure has a non-negative approximate distribution and the time response is almost indistinguishable from the exact response. (See Fig. 2.3.) The approximate response

$$g_0^{\mathrm{a}}(\omega) = \cfrac{i}{\omega - \cfrac{1}{\omega - \cfrac{2}{\omega - \cfrac{3+2\beta_1}{\omega + i\sqrt{2}D_1}}}} \tag{2.44}$$

is obtained using this closure, and is written here in continued fraction form for comparison with the expansion (2.34). The Hammett–Perkins closures for one, two, three, and four moments are plotted in Fig. 2.3.

One should note that there are some philosophical differences between the Hammett-Perkins Landau-fluid closure approach and the Kraichnan random-coupling approximation. The higher order Landau-fluid models fit the exact response somewhat better, particularly in the long-time decay where the random-coupling model has only an algebraic decay. In part, the improved fit arises because the derivation of the Landau-fluid approximation uses information known about the exact solution. The random-coupling model was derived without reference to the exact response, and is intended for more complicated problems where the distribution is most likely not Gaussian. While the Landau-fluid closure coefficients were chosen by fitting an idealized problem where the exact solution is know, it also is intended for use in more complicated problems where the exact solution is no longer known [such as happens when $\mathbf{E}\times\mathbf{B}$ nonlinearities are added to the Vlasov Eq. (3.5)]. The Landau-fluid closure is intended to model a subset of the physics known to reside in the more complicated problems. As we will find, the Hammett-Perkins closure works not only if the underlying distribution function is Gaussian, but it works in more general cases where the distribution function is sufficiently smooth that it can be written as a Gaussian times a few low order Hermite polynomials (no more than the number of moments being used).

2.4 Orthogonal Polynomials

The stochastic variable $y(t)$ is a continuous function of the frequency variable b and cannot therefore be fully characterized by a finite set of moments. Moment closure schemes attempt in some sense to estimate the effects of the missing or unresolved information. There are several interesting questions that one might ask. How does one estimate the PDF, given a finite set of moments? Is there a sensible definition of the 'unresolved scales' for this problem? What is a good estimate for the unresolved scales, given the observed moments? Note that answers to these questions can provide useful moment closure schemes. However, as was seen in the previous section, closures can be produced to fit the response functions without addressing any of these questions.

Expansions in orthogonal polynomials provide a natural translation from moments to underlying functions expressing those moments. Kraichnan (1970) noted that orthogonal polynomial expansions can be used to generate robust convergents to spectral densities given moments. Several results concerning linear closures for moment equations are readily expressed in terms of orthogonal polynomials.

2.4.1 Definition

Orthogonal polynomials are defined with respect to a positive weight function $w(x)$ for which the moments,

$$m_n = \int_{-\infty}^{\infty} x^n w(x)\, dx, \tag{2.45}$$

exist. It will be assumed that $m_0 = 1$ since $w(x)$ has the meaning of a probability density function. [The weight function $w(x)$ must decay faster than algebraically as $|x| \to \infty$ for all the moments to exist.]

Definition 3
Orthonormal polynomials with respect to a given weight function $w(x)$ are defined to be the polynomials in x,

$$P_n(x) = P_{n,0} + P_{n,1}x + P_{n,2}x^2 + \cdots + P_{n,n}x^n, \tag{2.46}$$

Polynomial	Definition	a_n	b_n	c_n
Hermite	$H_n(x) = (-1)^n \exp(x^2) \dfrac{d^n}{dx^n} \exp(-x^2)$	2	0	$2(n-1)$
Chebyshev	$U_n(x) = \dfrac{\sin((n+1)\arccos(x))}{\sin(\arccos(x))}$	2	0	1
Legendre	$P_n(x) = \dfrac{1}{2^n n!} \dfrac{d^n}{dx^n}(x^2-1)^n$	$\dfrac{2n-1}{n}$	0	$\dfrac{n-1}{n}$
Laguerre	$L_n(x) = \dfrac{1}{n!} \exp(x) \dfrac{d^n}{dx^n} \exp(-x)$	$-\dfrac{1}{n}$	$\dfrac{2n-1}{n}$	$\dfrac{n-1}{n}$

Table 2.1: Definitions of commonly used orthogonal polynomials and recursion coefficients such that $P_n(x) = (a_n x + b_n) P_{n-1}(x) - c_n P_{n-2}(x)$. Notation and normalizations are taken from Gradshteyn and Ryzhik (1980).

that satisfy the orthogonality conditions

$$\int_{-\infty}^{\infty} P_n(x) P_m(x) w(x)\, dx = \delta_{nm}. \tag{2.47}$$

(The Kronecker delta function is defined by $\delta_{nm} = 1$ if $n = m$ and $\delta_{nm} = 0$ otherwise.)

Orthonormal polynomials can be shown to satisfy a three-term recurrence relation,

$$P_n(x) = (a_n x + b_n)\, P_{n-1}(x) - c_n P_{n-2}(x). \tag{2.48}$$

The recurrence coefficients are related to the leading coefficients of the polynomials through

$$a_n = \frac{P_{n,n}}{P_{n-1,n-1}}, \qquad b_n = a_n \left(\frac{P_{n,n-1}}{P_{n,n}} - \frac{P_{n-1,n-2}}{P_{n-1,n-1}} \right), \qquad c_n = \frac{a_n}{a_{n-1}}. \tag{2.49}$$

2.4.2 Orthogonal Polynomial Expansion

Orthogonal polynomial moments of an arbitrary function $f(x)$ are defined by

$$f_n = \int_{-\infty}^{\infty} P_n(x) f(x)\, dx. \tag{2.50}$$

The inverse transform from moments to the function $f(x)$ is defined formally by

$$f(x) = \sum_{j=0}^{\infty} f_j P_j(x) w(x). \tag{2.51}$$

	weight $w(b)$	polynomial
Gaussian	$w_G(b) = \frac{1}{\sqrt{2\pi}} \exp(-b^2/2)$	$\frac{1}{\sqrt{n!2^n}} H_n(b/\sqrt{2})$
Spring	$w_s(b) = \begin{cases} \frac{1}{\pi}\sqrt{1-(b/2)^2} & (\lvert b\rvert < 2), \\ 0 & (\lvert b\rvert \geq 2) \end{cases}$	$U_n(b/2)$
Water Bag	$w_w(b) = \begin{cases} 1/2 & (\lvert b\rvert < 1), \\ 0 & (\lvert b\rvert \geq 1) \end{cases}$	$\sqrt{2n+1} P_n(b)$
Exponential	$w_e(b) = \begin{cases} \exp(-b) & (b > 0), \\ 0 & (b < 0) \end{cases}$	$L_n(b)$

Table 2.2: Orthonormal polynomials for weights corresponding to some PDFs of interest.

The form of these transforms is slightly asymmetric because one is expanding underlying distributions that decay rapidly for $|x| \to \infty$ in terms of moments that are polynomials, which diverge for large x. The weight function $w(x)$ appears in the moment expansion (2.51) to give the basic form of the modeled distributions.

It is possible to find functions whose orthogonal moment expansions do not converge pointwise or have poor pointwise convergence. Discontinuous functions, for example, will exhibit the ringing phenomenon observed in Fourier series expansions around discontinuities. The moment expansion does converge in an appropriately defined Hilbert space, however. The inner product

$$\langle f, g \rangle_w = \int_{-\infty}^{\infty} f(x)g(x)w(x)^{-1}\, dx \tag{2.52}$$

and corresponding norm $\|\cdot\|_w$ define a Hilbert space of distribution functions $\mathcal{H}_w$. If the set of functions $E_n = P_n(x)w(x)$ form a complete basis for $\mathcal{H}_w$, then the Fourier series

$$f = \sum_{j=0}^{\infty} \langle E_n, f \rangle_w \, E_n \tag{2.53}$$

converges for all $f \in \mathcal{H}_w$ [Theorem 4.13 of Conway (1990)]. Kraichnan (1970) demonstrates completeness for a broad class of $w(x)$. The moment expansion (2.51) can therefore be viewed as an orthonormal series expansion in $\mathcal{H}_w$, since from Eqs. (2.50) and (2.52) the expansion coefficients are given by $f_n = \langle E_n, f \rangle_w$.

2.5 Orthogonal Moments of the Stochastic Oscillator

The closure problem for stochastic oscillator moments is best studied in terms of polynomial moments, where the polynomials are *orthogonal with respect to the underlying PDF*. The main advantage to this orthogonal-polynomial expansion is demonstrated in Result 4, where it will be shown that matching in the high-frequency limit is simply accomplished by setting closure coefficients to zero. As well, projection onto orthogonal functions preserves the anti-Hermitian nature of the operator ib, so simple truncation at least gives solutions that are bounded in time.

Consider now the stochastic oscillator problem with underlying distribution written as an orthogonal-polynomial expansion about some positive weight function $w(b)$,

$$\rho(b) = \sum_{j=0}^{m} C_j P_j(b) w(b). \tag{2.54}$$

[This general form of the problem is useful when the results are carried over to the fluid moment problem where the initial conditions are of a form $\propto v f_M(v)$, which is a polynomial multiplied by a positive density function.] The *orthogonal-polynomial moments* are defined by

$$\alpha_n(t) = \langle P_n(b) y(t) \rangle , \tag{2.55}$$

where $P_n(b)$ are taken to be the orthonormal polynomials with respect to the same weight function $w(b)$. The general linear closure for the nth orthogonal-polynomial moment is then written as

$$\alpha_n(t) = \sum_{j=0}^{n-1} A_j \alpha_j(t). \tag{2.56}$$

2.5.1 Equivalence to b^n Moments

The first n polynomial moments $\{\alpha_0(t), \ldots, \alpha_{n-1}(t)\}$ contain exactly the same information as the first n moments $\{g_0(t), \ldots, g_{n-1}(t)\}$, so the resulting linear systems are equivalent. The translation from the problem with b^n moments $g_i(t)$, underlying distribution $\rho(b) = \sum_{j=0}^{m} C'_j b^j w(b)$ and closure $g_n(t) = \sum_{j=0}^{n-1} A'_j g_j(t)$ to the problem with polynomial moments (2.55), distribution (2.54), and closure (2.56) can be accomplished through

$$\begin{bmatrix} \alpha_0(t) \\ \alpha_1(t) \\ \vdots \\ \alpha_{n-1}(t) \end{bmatrix} = \mathsf{D}_{n-1} \begin{bmatrix} g_0(t) \\ g_1(t) \\ \vdots \\ g_{n-1}(t) \end{bmatrix}, \tag{2.57}$$

$$\begin{bmatrix} C_0 & C_1 & \dots & C_m \end{bmatrix} = \begin{bmatrix} C_0' & C_1' & \dots & C_m' \end{bmatrix} \mathsf{D}_m^{-1}, \tag{2.58}$$

$$\begin{bmatrix} A_0 & A_1 & \dots & A_n & -1 \end{bmatrix} = d_{nn} \begin{bmatrix} A_0' & A_1' & \dots & A_{n-1}' & -1 \end{bmatrix} \mathsf{D}_n^{-1}, \tag{2.59}$$

where the matrix of coefficients D is defined by

$$\mathsf{D}_k = \begin{bmatrix} P_{0,0} & 0 & \dots & 0 \\ P_{1,0} & P_{1,1} & \dots & 0 \\ \vdots & \vdots & \ddots & \vdots \\ P_{k,0} & P_{k,1} & \dots & P_{k,k} \end{bmatrix}. \tag{2.60}$$

2.5.2 Exact Solution

Upon taking orthogonal-polynomial moments of the exact solution (2.7) in the limit $\nu = 0$, one obtains the general response

$$\alpha_k(t) = \sum_{j=0}^{m} \mathsf{R}_{kj}(t) C_j, \tag{2.61}$$

$$\mathsf{R}_{kj}(t) = \int_{-\infty}^{\infty} e^{-ibt} P_k(b) P_j(b) w(b)\, db. \tag{2.62}$$

The first result obtained here shows that the general element of the transformed response matrix

$$\mathsf{R}_{kj}(\omega) = \int_0^{\infty} e^{i\omega t} \int_{-\infty}^{\infty} e^{-ibt} P_k(b) P_j(b) w(b)\, db\, dt \tag{2.63}$$

can be expressed in terms of the basic response element $\mathsf{R}_{00}(\omega)$, the orthogonal polynomials $P_n(\omega)$, and a set of numerator polynomials $Q_n(\omega)$ defined here.

Definition 4
Given an orthonormal set of polynomials $P_n(x)$ satisfying the recurrence relation (2.48), the conjugate *or* numerator *polynomials $Q_n(x)$ are defined to be the set of polynomials satisfying the same recurrence relation (2.48), with $Q_0(x) = 0$ and $Q_1(x) = a_1$.*

Note that the polynomial $Q_n(x)$ has degree $n-1$, whereas $P_n(x)$ has degree n. It is easily shown that

$$P_{n-1}(x) Q_n(x) - P_n(x) Q_{n-1}(x) = a_n. \tag{2.64}$$

This identity is easily proved using induction, the recurrence relation (2.48), and the fact $c_n a_{n-1} = a_n$, which follows from orthonormality. In general there is no guarantee that the conjugate polynomials Q_n corresponding to common orthogonal polynomials can be expressed simply. Two exceptions worth mentioning are the Chebyshev polynomials $U_n(x)$, for which $Q_n(x) = U_{n-1}(x)/2$, and the Hermite polynomials, which can be defined along with their conjugates by

$$(d/d\zeta)^n Z(\zeta) = H_n(\zeta)Z(\zeta) + Q_n(\zeta). \tag{2.65}$$

Lemma 1
The response function $\mathsf{R}_{0j}(t)$ has a Taylor series at $t = 0$ whose first j coefficients vanish. In other words,

$$\mathsf{R}_{0j}(t) = 0 + 0t + \cdots + 0t^{j-1} + c_j t^j + \cdots . \tag{2.66}$$

PROOF. Upon evaluating the kth derivative of the response (2.62), one finds that

$$\begin{aligned} \left|(\partial/\partial t)^k \mathsf{R}_{0j}(t)\right|_{t\,=\,0} &= \left|(\partial/\partial t)^k \int_{-\infty}^{\infty} e^{-ibt} P_j(b)w(b)\,db\right|_{t\,=\,0} \\ &= (-i)^k \int_{-\infty}^{\infty} b^k P_j(b)w(b)\,db. \end{aligned} \tag{2.67}$$

By definition, $P_j(b)$ is orthogonal to a complete set of polynomials with degree less than j, so the right-hand side of Eq. (2.67) is zero if $k < j$. $\square$

An immediate corollary to this is that the first term in the asymptotic series of the frequency response $\mathsf{R}_{0j}(\omega)$ is $\mathcal{O}(\omega^{-j-1})$. In other words,

$$\mathsf{R}_{0j}(\omega) \sim i\frac{i^j j! c_j}{\omega^{j+1}} + i\frac{i^{j+1}(j+1)! c_{j+1}}{\omega^{j+2}} + \cdots \qquad (\omega \to \infty). \tag{2.68}$$

This result follows from application of Watson's lemma (Bender and Orszag 1978) to the Laplace transform integral.

Lemma 2
The frequency responses of the lowest moment α_0 are related to $\mathsf{R}_{00}(\omega)$ by

$$\mathsf{R}_{0j}(\omega) = P_j(\omega)\mathsf{R}_{00}(\omega) - iQ_j(\omega). \tag{2.69}$$

PROOF. From the recurrence relation (2.48) it is easy to show that the response defined in Eq. (2.62) satisfies the recurrence relation

$$\mathsf{R}_{0,j}(t) = \left(a_j i\frac{\partial}{\partial t} + b_j\right) \mathsf{R}_{0,j-1}(t) - c_j \mathsf{R}_{0,j-2}(t). \tag{2.70}$$

Taking the Laplace transform (2.1) and integrating by parts gives

$$\mathsf{R}_{0,j}(\omega) = (a_j\omega + b_j)\,\mathsf{R}_{0,j-1}(\omega) - c_j \mathsf{R}_{0,j-2}(\omega) - ia_n \left|\mathsf{R}_{0,j-1}(t)\right|_{t=0}. \tag{2.71}$$

Now $\mathsf{R}_{0,0}(t=0)=1$ and $\mathsf{R}_{0,j}(t=0)=0$ for $j \geq 1$ from the previous lemma. The recurrence equation (2.71) therefore yields

$$\begin{aligned} \mathsf{R}_{0,0}(\omega) &= 1\mathsf{R}_{0,0}(\omega) - i0, \\ \mathsf{R}_{0,1}(\omega) &= P_1(\omega)\mathsf{R}_{0,0}(\omega) - ia_1, \\ \mathsf{R}_{0,j}(\omega) &= (a_j\omega + b_j)\,\mathsf{R}_{0,j-1}(\omega) - c_j\mathsf{R}_{0,j-2}(\omega) \qquad (j > 1). \end{aligned} \tag{2.72}$$

The result follows from the fact that P_n and Q_n satisfy the recurrence relation. □

From the asymptotic behavior of $\mathsf{R}_{0m}(\omega)$ in Eq. (2.68) one can see that the formula for $\mathsf{R}_{0m}(\omega)$, Eq. (2.69), implies that

$$\mathsf{R}_{00}(\omega) - i\frac{Q_j(\omega)}{P_j(\omega)} \sim \mathcal{O}\Big(\frac{1}{\omega^{2j+1}}\Big) \qquad (\omega \to \infty). \tag{2.73}$$

It turns out, therefore, that the ratios $iQ_j(\omega)/P_j(\omega)$ are Padé approximations to the asymptotic series of the response function.

In fact, this relation between orthogonal polynomials and the Padé approximations for this problem is a classical result of Padé theory. There is an intimate connection between orthogonal polynomials, moments, and Padé approximations. Upon exchanging the order of integration in the definition of the frequency response (2.63), one finds that

$$\frac{i}{z}\mathsf{R}_{00}\Big(-\frac{1}{z}\Big) = \int_{-\infty}^{\infty} \frac{w(b)\,db}{1+zb}, \tag{2.74}$$

which is the definition of the Hamburger function for the measure $w(b)\,db$ [Eq. (6.1) of Baker and Graves-Morris (1996)]. An elementary result in the theory of the Hamburger moment problem is that the denominators of the Padé approximations to this function around $z=0$ are just the orthogonal polynomials with respect to the measure $w(b)\,db$. The resulting Padé approximations are only guaranteed to converge for z in regions of the complex plane that are separated from the real axis by some minimum distance. Convergence for real z generally occurs only when a constant C exists such that the distribution satisfies $w(b)=0$ for $|b|>C$, and even then is only guaranteed for $|z|$ larger than some constant.

Result 1

The general element $\mathsf{R}_{kj}(\omega)$ *of the transformed response matrix is given by*

$$\mathsf{R}_{kj}(\omega) = P_{\min(k,j)}(\omega)\left[P_{\max(k,j)}(\omega)\mathsf{R}_{00}(\omega) - iQ_{\max(k,j)}(\omega)\right]. \tag{2.75}$$

Proof. Assume for the moment that $k \leq j$. The time response (2.62) may be rewritten

$$\begin{aligned} \mathsf{R}_{kj}(t) &= P_k(i\partial/\partial t)\int_{-\infty}^{\infty} e^{-ibt}P_j(b)w(b)\,db, \\ &= P_k(i\partial/\partial t)\mathsf{R}_{0j}(t). \end{aligned} \tag{2.76}$$

Recall that the Laplace transform of $(i\partial/\partial t)^n f(t)$ is just $\omega^n \widehat{f}(\omega) - i\omega^{n-1} f(0) - \cdots - f^{(n-1)}(0)$. By lemma 1 the first j derivatives of $\mathsf{R}_{0j}(t)$ vanish at $t = 0$, so the assumption $k \leq j$ implies that

$$\mathsf{R}_{kj}(\omega) = P_k(\omega)\mathsf{R}_{0j}(\omega). \tag{2.77}$$

The result then follows from lemma 2. □

This expression for the exact response function is useful for deriving and evaluating the approximate response. The notation

$$\{PQ\}_{kj}(\omega) = P_{\min(k,j)}(\omega) Q_{\max(k,j)}(\omega) \tag{2.78}$$

helps to simplify the resulting expressions. The previous result becomes simply

$$\mathsf{R}_{kj}(\omega) = P_k(\omega)P_j(\omega)\mathsf{R}_{00}(\omega) - i\,\{PQ\}_{kj}(\omega). \tag{2.79}$$

2.6 Approximate Response

In matrix form, the closed linear system of orthogonal-polynomial moments becomes

$$i\mathsf{A}\begin{bmatrix} \alpha_0(\omega) \\ \alpha_1(\omega) \\ \vdots \\ \alpha_{n-1}(\omega) \end{bmatrix} = \begin{bmatrix} C_0 \\ \vdots \\ C_m \\ 0 \\ \vdots \\ 0 \end{bmatrix}, \tag{2.80}$$

where

$$\mathsf{A} = \begin{bmatrix} -\omega - \dfrac{b_1}{a_1} & \dfrac{1}{a_1} & 0 & \dots & 0 \\ \dfrac{c_2}{a_2} & -\omega - \dfrac{b_2}{a_2} & \dfrac{1}{a_2} & \dots & 0 \\ 0 & \dfrac{c_3}{a_3} & -\omega - \dfrac{b_3}{a_3} & \dots & 0 \\ \vdots & \vdots & \vdots & \ddots & \vdots \\ \dfrac{A_0}{a_n} & \dfrac{A_1}{a_n} & \dfrac{A_2}{a_n} & \dots & \dfrac{A_{n-1}}{a_n} - \omega - \dfrac{b_n}{a_n} \end{bmatrix}. \tag{2.81}$$

The fact that the initial distribution constants $\{C_0, C_1, \ldots, C_m\}$ enter the problem in the equations for the first m moments only is a property of the orthogonal-polynomial-moment expansion. The solution to this matrix problem

$$\alpha_k = \sum_{j=0}^{m} \mathsf{R}^{\mathrm{a}}_{kj}(\omega) C_j \tag{2.82}$$

defines the approximate response matrix $\mathsf{R}^{\mathrm{a}} = -i\mathsf{A}^{-1}$.

Several important questions can be considered. Is there a general procedure for choosing the coefficients $\{A_0, A_1, \ldots, A_{n-1}\}$ for the n-moment system? Does the approximate response converge? Does $\mathsf{R}^{\mathrm{a}}_{kj}(\omega) \to \mathsf{R}_{kj}(\omega)$ as $n \to \infty$? Does $\mathsf{R}^{\mathrm{a}}_{kj}(t) \to \mathsf{R}_{kj}(t)$ as $n \to \infty$? The approximate response functions $\mathsf{R}^{\mathrm{a}}_{kj}(\omega)$ are Padé approximations in ω and have poles in the complex plane. Causality requires that these poles lie in the lower-half complex plane, and closures that give poles in the upper-half complex plane will generate systems that are exponentially unstable. What is the behavior of the poles of the approximate response function as a function of the number of moments? The following sections will attempt to address these questions.

2.6.1 Form and Asymptotics of the Approximate Response

Result 2

The coefficients of the approximate response matrix $\mathsf{R}^{\mathrm{a}}_{kj}(\omega)$ for the closed system of n orthogonal-polynomial moments, Eq. (2.80), are given by

$$\begin{aligned}\mathsf{R}^{\mathrm{a}}_{kj}(\omega) = &- i\,\{PQ\}_{kj}(\omega) \\ &+ iP_k(\omega)\frac{\{PQ\}_{nj}(\omega) - A_{n-1}\{PQ\}_{n-1,j}(\omega) - \cdots - A_0\{PQ\}_{0j}(\omega)}{P_n(\omega) - A_{n-1}P_{n-1}(\omega) - \cdots - A_0P_0(\omega)}.\end{aligned} \tag{2.83}$$

Proof. Verification that $\sum_{k=0}^{n-1} i\mathsf{A}_{mk}\mathsf{R}^{\mathrm{a}}_{kj}(\omega) = \delta_{mj}$ involves straightforward algebra. Note that

$$\frac{c_j}{a_j}\{PQ\}_{j-1,l} - \left(\omega + \frac{b_j}{a_j}\right)\{PQ\}_{j,l} + \frac{1}{a_j}\{PQ\}_{j+1,l} = \delta_{jl}, \tag{2.84}$$

follows from the recurrence relation (2.48) and the conjugacy relation (2.64). □

As with the exact response, one can attempt to relate the general approximate response to the basic response $\mathsf{R}^{\mathrm{a}}_{00}(\omega)$, which takes the form

$$\mathsf{R}^{\mathrm{a}}_{00}(\omega) = i\frac{Q_n(\omega) - A_{n-1}Q_{n-1}(\omega) - \cdots - A_0Q_0(\omega)}{P_n(\omega) - A_{n-1}P_{n-1}(\omega) - \cdots - A_0P_0(\omega)}. \tag{2.85}$$

Using the definition of $\{PQ\}_{kj}$, the general solution can be written as

$$\begin{aligned}\mathsf{R}^{\mathrm{a}}_{kj}(\omega) =&P_k(\omega)P_j(\omega)\mathsf{R}^{\mathrm{a}}_{00}(\omega) - i\,\{PQ\}_{kj}(\omega) \\ &+ iP_k(\omega)\frac{\sum_{r=0}^{j-1} A_r\left[P_j(\omega)Q_r(\omega) - P_r(\omega)Q_j(\omega)\right]}{P_n(\omega) - A_{n-1}P_{n-1}(\omega) - \cdots - A_0P_0(\omega)}.\end{aligned} \tag{2.86}$$

From this form of the approximate response, it is easy to obtain the first major result concerning the error in the response function defined by

$$\Delta_{kj}(\omega) = \mathsf{R}^{\mathrm{a}}_{kj}(\omega) - \mathsf{R}_{kj}(\omega). \tag{2.87}$$

Subtracting the exact response (2.79) from the approximate response (2.86) yields the following result.

Result 3
For the orthogonal-polynomial moment system with closure, setting the first p closure coefficients to zero ($A_0 = \cdots = A_{p-1} = 0$) enables the errors in the response functions corresponding to $C_0, \ldots, C_p$ to be related to each other by the formula

$$\Delta_{kj}(\omega) = P_k(\omega)P_j(\omega)\Delta_{00}(\omega) \qquad (j \leq p). \tag{2.88}$$

Fitting the basic response $\mathsf{R}_{00}(\omega)$ well therefore ensures a good fit for all the response functions $\mathsf{R}_{kj}(\omega)$ with $j \leq p$ if the first p coefficients are set to zero. Fitting those components of the response function ensures that the response to distributions of the form $\rho(b) = [C_0 P_0(b) + \cdots + C_p P_p(b)]\, w(b)$ is modeled well. Increasing p therefore enables one to uniformly approximate a greater variety of initial conditions. Setting the first p coefficients to zero also ensures a good fit of the basic response in the $\omega \to \infty$ limit.

Result 4
Setting the first p closure coefficients to zero ($A_0 = \cdots = A_{p-1} = 0$) improves the asymptotic fit of the approximate response function by a factor of ω^{-p}. The approximate response behaves as

$$\mathsf{R}^{\mathrm{a}}_{00}(\omega) - \mathsf{R}_{00}(\omega) \sim \mathcal{O}\Big(\frac{1}{\omega^{n+1+p}}\Big) \qquad (\omega \to \infty). \tag{2.89}$$

Proof. The asymptotic result expressed in Eq. (2.73) implies that $P_j(\omega)\mathsf{R}_{00}(\omega) - iQ_j(\omega) \sim \mathcal{O}(\omega^{-(j+1)})$ as $\omega \to \infty$. The asymptotic behavior of the linear combination

$$\begin{aligned}&[P_n(\omega) - A_{n-1}P_{n-1}(\omega) - \cdots - A_p P_p(\omega)]\, \mathsf{R}_{00}(\omega)\\ &\quad - i\,[Q_n(\omega) - A_{n-1}Q_{n-1}(\omega) - \cdots - A_p Q_p(\omega)] \sim \mathcal{O}\Big(\frac{1}{\omega^{p+1}}\Big) \qquad (\omega \to \infty),\end{aligned} \tag{2.90}$$

is given by the worst term $A_p P_p(\omega)\mathsf{R}_{00}(\omega) - iA_p Q_p(\omega)$. The result follows using the definition of $\mathsf{R}^{\mathrm{a}}_{00}(\omega)$ in Eq. (2.85) after dividing Eq. (2.90) by the denominator of $\mathsf{R}^{\mathrm{a}}_{00}(\omega)$. □

Thus there are two benefits to setting the lowest closure coefficients to zero. The asymptotic response is improved and the approximate response models initial conditions with more degrees of freedom. Why not simply take the maximum possible choice $p = n$, which corresponds to moment truncation [$\alpha_n(t) = 0$]? The resulting approximate response

$$\mathsf{R}^{\mathrm{a}}_{00}(\omega) = i\frac{Q_n(\omega)}{P_n(\omega)} \tag{2.91}$$

matches the exact response to $\mathcal{O}(\omega^{-(2n+1)})$ as $\omega \to \infty$, a significant improvement over truncation in b^n moments, which leads to the Taylor-series approximation (2.17), which matches the exact response to $\mathcal{O}(\omega^{-(n+1)})$ as $\omega \to \infty$. The denominator of this approximation, $P_n(\omega)$, is an orthogonal polynomial with respect to a positive weight function, and therefore has n zeroes on the real axis. This approximation yields solutions that are oscillatory in time and fail to model the phase-mixing decay.

2.6.2 Two-Point Approximation

The question remains how to choose the remaining coefficients if some are to be left nonzero ($p < n$). Matching in the $\omega \to \infty$ limit forces more coefficients to be zero, so some other part of the response function must be looked at. One is therefore naturally led to consider generalized Padé approximants involving other limits. Multipoint Padé approximations are sometimes called rational interpolants or Newton–Padé approximants. Various definitions exist for two-point approximants since one point may be infinite and there is a degree of freedom in how to split the total number of matching conditions between the two points. The particular definition chosen here corresponds to the problem at hand where the approximate response function is a ratio of polynomials that naturally matches the exact response in the $\omega \to \infty$ limit, and one wishes to fix coefficients by matching at a point elsewhere.

Definition 5
Suppose a function $f(z)$ has an asymptotic series and power series representation

$$f(z) = \frac{c_1}{z} + \frac{c_2}{z^2} + \cdots \qquad (z \to \infty), \tag{2.92}$$

$$f(z) = d_0 + d_1(z - z_0) + d_2(z - z_0)^2 + \cdots \qquad (z \to z_0). \tag{2.93}$$

The $[N, q]$ two-point Padé approximant to f is defined by

$$f^{[N,\,q,\,z_0]}(z) = \frac{Q^{[N,q,z_0]}(z)}{P^{[N,q,z_0]}(z)}, \tag{2.94}$$

where $Q^{[N,q,z_0]}(z)$ is a polynomial of degree $N-1$, $P^{[N,q,z_0]}(z)$ is a polynomial of degree N, $f^{[N,\,q,\,z_0]}(z) - f(z) \sim \mathcal{O}(z^{-(2N+1-q)})$ as $z \to \infty$, and $f^{[N,\,q,\,z_0]}(z) - f(z) \sim \mathcal{O}((z - z_0)^q)$ as $z \to z_0$. (There are $2N$ degrees of freedom in the choice of coefficients of the polynomials and $2N$ terms have been matched in the two series.)

With the first p closure coefficients set to zero, the approximate response

$$\mathsf{R}^{\mathrm{a}}_{00}(\omega) = i\frac{Q_n(\omega) - A_{n-1}Q_{n-1}(\omega) - \cdots - A_pQ_p(\omega)}{P_n(\omega) - A_{n-1}P_{n-1}(\omega) - \cdots - A_pP_p(\omega)}. \tag{2.95}$$

matches the exact response to order $\mathcal{O}(\omega^{n+1+p})$. The approximate response therefore becomes the $[n, q, \omega_0]$ Padé approximant to the exact response for $q = n - p$ if the q remaining coefficients can be chosen to match the first q terms of the Taylor series

$$\mathsf{R}_{00}(\omega) = r_0 + r_1(\omega - \omega_0) + r_2(\omega - \omega_0)^2 + \cdots. \tag{2.96}$$

Upon expressing the polynomials in terms of $(\omega - \omega_0)$,

$$\begin{aligned} P_j(\omega) &= P_{j,0} + P_{j,1}\omega + \cdots + P_{j,j}\omega^j \\ &= P^{\omega_0}_{j,0} + P^{\omega_0}_{j,1}(\omega - \omega_0) + \cdots + P_{j,j}(\omega - \omega_0)^j, \end{aligned} \tag{2.97}$$

one obtains the matrix equation for the remaining coefficients,

$$\left(\begin{bmatrix} r_0 & 0 & \dots & 0 \\ r_1 & r_0 & \dots & 0 \\ \vdots & \vdots & \ddots & \vdots \\ r_{q-1} & r_{q-2} & \dots & r_0 \end{bmatrix}\begin{bmatrix} P^{\omega_0}_{n-1,0} & P^{\omega_0}_{n-2,0} & \dots & P^{\omega_0}_{p,0} \\ P^{\omega_0}_{n-1,1} & P^{\omega_0}_{n-2,1} & \dots & P^{\omega_0}_{p,1} \\ \vdots & \vdots & \ddots & \vdots \\ P^{\omega_0}_{n-1,q} & P^{\omega_0}_{n-2,q} & \dots & P^{\omega_0}_{p,q} \end{bmatrix} - i\begin{bmatrix} Q^{\omega_0}_{n-1,0} & Q^{\omega_0}_{n-2,0} & \dots & Q^{\omega_0}_{p,0} \\ Q^{\omega_0}_{n-1,1} & Q^{\omega_0}_{n-2,1} & \dots & Q^{\omega_0}_{p,1} \\ \vdots & \vdots & \ddots & \vdots \\ Q^{\omega_0}_{n-1,q} & Q^{\omega_0}_{n-2,q} & \dots & Q^{\omega_0}_{p,q} \end{bmatrix}\right) \times \begin{bmatrix} A_{n-1} \\ A_{n-2} \\ \vdots \\ A_p \end{bmatrix}$$
$$= \begin{bmatrix} r_0 & 0 & \dots & 0 \\ r_1 & r_0 & \dots & 0 \\ \vdots & \vdots & \ddots & \vdots \\ r_{q-1} & r_{q-2} & \dots & r_0 \end{bmatrix}\begin{bmatrix} P^{\omega_0}_{n,0} \\ P^{\omega_0}_{n,1} \\ \vdots \\ P^{\omega_0}_{n,q} \end{bmatrix} - i\begin{bmatrix} Q^{\omega_0}_{n,0} \\ Q^{\omega_0}_{n,1} \\ \vdots \\ Q^{\omega_0}_{n,q} \end{bmatrix}. \quad (2.98)$$

Definition 6
Coefficients $\{A_{n-1}, A_{n-2}, \dots, A_p\}$ *satisfying the* $\omega \to \omega_0$ *conditions of Eq. (2.98) will be called the* $[n, q, \omega_0]$ *closure. The approximate response functions obtained using these closure coefficients will be denoted by* $\mathsf{R}^{[n,\,q,\,\omega_0]}_{kj}(\omega)$ *and the response function errors by* $\Delta^{[n,\,q,\,\omega_0]}_{kj}(\omega)$.

Padé convergents often provide excellent approximations even where the asymptotic series diverges. There are no general guarantees, however, that this type of two-point Padé approximation converges or even gives reasonable results. There are several things that can go wrong with the closures generated in this fashion. First, coefficients satisfying Eq. (2.98) may fail to exist if the matrix is singular. Second, the approximate response functions may have poles in the upper-half complex plane and therefore give exponential instabilities in the time solution instead of phase-mixing decay. Third, even if reasonable response functions are produced, they may fail to match the exact response at points other than $\omega = 0$ and $\omega \to \infty$. The convergence properties of this approximation scheme will be studied numerically in the following sections for several common distributions.

2.7 Convergence of the Two-Point Approximation Closure

As will be demonstrated in the next chapter, this two-point approximation closure is a generalization of the Landau-fluid closure of Hammett and Perkins (1990). Proof of convergence of the linear theory for increasing numbers of moments does not exist for

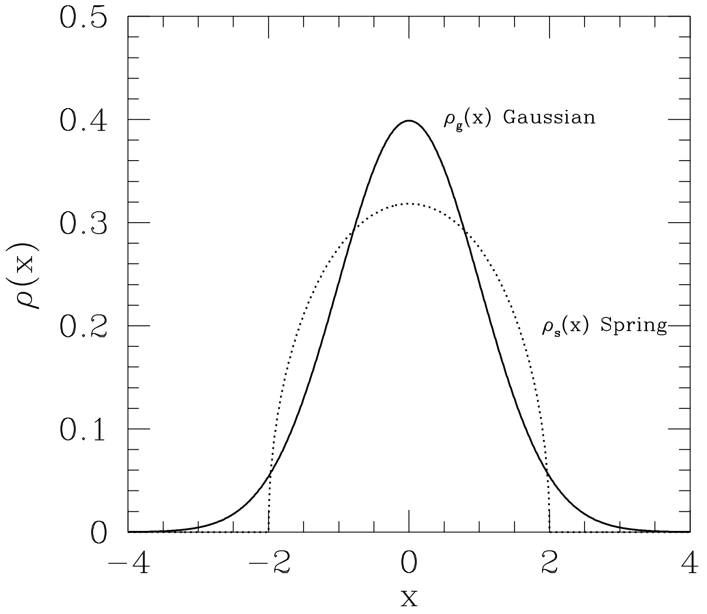

Figure 2.4: The Gaussian distribution and mass–spring distribution. Both distributions have mean 0 and variance 1.

the fluid closure problem. Here numerical evidence of convergence for these closures is presented for the two background distributions plotted in Fig. 2.4.

There is no guarantee that these closures give reasonable solutions for arbitrary n, q, and ω_0. For the subset of closures with $q = 1$, however, the two-point approximation closure yields exponentially decaying solutions that correspond to non-negative approximate distributions.

Result 5

For the general orthogonal moment linear system with positive underlying probability distribution $w(b) > 0$, the $[n, 1, \omega_0]$ closure corresponds to a non-negative approximate distribution and the resulting approximate response functions have poles that all lie in the lower half plane.

PROOF. The coefficient for the $[n, 1, \omega_0]$ closure is determined by the equation

$$\begin{aligned} 0 &= \left|\mathsf{R}_{00}(\omega) - \mathsf{R}^{\mathrm{a}}_{00}(\omega)\right|_{\omega=\omega_0} \\ &= \mathsf{R}_{00}(\omega_0) - i\frac{Q_n(\omega_0) - A_{n-1}Q_{n-1}(\omega_0)}{P_n(\omega_0) - A_{n-1}P_{n-1}(\omega_0)}. \end{aligned} \tag{2.99}$$

From the form of the response (2.63) one can show that $\mathrm{Re}(\mathsf{R}_{00}(\omega)) = \pi\, w(b)|_{b=\omega}$, so taking the real part of this equation results in

$$-A^i_{n-1}/a_n = \pi w(\omega_0)\left\{\left[P_n(\omega_0) - A^r_{n-1}P_{n-1}(\omega_0)\right]^2 + \left[A^i_{n-1}P_{n-1}(\omega_0)\right]^2\right\}. \tag{2.100}$$

[The conjugacy condition (2.64) has been used and the coefficient has been split into real and imaginary parts as $A_{n-1} = A^r_{n-1} + iA^i_{n-1}$.] The right-hand side of this equation is positive and nonzero because the zeroes of P_n and P_{n-1} are interlaced due to orthogonality. The quantity $-A^i_{n-1}/a_n$ must therefore be positive. Using the definition of the approximate distribution from Eq. (2.15) one can show that

$$\rho^{\mathrm{a}}(b) = \frac{1}{\pi}\frac{-A^i_{n-1}/a_n}{\left[P_n(b) - A^r_{n-1}P_{n-1}(b)\right]^2 + \left[A^i_{n-1}P_{n-1}(b)\right]^2}. \tag{2.101}$$

Hence, the approximate distribution for this system is defined and positive for all b. The evolution of the sum of squares of the moments

$$\frac{d}{dt}\sum_{j=0}^{n-1}|\alpha_j(t)|^2 = 2\frac{A^i_{n-1}}{a_n}|\alpha_{n-1}(t)|^2, \tag{2.102}$$

can be derived for the closed linear system (2.80) assuming $q = 1$. Any pole of the response in the upper-half complex plane would imply an exponentially growing solution, which cannot satisfy Eq. (2.102) with A^i_{n-1}/a_n negative. The squared absolute value, $\left[P_n(\omega) - A^r_{n-1}P_{n-1}(\omega)\right]^2 + \left[A^i_{n-1}P_{n-1}(\omega)\right]^2$, of the denominator of the approximate response $\mathsf{R}^{\mathrm{a}}_{00}(\omega)$ is nonzero because A_{n-1} has nonzero imaginary part and zeroes of P_n cannot coincide with zeroes of P_{n-1}. Therefore, all poles of the approximate response function must lie off the real axis in the lower-half complex plane. □

Thus for completely arbitrary background distribution, the closures with $q = 1$ are guaranteed to correspond to non-negative approximate distributions for any number of moments n. The $q = 1$ set of closures may fail to converge or converge slowly, however. There is no general theorem for closures with $q > 1$. As an example, consider the pathological bi-Gaussian density

$$w(b) = \frac{1}{\sqrt{2\pi}}\left[\frac{3}{5}\exp(-b^2/2) + 4\exp(-10^2b^2/2)\right]. \tag{2.103}$$

The behavior of the response at $\omega = 0$ is dominated by the narrow Gaussian containing less than half the total density. The $[4, 2, 0]$ closure for this distribution was computed numerically and found to have a pole at $\sim 10.76i$ and therefore gives non-physical exponentially growing solutions and violates causality. Note that this distribution was constructed to behave strangely at the point ω_0 where the matching was done to obtain closure coefficients. For the two typical distributions considered in the following sections, all of the closures had poles confined to the lower half of the

$[n, q, \omega_0]$	closure
$[1, 1, 0]$	$\langle by \rangle = -i\sqrt{\frac{2}{\pi}} \langle y \rangle$
$[2, 1, 0]$	$\langle b^2 y \rangle - \langle y \rangle = -i\sqrt{\frac{\pi}{2}} \langle by \rangle$
$[3, 1, 0]$	$\langle b^3 y \rangle - 3 \langle by \rangle = -i2\sqrt{\frac{2}{\pi}} \left(\langle b^2 y \rangle - \langle y \rangle\right)$
$[3, 2, 0]$	$\langle b^3 y \rangle - 3 \langle by \rangle = -i\frac{\sqrt{2\pi}}{4-\pi} \left(\left\langle b^2 y \right\rangle - \langle y \rangle\right) + \frac{3\pi - 8}{4 - \pi} \langle by \rangle$
$[4, 1, 0]$	$\langle b^4 y \rangle - 6 \langle b^2 y \rangle + 3 \langle y \rangle = -i\frac{3}{4}\sqrt{2\pi} \left(\left\langle b^3 y \right\rangle - 3 \langle by \rangle\right)$
$[4, 2, 0]$	$\langle b^4 y \rangle - 6 \langle b^2 y \rangle + 3 \langle y \rangle = -i\sqrt{2\pi}\frac{2}{3\pi - 8} \left(\left\langle b^3 y \right\rangle - 3 \langle by \rangle\right) + \frac{32 - 9\pi}{3\pi - 8} \left(\left\langle b^2 y \right\rangle - \langle y \rangle\right)$

Table 2.3: Two-point approximation closures assuming a Gaussian weight function for some small values of n and q expressed in terms of the original b^n moments.

complex plane. This example serves as a warning, however, that it is possible to obtain unphysical results if one is not careful. Alternatively, one could expand this weight function about a Gaussian by

$$w(b) \approx \exp(-b^2/2) \sum_{j=0}^{m} C_j H_j(b/\sqrt{2}). \tag{2.104}$$

The two-point closure for the Gaussian case can then be applied to this system. By result 3 the n moment closure with a given q would correspond to allowing up to $m = n - q$ Hermite polynomials in the approximation to $w(b)$. This procedure would retain the advantages that will be observed for the Gaussian case (causality and fast convergence). In principle, any arbitrary distribution function $w(b)$ could be thus represented, though the convergence rate with n may be very slow in some cases.

The fitness of a given closure can be measured by how accurately the response function for the closed system matches the exact response. There are several choices, however, of how to measure the discrepancy. Clearly a good first requirement on the closed system is that the response function has all its poles in the lower-half complex plane. This requirement ensures that the time response decays as $t \to \infty$. As a second measure of fitness, the maximum error of the frequency response along the real axis is calculated in the following section. In applications of these closures in

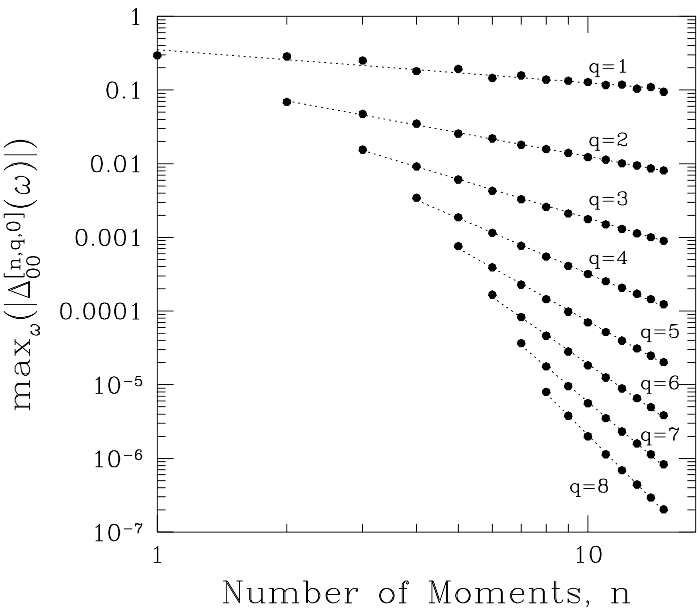

Figure 2.5: The maximum absolute error between the approximate response function and the exact response along the real axis for various two-point closures $[n, q, 0]$ in the Gaussian case is plotted against the number of moments n in the approximate system. The dotted lines are least-squares fits through the points corresponding to various choices of q, the number of times the response function is matched in the $\omega \to 0$ limit. The slopes of these fits for q from 1 through 8 are approximately $[-0.45, -1.1, -1.8, -2.5, -3.3, -4.1, -4.9, -5.8]$.

plasma physics, one is interested in accurately obtaining the growth rates of unstable modes. If the approximate response has no poles in the upper half complex plane, then the maximum modulus principle (Carrier et al. 1983, pg. 42) guarantees that the maximum error in the entire upper half plane is bounded by the maximum error along the real axis. Therefore if pointwise convergence is demonstrated on the real axis with increasing numbers of moments, the calculated growth rates for unstable modes will converge.

2.7.1 Gaussian Case

The initial study of Landau-fluid closures by Hammett and Perkins (1990) consisted essentially of application of this two-point approximation for a Gaussian distribution

$$w_G(b) = \frac{1}{\sqrt{2\pi}} \exp(-b^2/2). \tag{2.105}$$

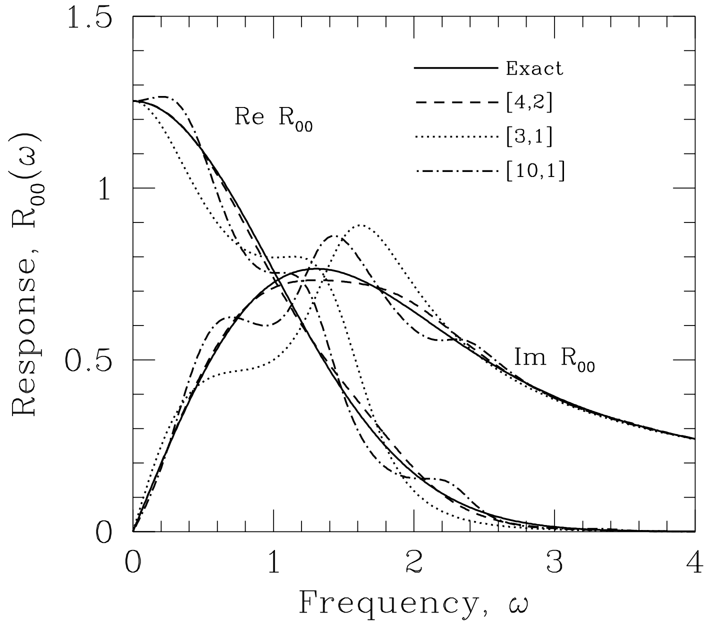

Figure 2.6: The exact response function $\mathsf{R}_{00}(\omega)$ for a Gaussian weight function (solid lines) and three of the two-point approximation closure response functions (dashed lines) corresponding to $[n = 4, q = 2]$, $[n = 3, q = 1]$ and $[n = 10, q = 1]$.

This case is of primary interest in plasma physics where velocities are assumed to have a Maxwellian distribution, so the frequencies $k_{\|}v$ have a Gaussian PDF. The exact response from Eq. (2.32) is just

$$\mathsf{R}_{00}(\omega) = \frac{-i}{\sqrt{2}} Z(\omega/\sqrt{2}). \tag{2.106}$$

For the Vlasov equation the initial conditions (which act as the distribution of frequencies $\rho(b)$) are of the form $bw_G(b)$. The appropriate response function to consider is

$$\mathsf{R}_{01}(\omega) = -i \left[1 + \frac{\omega}{\sqrt{2}} Z(\omega/\sqrt{2}) \right]. \tag{2.107}$$

Provided closures with $p \geq 1$ are considered, however, the approximate response errors are related by $[\mathsf{R}^{\mathrm{a}}_{01}(\omega) - \mathsf{R}_{01}(\omega)] = \omega[\mathsf{R}^{\mathrm{a}}_{00}(\omega) - \mathsf{R}_{00}(\omega)]$.

Since the response function satisfies the symmetry $\mathsf{R}_{00}(-\omega) = \mathsf{R}^*_{00}(\omega)$, it is natural to consider $\omega_0 = 0$, in other words to match in the $\omega \to 0$ limit. For reference, some of the $[n, q, 0]$ closures are listed in Table 2.3 in terms of the original b^n moments.

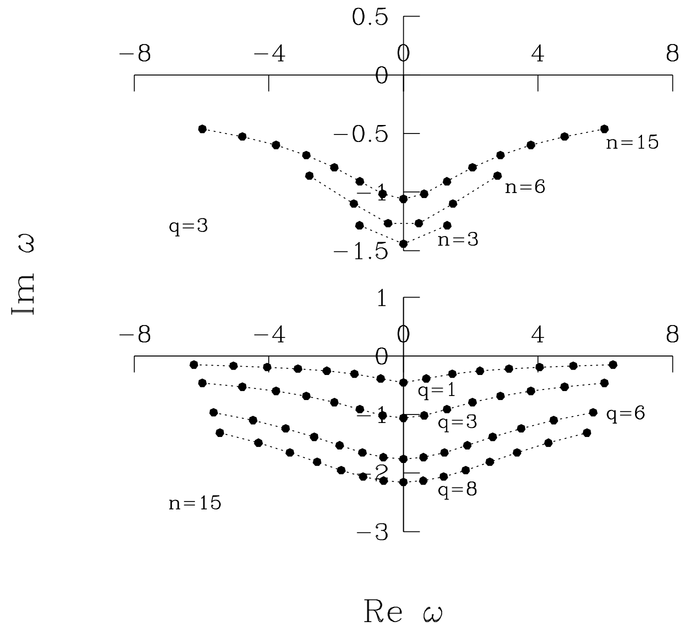

Figure 2.7: The locations in the complex plane of the poles of the approximate response function are shown for several different moment closures. In the top graph, where q is fixed at 3, the poles move towards the real axis with increasing numbers of moments. For a fixed number of moments ($n = 15$ in the lower graph), the poles move away from the real axis as q is increased.

The closures of Hammett and Perkins (1990) correspond to the $[3, 1, 0]$ and $[4, 2, 0]$ closures here.

The maximum error $\Delta_{00}(\omega)$ for real ω was computed for various closures and plotted in Fig. 2.5 against the total number of moments n. The errors seem to scale $\propto n^{-C(q)}$, where $C(q)$ is an increasing function of q. While the $q = 1$ closure have been proven to produce causal response functions, they converge poorly with increasing numbers of moments, the error scaling roughly as $n^{-0.45}$. A few of the approximate response functions are plotted in Fig. 2.6 along with the exact response. Compare the two responses from the $q = 1$ closures plotted with $n = 3$ and $n = 10$ to see the nature of the slow convergence for $q = 1$. The response from the $n = 10$ closure oscillate more around the true solution, but is only a slight improvement over that from the $n = 3$ closure. In contrast, the $[n = 4, q = 2]$ closure yields a response function that is already very close to the exact answer.

The poles of the approximate response function are plotted in the complex plane in Fig. 2.7. The upper plot shows poles for fixed $q = 3$ and three choices of n. The

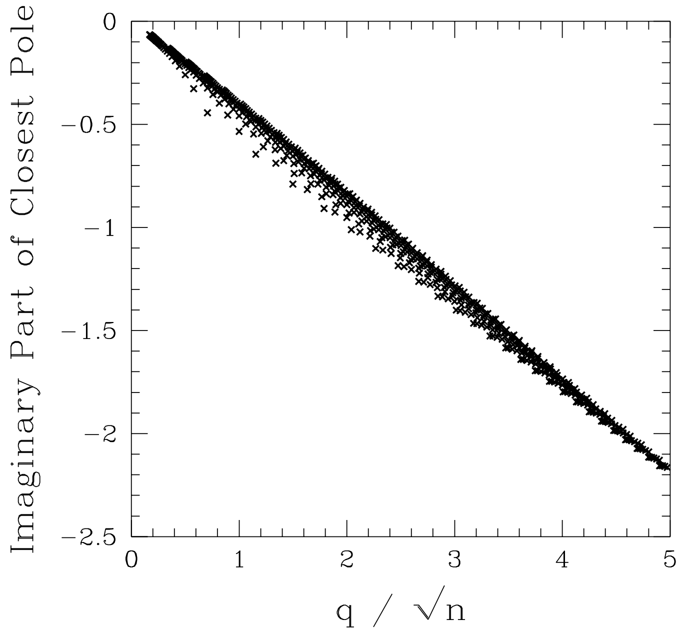

Figure 2.8: The maximum imaginary part of the poles of the $[n, q, 0]$ closure is plotted against $q/\sqrt{n}$. All closures with $1 \leq q < n \leq 35$ are included in this plot.

poles move closer to the axis with increasing number of moments and spread out. The lower plot shows poles for fixed $n = 15$ with four choices of q. The poles move away from the axis with increasing q. The response function appears to converge uniformly on the real axis as $n \to \infty$ even though the poles move progressively closer to the real axis. The distance of the closest pole to the real axis plotted in Fig. 2.8 was found empirically to scale as $q/\sqrt{n}$.

In summary, the main result obtained here is that there is strong numerical evidence that for the Gaussian case the linear response functions obtained using the two-point approximation closures converge with increasing numbers of moments. The convergence rate depends on q, the number of times the response function is matched in the $\omega \to 0$ limit. Convergence is faster for larger q. For all the cases considered, the poles lie in the lower-half complex plane, so the closures obtained in this fashion all give causal behavior.

2.7.2 Spring Response

The semi-infinite mass–spring system portrayed in Fig. (2.9) is an interesting physical model that can be used to illustrate the behavior of closures. With an infinite num-

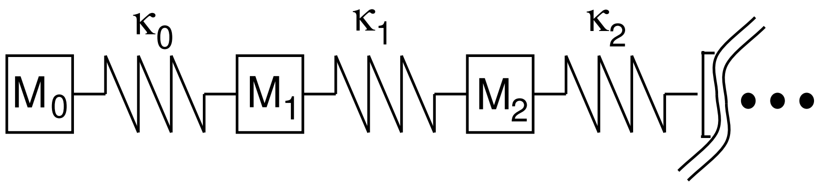

Figure 2.9: A simple one-dimensional semi-infinite mass–spring system consisting of objects, each with mass M_j, connected by springs with spring constant κ_j. The displacement of the jth mass $x_j(t)$ is measured relative to an initial state where the springs exert no forces.

ber of masses in such a system, there is a continuum of normal modes, so the system exhibits phase-mixing behavior analogous to that in the stochastic oscillator problem. The connection between the general mass–spring system and the phase-mixing problem in fluid moment equations with a Gaussian background was first illustrated by Hammett et al. (1993). Here the case with uniform spring constants $\kappa_j = \kappa$ and masses $M_j = M$ is considered as well.

The displacements of the masses $x_j(t)$ and velocities $v_j(t)$ evolve according to the equations

$$\begin{aligned} \dot{x}_0(t) &= v_0(t), \\ M_0\dot{v}_0(t) &= \kappa_0 \left[x_1(t) - x_0(t)\right] \\ \dot{x}_1(t) &= v_1(t), \\ M_1\dot{v}_1(t) &= \kappa_1 \left[x_2(t) - x_1(t)\right] - \kappa_0 \left[x_1(t) - x_0(t)\right], \\ &\vdots \end{aligned} \tag{2.108}$$

where $\dot{f}(t)$ represents df/dt. This infinite set of equations can be written in Hamiltonian form and describes a system that is reversible and conserves energy. At low frequencies, however, this system can act like an irreversibly damped mass.

With the set of suitably normalized variables

$$\begin{aligned} \alpha_0(t) &= v_0(t), & \alpha_1(t) &= i\sqrt{\frac{\kappa_0}{M_0}}\left(x_1 - x_0\right), \\ \alpha_2(t) &= -\sqrt{\frac{M_1}{M_0}}v_1(t), & \alpha_3(t) &= -i\sqrt{\frac{\kappa_1}{M_0}}\left(x_2 - x_1\right), \\ &\vdots & &\vdots \\ \alpha_{2j}(t) &= (-1)^j\sqrt{\frac{M_j}{M_0}}v_j(t), & \alpha_{2j+1}(t) &= i(-1)^j\sqrt{\frac{\kappa_j}{M_0}}\left(x_{j+1} - x_j\right), \end{aligned} \tag{2.109}$$

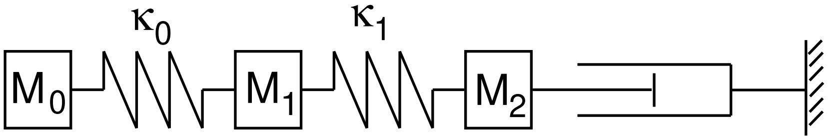

Figure 2.10: The $q = 1$ closure from the stochastic oscillator problem corresponds to adding a damping force proportional to the velocity of the last mass. This picture represents the $[5, 1]$ closure by attaching a viscous damper to the last mass.

the Laplace transform of the mass–spring system can be expressed in matrix form

$$i \begin{bmatrix} -\omega & \sqrt{\frac{\kappa_0}{M_0}} & 0 & 0 & 0 & \dots \\ \sqrt{\frac{\kappa_0}{M_0}} & -\omega & \sqrt{\frac{\kappa_0}{M_1}} & 0 & 0 & \dots \\ 0 & \sqrt{\frac{\kappa_0}{M_1}} & -\omega & \sqrt{\frac{\kappa_1}{M_1}} & 0 & \dots \\ 0 & 0 & \sqrt{\frac{\kappa_1}{M_1}} & -\omega & \sqrt{\frac{\kappa_1}{M_2}} & \dots \\ 0 & 0 & 0 & \sqrt{\frac{\kappa_1}{M_2}} & -\omega & \dots \\ \vdots & \vdots & \vdots & \vdots & \vdots & \ddots \end{bmatrix} \begin{bmatrix} \alpha_0(\omega) \\ \alpha_1(\omega) \\ \alpha_2(\omega) \\ \alpha_3(\omega) \\ \alpha_4(\omega) \\ \vdots \end{bmatrix} = \begin{bmatrix} \alpha_0(t)|_{t=0} \\ \alpha_1(t)|_{t=0} \\ \alpha_2(t)|_{t=0} \\ \alpha_3(t)|_{t=0} \\ \alpha_4(t)|_{t=0} \\ \vdots \end{bmatrix}. \tag{2.110}$$

This system is similar in form to the general linear system of orthogonal-polynomial moments, Eq. (2.80). There can be a direct correlation for a choice of spring constants and masses that correspond to the recursion coefficients of the orthogonal polynomials. For example, taking $\kappa_j = (2j + 1)M_j$ and $M_j = (2j)!/4^j(j!)^2$, a series of increasingly stiffer springs and smaller masses ($M_j \sim 1/\sqrt{\pi j}$ as $j \to \infty$), gives a system of equations corresponding precisely to the Hermite moment case.

The mass–spring system provides a physical picture of the moment coupling problem. Typically one considers initial distributions that correspond to low-order moments. In the mass–spring system, such initial conditions correspond to perturbations in the left-most masses and springs. As time evolves, the distribution of $y(t)$ in the stochastic oscillator goes to finer scales in b and is therefore represented by higher-order orthogonal polynomials, which 'wiggle' more. In the mass–spring system, the initial perturbation travels as a wave to the right to masses that represent higher-order polynomials. Truncation at an odd term $[\alpha_{2n+1}(t) = 0]$ in the mass–spring system corresponds physically to cutting the nth spring and truncation at an even term $[\alpha_{2n}(t) = 0]$ corresponds to stapling the nth mass to a fixed point in space. In the truncated system, therefore, waves will reflect off the rightmost boundary and return to the low moments, unlike the semi-infinite system where waves are free to carry their energy off to infinity.

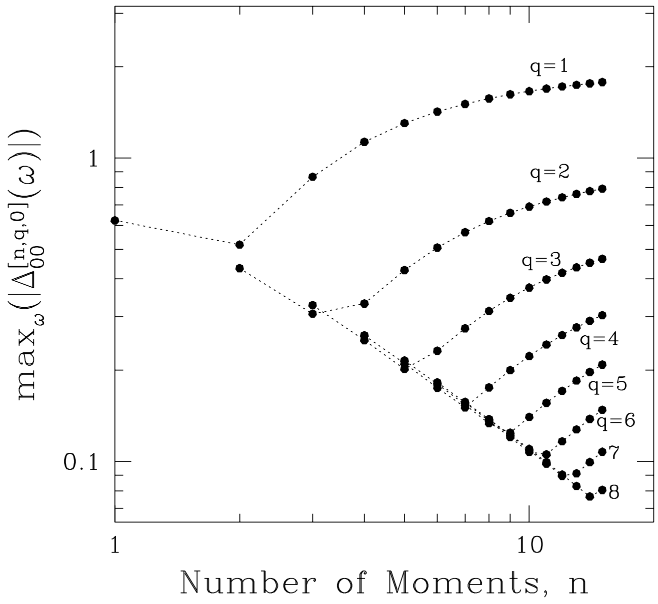

Figure 2.11: The maximum absolute error between the approximate response function and the exact response along the real axis for various two-point closures $[n, q, 0]$ for the Mass–Spring distribution is plotted against the number of moments n in the approximate system. Dotted lines connect the closures for a given q, the number of times the response function is matched in the $\omega \to 0$ limit. For fixed q the approximation improves with increasing number of moments n until $n \sim 2q$, at which point the error increases with increasing n.

The $q = 1$ closure for an odd moment $\alpha_{2n+1}(t) = -iC\alpha_{2n}(t)$ has the physical interpretation of cutting the nth spring and adding a damping force proportional to the velocity on the nth mass. The guarantee of Result 5 that solutions using the $q = 1$ closure are exponentially damped in time has a simple physical interpretation here, since the system conserves energy except for the damping term, which only removes energy from the system. Selecting the size of the damping term by matching in the $\omega \to 0$ limit is analogous to impedance matching at the end of an electrical cable. The chain of springs is a reactive system that is coupled to a dissipative element chosen to minimize the reflection of energy.

The Uniform Mass–Spring System

Consider now the case with uniform spring constants $\kappa_j = \kappa$ and masses $M_j = M$. The off-diagonal elements in the matrix system, Eq. (2.110), are then all 1. This form of the system corresponds to the recurrence relation for the polynomials $U_n(b/2)$ that

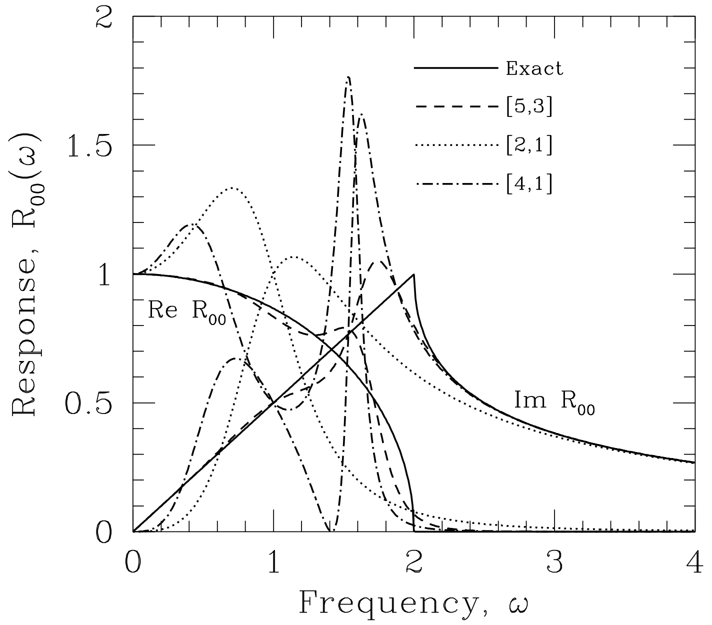

Figure 2.12: The exact response function $\mathsf{R}_{00}(\omega)$ (solid lines) for the uniform mass–spring system and three of the two-point approximation closure response functions (dashed lines) corresponding to $[n=5,q=3]$, $[n=2,q=1]$ and $[n=4,q=1]$.

are orthogonal with respect to the weight function

$$w_s(b) = \begin{cases} \dfrac{1}{\pi}\sqrt{1-(b/2)^2} & (|b|<2), \\ 0 & (|b| \geq 2), \end{cases} \tag{2.111}$$

which is plotted against a Gaussian in Fig. 2.4. This system provides an interesting test of the two-point approximation closure since the exact response to an initial velocity perturbation in the first mass,

$$\mathsf{R}_{00}(\omega) = v_0(\omega)/\left. |v_0(t)|\right|_{t=0} = \sqrt{1-(\omega/2)^2} + i\omega/2, \tag{2.112}$$

has two square-root singularities. [The square root is taken so that $\mathsf{R}_{00}(0) = 1$ and by analytic continuation above the two cuts at -2 and 2 in the complex plane. At large ω, the square-root term is imaginary and cancels the linear term to leading order so that $\mathsf{R}_{00}(\omega) \sim i/\omega$.] Toroidal fluid closures must model response functions that have square-root singularities (Beer and Hammett 1996).

Again the exact response is symmetric, so the q low-frequency conditions are computed by matching in the $\omega \to 0$ limit. The maximum error along the real axis

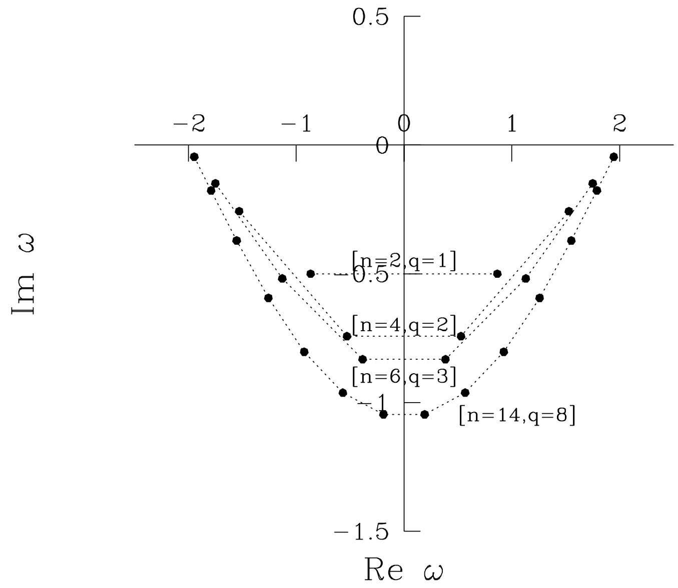

Figure 2.13: The locations in the complex plane of the poles of the approximate response functions for the mass–spring system are shown for several closures where the best q has been chosen. With increasing numbers of moments the poles move away from the real axis, with the exception of the poles at the end, which move towards the points of square-root singularity of the exact response function.

for the approximate responses is plotted in Fig. 2.11 against the number of moments n. Note the markedly different behavior in this case. With fixed q, the number of times the response is matched in the $\omega \to 0$ limit, the response functions *do not converge* with increasing numbers of moments n. For a given q, there appears to be an optimal number of moments $n \sim 2q$, beyond which the addition of extra moment equations degrades the approximation. Another way of interpreting this graph is to say that for a fixed number of moment equations n, convergence improves with increasing q until $q \sim n/2$, at which point matching additional times in the $\omega \to 0$ limits does not improve or degrade the convergence. The error does seem to scale as n^{-1}, however, for a sequence of closures such that $q > n/2$, so there can be convergence of the linear theory.

Three of the approximate responses are plotted in Fig. 2.12 along with the exact response for this system. The convergence behavior appears to be dominated by the square-root singularity at $\omega = 2$ (and $\omega = -2$). The case $[n = 4, q = 1]$ illustrates what goes wrong for $q < n/2$. The asymptotic behavior of the approximate response penetrates past the square-root singularity and gives large errors at lower ω. Matching sufficiently often in the $\omega \to 0$ limit gives more reasonable results as is demonstrated by the $[n = 5, q = 3]$ closure. The square-root singularity prevents the superb convergence obtained in the Gaussian case, however.

The poles of the response function are plotted in Fig. 2.13 for a sequence of 'optimal' closures where $n \sim 2q$. With increasing numbers of moments, there are some poles that move away from the real axis. Some of the additional poles move towards the two square-root singularities at $\omega = \pm 2$. It is reasonable to expect that convergence to response functions with such singularities will require that the approximate response function has poles near the singularities to model the non-analytic behavior there. The series of poles for a given closure can be viewed as an attempt to model the branch cuts leaving the singularities.

2.8 Summary

The issue of obtaining closures for equations evolving moments of the stochastic oscillator problem was considered here. This problem is easily solved exactly and moments exhibit *phase-mixing* decay. Simple truncation of the moment hierarchy leads to unphysical behavior as $t \to \infty$, the moments either increasing without bound (the Taylor-series approximation) or oscillating forever (for the cumulant-discard approach). The random-coupling model is a simple nonlinear closure used in fluid turbulence theories that yields decaying solutions.

A general linear closure has been introduced here, based on the Landau-fluid approach of Hammett and Perkins (1990) to obtaining fluid moment closures for collisionless plasmas. The n closure coefficients for the n-moment system are computed using conditions obtained by matching the response function for the closed moment system to the exact response function q times in the $\omega \to 0$ limit and $n - q$ times in the $\omega \to \infty$ limit. Results concerning the form of this closure are easily expressed for closures written in terms of polynomial moments where the polynomials are orthogonal with respect to the underlying distribution. A given closure for n moments is shown to match the linear response for background distributions that can be written as a polynomial of order $n - q$ in the frequency b multiplied by the given background distribution.

There is strong numerical evidence that the linear response of the closed moment system converges to the exact response for any choice of closure with increasing numbers of moments n, as long as there is some dissipation in the closure for the highest moment and the underlying distribution function is sufficiently smooth (i.e., can be represented as a Gaussian times a few low order Hermite polynomials). Convergence can be accelerated with a judicious choice of the closure dissipation, and is faster if q scales with n. However, if the underlying distribution function contains small scale features or sharp discontinuities (so its expansion in terms of Hermite polynomials requires high order polynomials), then convergence may be very slow, and a very large number of moments would be required. In some examples with sharp features in the distribution function, there was no convergence with n unless q also increased proportional to n. The poles of the approximate response functions were found to lie in the lower-half complex plane for a large number of choices of n and q.

Convergence of the response function of the closed moment system can become somewhat complicated for some underlying distributions. This approach to computing closure coefficients was applied to the semi-infinite uniform mass–spring system, which has a response function with two square-root type singularities. The response functions had well behaved poles for all the cases considered, but it appears that merely taking $n \to \infty$ does not yield converging response functions unless increasing values of q are taken as well. (The choice $q \sim n/2$ appears to work well.) The convergence properties of the semi-infinite mass–spring system indicate that care must be taken in any attempt to generalize toroidal gyrofluid equations to larger numbers of moments. The linear kinetic response function in toroidal geometry has a square-root type singularity that must be matched by the response of toroidal gyrofluid equations (Beer and Hammett 1996). In the toroidal case, the square-root branch cut is at $\omega = 0$ and so the usual method of matching the Taylor series expansion of the response at $\omega = 0$ doesn't work. Thus, Beer and Hammett (1996) chose closure coefficients to minimize the total error over a range of ω instead of only at $\omega = 0$.

2.9 Implication for Statistical Closures

The stochastic oscillator problem itself is merely a model problem. In the end, the choice of closure used for a particular problem will involve many considerations. The approach presented here is a natural one for application to fluid moment closures in plasma physics where the underlying distribution is known and numerical implementation greatly favors the lack of time history in the closure. However, when deriving closures for statistical moments in turbulence theories, one does not know ahead of time what the underlying distribution is.

In general, little is known about the convergence properties of statistical moment hierarchies in the study of turbulence. The linear results presented here are at least tangentially significant to the more general problem of nonlinear closures. The $q = 1$ closures for example, introduce a damping term in the highest moment only. The linear response for the $q = 1$ closures converges slowly for the Gaussian case and does not converge at all for the Mass–Spring problem with increasing numbers of moments even though information about the exact response is used in deriving the closure coefficient. For statistical closures in turbulence, where information about the exact nonlinear response is unavailable, one might expect even weaker convergence properties for similar closures that introduce only simple damping terms.

Chapter 3

Landau Fluid Equations

The Navier–Stokes equations for neutral fluids are highly effective at describing the flows of many gases and liquids under typical conditions. The short mean free path and high collision rate in most cases ensures that, from a macroscopic point of view, the particle distributions are very nearly Maxwellian, and the departures are well modeled by simple viscosity terms. The very low collision rate in tokamak plasmas leads to a breakdown of the standard Chapman–Enskog method for deriving the plasma fluid equations of Braginskii (1965). Plasma waves, especially those driven by temperature-gradient instabilities, can experience significant collisionless damping due to Landau damping. The approach to deriving plasma fluid equation by Hammett and Perkins (1990) was to derive the fluid closures by matching the linear kinetic response of a collisionless fluid. The resulting equations conserve particles, momentum and energy and at the same time accurately model the dissipation of electrostatic waves due to Landau damping.

The relation between fluid moment closures and the statistical moment closures considered in the previous chapter is illustrated by considering the one-dimensional Vlasov equation. With an appropriate change of variables, the linearized Vlasov equation is equivalent to the stochastic oscillator problem. The background particle distribution in the Vlasov theory takes the place of the frequency distribution for the oscillator problem. The results concerning general linear closures of stochastic oscillator moments carry over to linear closures of fluid moments.

Orthogonal-polynomial fluid moments can be defined analogously to the orthogonal-polynomial statistical moments. The natural background particle distribution is Maxwellian, so Hermite fluid moments form the natural basis for studying the Vlasov equation. The Hermite fluid moments are equivalent, in fact, to the coefficients of the Hermite series expansion of the Vlasov equation that has traditionally been used for one-dimensional plasma simulation (Armstrong et al. 1970). The connection between Hermite moments and cumulants is demonstrated for fluid moments as well.

Several insights can be gained from the transformations among coefficients in the series expansion of the Vlasov equation, fluid moments of the Vlasov equation, and statistical moments of the stochastic oscillator. Observations concerning the limitations of truncated series expansions have implications for fluid moment systems that evolve a finite number of moments. On the other hand, the general dissipative closure derived for fluid moments may be useful in applications to kinetic series solutions of the Vlasov equation.

Deriving closures from linear theory does not fully determine the nonlinear form of the closure. Closures with significantly different nonlinear features can be linearly identical. Two such closures are introduced in this chapter. The optimal nonlinear form of fluid closures is an interesting question that is only starting to be addressed.

3.1 Fluid Moments

Consider the one-dimensional kinetic theory of a distribution of particles at location z with velocity v given by $f(z,v,t)$. The standard fluid moments, number density n, mean velocity u, pressure p, heat flux q, and general higher moments r_n are defined by

$$\begin{aligned} n(z) &= \int_{-\infty}^{\infty} f(z,v)\,dv, & n(z)u(z) &= \int_{-\infty}^{\infty} v f(z,v)\,dv, \\ p(z) &= m\int_{-\infty}^{\infty} [v-u(z)]^2 f(z,v)\,dv, & q(z) &= m\int_{-\infty}^{\infty} [v-u(z)]^3 f(z,v)\,dv, \\ r(z) &= m\int_{-\infty}^{\infty} [v-u(z)]^4 f(z,v)\,dv, & &\dots \\ r_n(z) &= m\int_{-\infty}^{\infty} [v-u(z)]^{4+n} f(z,v)\,dv, \end{aligned} \tag{3.1}$$

where m is the particle mass. These moments are nonlinear functions of the particle distribution as a result of their definition with respect to the mean velocity $u(z)$. To connect plasma kinetic problems with the stochastic oscillator moments, the v^n moments are defined by

$$M_n(z) = \int_{-\infty}^{\infty} v^n f(z,v)\,dv. \tag{3.2}$$

The first n moments in either formulation contain exactly the same information. There is an algebraic transformation from either set of moments to the other given by

$$
\begin{aligned}
n(z) &= M_0(z), \\
u(z) &= \frac{M_1(z)}{M_0(z)}, \\
p(z) &= m\left[M_2(z) - \frac{M_1(z)^2}{M_0(z)}\right], \\
q(z) &= m\left[M_3(z) - 3\frac{M_2(z)M_1(z)}{M_0(z)} + 2\frac{M_1(z)^3}{M_0(z)^2}\right], \\
r(z) &= m\left[M_4(z) - 4\frac{M_3(z)M_1(z)}{M_0(z)} + 6\frac{M_2(z)M_1(z)^2}{M_0(z)^2} - 3\frac{M_1(z)^4}{M_0(z)^3}\right], \\
&\vdots
\end{aligned}
\tag{3.3}
$$

which translates v^n moments into fluid moments and by

$$
\begin{aligned}
M_0(z) &= n(z), \\
M_1(z) &= n(z)u(z), \\
M_2(z) &= \frac{p(z)}{m} + n(z)u(z)^2, \\
M_3(z) &= \frac{q(z) + 3u(z)p(z)}{m} + n(z)u(z)^3, \\
M_4(z) &= \frac{r(z) + 4u(z)q(z) + 6u(z)^2p(z)}{m} + n(z)u(z)^4, \\
&\vdots
\end{aligned}
\tag{3.4}
$$

which translates fluid moments into v^n moments. These transformations are nonlinear. A closure that is linear in fluid moments can therefore behave differently from a closure that is linear in v^n moments even if they are linearly equivalent. This difficulty is discussed in Section 3.4.

3.2 Vlasov Equation

The dynamics of particle motion along straight magnetic field lines is given by the one-dimensional kinetic equation,

$$
\left[\frac{\partial}{\partial t} + v\frac{\partial}{\partial z} - \frac{q}{m}\frac{\partial\phi(z,t)}{\partial z}\frac{\partial}{\partial v}\right] f(z,v,t) = \nu\frac{\partial}{\partial v}\left(v + {v_t}^2\frac{\partial}{\partial v}\right) f(z,v,t).
\tag{3.5}
$$

The model collision operator of Lenard and Bernstein (1958) is included, which models collisions with a thermalizing background with collision frequency ν and thermal velocity v_t. In the limit of small potential perturbations, $q\phi \ll m{v_t}^2$, the collision term will dominate, so to lowest order the particles have a Maxwellian distribution,

$$f_0(v) = \frac{n_0}{\sqrt{2\pi {v_t}^2}} \exp(-v^2/2{v_t}^2). \tag{3.6}$$

The potential ϕ is related linearly to the distribution $f(z, v, t)$ through Poisson's equation, so the resulting system is quadratically nonlinear.

Taking fluid moments of the Vlasov equation (3.5) yields a hierarchy of fluid moment equations,

$$\frac{\partial n}{\partial t} + \frac{\partial}{\partial z}(un) = 0, \tag{3.7}$$

$$\frac{\partial u}{\partial t} + u\frac{\partial u}{\partial z} + \frac{1}{mn}\frac{\partial p}{\partial z} + \nu u = -\frac{q}{m}n\frac{\partial \phi}{\partial z}, \tag{3.8}$$

$$\frac{\partial p}{\partial t} + u\frac{\partial p}{\partial z} + 3p\frac{\partial u}{\partial z} + \frac{\partial q}{\partial z} + \nu\left[p - m(u^2 + {v_t}^2)n\right] = 0, \tag{3.9}$$

$$\vdots$$

These equations are nonlinear as a result of the moment definition with respect to the mean velocity. The v^n moment equations,

$$\begin{aligned}
&\frac{\partial M_0}{\partial t} + \frac{\partial M_1}{\partial z} = 0, \\
&\frac{\partial M_1}{\partial t} + \frac{\partial M_2}{\partial z} + \nu M_1 = -\frac{qM_0}{m}\frac{\partial \phi}{\partial z}, \\
&\quad\vdots \\
&\frac{\partial M_j}{\partial t} + \frac{\partial M_{j+1}}{\partial z} + \nu j\left[M_j - (j-1)M_{j-2}\right] = -\frac{eM_{j-1}}{m}\frac{\partial \phi}{\partial z},
\end{aligned} \tag{3.10}$$

are linear equations and slightly simpler than the fluid moment equations. One very nice feature of the fluid moment equations, however, is that the potential only appears in one equation, the one for the velocity u, in contrast to v^n moment equations where it enters in every equation.

In Fourier space, the term $v\partial/\partial z\, f(z, v, t)$ becomes $ikvf(k, v, t)$, which is analogous to the $iby(t)$ in the stochastic oscillator. Fluid moments can therefore experience phase-mixing decay, since the frequencies kv are continuously distributed. Simple truncation schemes applied to either of these moment hierarchies leads to unphysical behavior. The truncation $M_n(z, t) = 0$ leads to a solution for the lower moments that is essentially a truncation of the Taylor series representing the true solution, and therefore blows up as $t \to \infty$. The fluid moment truncation $q(z, t) = 0$, on the other hand, leads to a set of equations that conserves the total density, momentum and energy and therefore has a solution that does not diverge at large times. Still, the system fails to exhibit phase-mixing decay.

	Stochastic Oscillator	Vlasov Equation
frequency	b	$\|k\|v$
moments	$g_n(t) = \langle b^n y(t) \rangle$	$M_n(k,t) = \int_{-\infty}^{\infty} v^n f(k,v,t)\,dv$
orthogonal functions	$P_n(b)w(b)$	$\frac{1}{\sqrt{2^n n!}} H_n(v/\sqrt{2}v_t) \frac{e^{-v^2/2v_t{}^2}}{\sqrt{2\pi v_t{}^2}}$
frequency distribution	$\rho(b)$	$\frac{ike}{m}\frac{\partial}{\partial v} f_0(v)$
oscillator variable	$y(t)\rho(b)$	$Y(k,v,t)$
Response	$\mathsf{R}_{01}(\omega)$	$R(\zeta)$

Table 3.1: Equivalent concepts for the stochastic oscillator problem and the linearized Vlasov equation.

Hammett and Perkins (1990) obtained a dissipative closure model by matching the response of the closed moment system with the linear response to a small potential assuming the near-equilibrium density, $f(z,v,t) = f_0(v) + \tilde{f}(z,v,t)$. The Fourier transformed, linearized Vlasov equation in the collisionless limit $\nu = 0$ is just

$$\left(\frac{\partial}{\partial t} + ikv\right) \tilde{f}(k,v,t) = \frac{q}{m} ik\phi(k,t) \frac{\partial}{\partial v} f_0(v). \tag{3.11}$$

The response for this linear problem with the background Maxwellian defined in Eq. (3.6) can be written simply as

$$\tilde{n}(k,\omega) = -\frac{qn_0}{mv_t{}^2} \phi(k,\omega) R(\zeta), \tag{3.12}$$

where the Laplace transform $t \to \omega$ has been taken, the response function is given by $R(\zeta) = 1 + \zeta Z(\zeta)$, and the normalized frequency

$$\zeta = \frac{\omega}{\sqrt{2}|k|v_t} \tag{3.13}$$

is used.

This system is very similar to the stochastic oscillator equation (2.6). To connect the two problems, note that the solution to the linearized Vlasov equation (3.11) can be written as $\tilde{f}(k,v,t) = \int_{-\infty}^{t} Y(k,v,t-t_1)\phi(k,t_1)\,dt_1$, where the Green's function $Y(k,v,\tau)$ is the solution to

$$\left(\frac{\partial}{\partial t} + ikv\right) Y(k,v,t) = 0, \qquad Y(k,v,0) = \frac{q}{m} ik \frac{\partial}{\partial v} f_0(v). \tag{3.14}$$

This initial-value problem is essentially the stochastic oscillator problem (2.6). The frequency for this system is kv instead of b. The Green's function $Y(k,v,t)$ corresponds to $y(t)\rho(b)$, the oscillator variable weighted by the frequency PDF. The driving term $(q/m)\,ik\phi\,(\partial/\partial v)\,f_0(v)$ in the Vlasov equation corresponds to the distribution of frequencies of the stochastic oscillator. For a Maxwellian, $(\partial/\partial v)f_0(v) \propto v f_0(v)$, so the response function $R(\zeta)$ corresponds to the $\mathsf{R}_{01}(\omega)$ response of the stochastic oscillator with a Gaussian distribution of frequencies. The correspondence between the two problems is summarized in Table 3.1.

Note that for the stochastic oscillator problem the frequency variable b is the same variable that appears in the distribution and the orthogonal polynomial expansion, whereas the frequency variable kv in the Vlasov equation is different from the combination v/v_t that appears in the distribution and the orthogonal polynomials. This difference could be eliminated by transforming the time variable in the Vlasov equation by $\tau = kv_t t$, which results in the now dimensionless frequency v/v_t. This transformation does not quite work, however, since the phase-mixing decay should occur in the limit $t \to -\infty$, and negative wave numbers k effectively reverse the direction of time with this transformation. The transformation of variables

$$\tau = |k| v_t t, \qquad b = \frac{k}{|k|}\frac{v}{v_t} \tag{3.15}$$

preserves the direction of time. The transformed Green's function equation for the linearized Vlasov equation with background Maxwellian becomes

$$\left(\frac{\partial}{\partial\tau} + ib\right) Y(k,b,\tau) = 0, \qquad Y(k,b,0) = \frac{q}{m{v_t}^2} i\phi(k,\tau)\frac{n_0}{\sqrt{2\pi {v_t}^2}}\frac{\partial}{\partial b}\exp(-b^2/2). \tag{3.16}$$

The solution to this equation is precisely the solution of the stochastic oscillator problem with underlying distribution $\rho(b) \propto b\exp(-b^2/2)$. (Strictly speaking this PDF is not a probability distribution, but the linear response theory developed in the preceding chapter does not depend on the positivity of the underlying distribution.) The transformation from the stochastic oscillator problem to the linearized Vlasov equation is summarized in Table 3.1.

With the transformation (3.15) it is possible to convert the stochastic oscillator closures to fluid moment closures. The linear frequency in the Vlasov equation is given by the combination kv, so an appropriate dissipative closure for fluid moments should introduce damping on the order of $|k|v_t$, which is a measure of the spread of frequencies. Landau-fluid closures involve operators in wave-number space that are proportional to the absolute value of the wave number (Hammett and Perkins 1990). The $|k|$ operator arises because the quantity $k/|k|$ enters the transformation of closures from the stochastic oscillator problem to fluid moments. The stochastic oscillator moments are polynomials in $b = kv/|k|v_t$, whereas the fluid moments involve polynomials in v.

3.3 Hermite Moments

Before relating the stochastic oscillator moment closures to fluid moment closures, the definition of orthogonal-polynomial moments for the Vlasov equation will be considered. Early studies of the Vlasov equation (Weissglas 1962; Engelmann et al. 1963; Armstrong 1967; Grant and Feix 1967; Armstrong et al. 1970) used a series expansion about the background Maxwellian in terms of Hermite polynomials in velocity,

$$f(z,v,t) = \frac{1}{\sqrt{2\pi {v_t}^2}} \sum_{n=0}^{\infty} a_n(z,t) \frac{1}{\sqrt{2^n n!}} H_n(v/\sqrt{2}v_t) e^{-v^2/2{v_t}^2}. \tag{3.17}$$

The thermal velocity v_t is taken to be a constant for now. This series expansion represents the background distribution $f_0(v)$ with one nonzero term, $a_0 = n_0$, and therefore works well for problems with near-Maxwellian distributions.

Substituting this series expansion into the Vlasov equation (3.5) yields evolution equations for the coefficients,

$$\begin{aligned}
&\frac{\partial a_0}{\partial t} + v_t \frac{\partial a_1}{\partial z} = 0, \\
&\frac{\partial a_1}{\partial t} + v_t \left(\frac{\partial a_0}{\partial z} + \sqrt{2} \frac{\partial a_2}{\partial z} \right) + \nu a_1 = -\frac{q a_0}{v_t m} \frac{\partial \phi}{\partial z}, \\
&\quad \vdots \\
&\frac{\partial a_j}{\partial t} + v_t \left(\sqrt{j} \frac{\partial a_{j-1}}{\partial z} + \sqrt{j+1} \frac{\partial a_{j+1}}{\partial z} \right) + \nu j a_j = -\frac{q \sqrt{j} a_{j-1}}{v_t m} \frac{\partial \phi}{\partial z}.
\end{aligned} \tag{3.18}$$

This 'kinetic' series solution of the Vlasov equation is in fact equivalent to the moment approach. Using the orthogonality of the Hermite polynomials, the series coefficients in Eq. (3.17) can be expressed as *Hermite moments*,

$$a_n(z,t) = \int_{-\infty}^{\infty} \frac{1}{\sqrt{2^n n!}} H_n(v/\sqrt{2}v_t) f(z,v,t)\, dv. \tag{3.19}$$

The first n Hermite moments and the first n fluid moments contain exactly the same information, since the polynomials $\{1, v, (v-u), \ldots, (v-u)^n\}$ span the same space as $\{H_0(v), H_1(v), \ldots, H_n(v)\}$. Each Hermite moment can be expressed in terms of fluid moments of equal or lower order by

$$
\begin{aligned}
a_0(z) &= n(z), \\
a_1(z) &= \frac{n(z)u(z)}{v_t}, \\
a_2(z) &= \frac{mu(z)^2 n(z) + \left[p(z) - m{v_t}^2\right] n(z)}{\sqrt{2} m{v_t}^2}, \\
a_3(z) &= \frac{q(z) + mu(z)^3 n(z) + 3u(z)\left[p(z) - m{v_t}^2 n(z)\right]}{\sqrt{6} m{v_t}^3}, \\
&\vdots
\end{aligned}
\tag{3.20}
$$

and each fluid moment can be expressed in terms of Hermite moments of equal or lower order by

$$
\begin{aligned}
n(z) &= a_0(z), \\
u(z) &= v_t \frac{a_1(z)}{a_0(z)}, \\
p(z) &= m{v_t}^2 \left[\sqrt{2} a_2(z) + a_0(z) - \frac{a_1(z)^2}{a_0(z)}\right], \\
q(z) &= m{v_t}^3 \left[\sqrt{6} a_3(z) - 3\frac{\sqrt{2} a_2(z) a_1(z)}{a_0(z)} + 2\frac{a_1(z)^3}{a_0(z)^2}\right], \\
&\vdots
\end{aligned}
\tag{3.21}
$$

Thus, there is a nonlinear transformation from fluid moments to v^n moments and from fluid moments to Hermite moments. The transformation from v^n moments to Hermite moments is just the linear transformation to orthogonal-polynomial moments discussed in Section 2.5.1. The theory from the previous chapter gives a systematic approach to developing linear closures that yield good approximations to the linear responses. As yet there is no theory to specify the nonlinear form of closures, leaving ambiguity in the choice of closure. Note that a linear closure in fluid moments translates to a nonlinear closure for Hermite moments and vice versa.

3.4 Nonlinear Aspect of Moment Closures

To demonstrate some of the nonlinear features of closures, two closures with the same linear behavior are presented here. Consider the heat-flux closure

$$
q(z) = -i\frac{2\sqrt{2}}{\sqrt{\pi}} v_t \frac{k}{|k|}\left[p(z) - m{v_t}^2 n(z)\right]
\tag{3.22}
$$

of Hammett and Perkins (1990), where the $k/|k|$ operator is understood to represent the transformation to k space, multiplication by $k/|k|$, and transformation back to z space. Direct translation of the third Hermite moment closure

$$a_3(k,t) = -i\frac{k}{|k|}\frac{2\sqrt{2}}{\sqrt{3\pi}}a_2(k,t) \tag{3.23}$$

to fluid moments using Eq. (3.20) yields a significantly more complicated expression,

$$\begin{aligned} q(z) =& 3u(z)\left[m{v_t}^2 n(z) - p(z)\right] - mu(z)^3 n(z) \\ &- i\frac{2\sqrt{2}}{\sqrt{\pi}}v_t\frac{k}{|k|}\left\{p(z) + mn(z)\left[u(z)^2 - {v_t}^2\right]\right\}. \end{aligned} \tag{3.24}$$

Linear equivalence of these closures is demonstrated by splitting the moments into equilibrium and fluctuating components; for example $n(z) = n_0 + \tilde{n}(z)$ where $n_0 = \int_{-\infty}^{\infty} f_0(v)\,dv$ and $\tilde{n}(z) = \int_{-\infty}^{\infty} \tilde{f}(z,v)\,dv$. The odd equilibrium moments are zero ($u_0 = 0, q_0 = 0, \ldots$) and the even equilibrium moments can be expressed in terms of powers of v_t ($p_0 = m{v_t}^2 n_0, r_0 = 3m{v_t}^4 n_0, \ldots$). Assuming the fluctuating components are small, expanding both the Hammett–Perkins closure (3.22) and the transformed Hermite moment closure (3.24) give the same result to first order,

$$\tilde{q}(z) \sim -i\frac{2\sqrt{2}}{\sqrt{\pi}}v_t\frac{k}{|k|}\left[\tilde{p}(z) - m{v_t}^2\tilde{n}(z)\right], \tag{3.25}$$

but have different second-order terms. There is clearly great freedom in choosing closures that have the same linear behavior. For example, the linear combination $p(z) - m{v_t}^2 n(z)$, could be replaced by $n_0[T(z) - T_0(z)]$ where the temperature $T(z) = p(z)/n(z)$ is a nonlinear quantity that gives the same behavior to first order. Since $u_0 = 0$, any arbitrary expression multiplied by $u(z)^2$ may be added to the closure without affecting the linear behavior.

Note as well that both closures contain equilibrium constants, v_t and n_0. In simulations that assume a fixed background gradient, these parameters are constants that are input to the simulation. Extending closures to cases with a background equilibrium that vary in space or time may be nontrivial. In turbulence, the average density and energy along a field line vary slowly compared to the fluctuations themselves, so averaging the density $n(z)$ and the local thermal velocity $v_t(z) = \sqrt{p(z)/mn(z)}$ provides reasonable estimates for n_0 and v_t. The derivation of closure coefficients, however, assumes that these quantities are constant in time.

These questions have yet to be addressed satisfactorily. The following chapter presents a model nonlinear problem, the plasma echo, that can be accurately modeled provided enough moments are kept. Additional moments serve to approximate finer scales of the distribution function. It may be that the precise nonlinear form of the closure is irrelevant provided enough moments are kept. (Accurate simulations require a good linear closure, however, as is clear from the unphysical results obtained with the simplest moment discard approaches.)

3.5 Cumulants

The standard approach to deriving Landau-fluid closures expresses the fourth-moment closure in terms of the combination

$$\delta r(z) = r(z) - 3\frac{p(z)^2}{mn(z)}. \tag{3.26}$$

The term $3p(z)^2/mn(z)$ is often justified on the grounds that for a Maxwellian distribution, it is exactly equal to $r(z)$. For another point of view, one can examine the linear form of $\delta r(z)$. Formally, let us suppose that

$$f(z,v,t) = f_0(v) + \epsilon\tilde{f}(z,v,t), \tag{3.27}$$

where $f_0(v)$ is the background Maxwellian of Eq. (3.6) and ϵ is a formal ordering parameter assumed to be small. With this expansion we find that

$$\begin{aligned}\delta r(z) &= \epsilon\left[\tilde{r}(z) - 6\frac{p_0}{mn_0}\tilde{p}(z) + 3m{v_t}^4\tilde{n}(z)\right] + \mathcal{O}(\epsilon^2)\\ &= \epsilon m\int_{-\infty}^{\infty}\left(v^4 - 6{v_t}^2v^2 + 3{v_t}^4\right)\tilde{f}(z,v)\,dv + \mathcal{O}(\epsilon^2)\\ &= \epsilon m{v_t}^4\int_{-\infty}^{\infty} H_4(v/\sqrt{2}v_t)\tilde{f}(z,v)\,dv + \mathcal{O}(\epsilon^2).\end{aligned} \tag{3.28}$$

So to first order in the expansion parameter ϵ, we find that $\delta r(z)$ is proportional to the Hermite moment $a_4(z)$. In fact the moments that are typically used to express closures, $\tilde{n}(z)$, $\tilde{u}(z)$, $\tilde{T}(z) = [\tilde{p}(z) - T_0\tilde{n}(z)]/n_0$ and $\tilde{q}(z)$, are all proportional to Hermite moments. The effectiveness of this basis arises from the orthogonality property of the moments.

Cumulant expansions can be used to systematically generate terms such as $\delta r(z)$ that vanish for a Maxwellian and linearly match the Hermite moments. Velocity averages are defined by

$$\langle g(v)\rangle = \frac{\int_{-\infty}^{\infty} g(v)f(z,v)\,dv}{\int_{-\infty}^{\infty} f(z,v)\,dv}, \tag{3.29}$$

and cumulant averages in this case are defined by identifying powers of x in the equation

$$\exp\left(\sum_{n=1}^{\infty}\langle v^n\rangle_c\frac{x^n}{n!}\right) = \langle\exp(vx)\rangle. \tag{3.30}$$

The cumulants can be formally expanded as $\langle v^n\rangle_c = \langle v^n\rangle_c^0 + \epsilon\langle v^n\rangle_c^1 + \cdots$. Upon substituting this expansion in the cumulant definition (3.30) and using the formal expansion of the distribution (3.27) in the equation for the averages (3.29), one finds the expression for the first-order part of the cumulant average,

$$\begin{aligned}\sum_{n=1}^{\infty} \langle v^n \rangle_c^1 \frac{x^n}{n!} &= \frac{1}{n_0}\left[\exp(-{v_t}^2 x^2/2)\int_{-\infty}^{\infty} \exp(xv)\tilde{f}(z,v)\,dv - \int_{-\infty}^{\infty} \tilde{f}(z,v)\,dv\right] \\ &= \frac{1}{n_0}\int_{-\infty}^{\infty} \sum_{n=1}^{\infty} \left(v_t/\sqrt{2}\right)^n H_n(v/\sqrt{2}v_t)\frac{x^n}{n!}\tilde{f}(z,v)\,dv. \end{aligned} \tag{3.31}$$

This result uses the Hermite polynomial generating function (2.25). The cumulant averages $\langle v^n \rangle_c$ are therefore linearly equivalent to multiples of the Hermite moments.

Cumulant averages therefore provide an alternative nonlinear basis of moments with which to form closures that are linearly equivalent to those formed from Hermite moments. The first few cumulant moments are

$$\begin{aligned} \langle v \rangle_c &= u(z), & \left\langle v^2 \right\rangle_c &= \frac{p(z)}{mn(z)}, \\ \left\langle v^3 \right\rangle_c &= \frac{q(z)}{mn(z)}, & \left\langle v^4 \right\rangle_c &= \frac{mn(z)r(z) - 3p(z)^2}{m^2 n(z)^2}. \end{aligned} \tag{3.32}$$

3.6 Summary

Transformations have been presented here that enable several problems involving closures to be identified with one another. The linearized Vlasov equation has been shown to be equivalent to the stochastic oscillator problem. The fluid moment closure problem in this case is therefore equivalent to a statistical moment closure problem. It has also been shown that the fluid moments of the Vlasov equation are equivalent to Hermite polynomial moments, which in turn are equivalent to coefficients in the Hermite series that has traditionally been used in simulations of the Vlasov equation. Fluid moment cumulants are linearly equivalent to Hermite moments. This equivalence is responsible for the nice properties of closures expressed in terms of cumulants.

Note that the transformation from fluid moments to Hermite moments is nonlinear, so linear closures with the same first-order behavior can produce different results at higher order. The correct nonlinear form of fluid moment closures is an issue that has yet to be addressed. In the following chapter, results are presented that indicate that higher-order behavior is more sensitive to the number of fluid moments retained in a model than to the precise form of the closure.

Chapter 4

Nonlinear Tests of One-Dimensional Closures

The linear theory of Landau-fluid equations works very well, and improves with the number of moments used. A relevant question, however, is whether the fluid equations can reproduce second-order nonlinear effects, such as ion Compton scattering. Mattor (1992) has questioned the ability of Landau-fluid equations to reproduce this effect near marginal stability. The analysis of Compton scattering is inherently 3D. However, the essential nature of the approximation of the second-order propagator can be illustrated in the simple exactly solvable one-dimensional problem of electron plasma echoes.

Plasma echoes (Gould et al. 1967) are an effect that can occur in highly collisionless plasmas due to the Hamiltonian nature of flows in phase space. Spatial perturbations that appear to have decayed have in reality become convoluted in phase space and disappeared in an averaged sense only. In some circumstances, additional perturbations can interact with the existing convoluted perturbations to produce a second-order perturbation that unfolds in time to produce a response much later, *the echo*. The simplest possible derivation of an electron plasma echo is presented here. There is an exact kinetic solution for this problem. The problem is solved using a finite moment system with closure and compared to the exact solution. An estimate for the number of moments required to accurately model second-order effects is therefore obtained. Finally the form of the second-order propagator obtained from the moment system is computed to illustrate the nature of the approximation being made.

4.1 Plasma Echoes

Plasma wave echoes (Gould et al. 1967; O'Neil and Gould 1968) are a second-order effect arising in the one-dimensional Vlasov equation. If the plasma is perturbed at a given wavelength, a density perturbation is excited and will die away due to

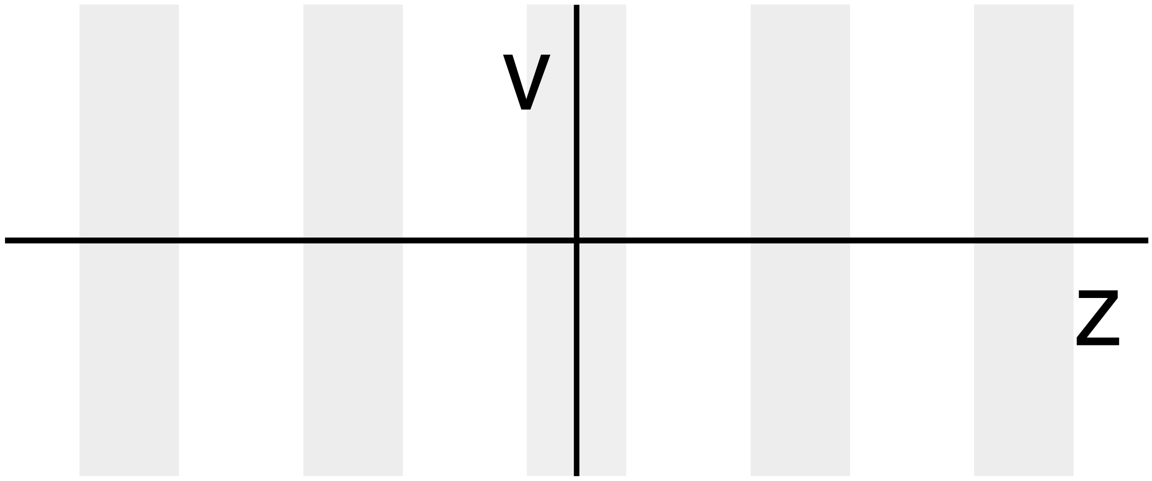

Initial perturbation with $k = 3$.

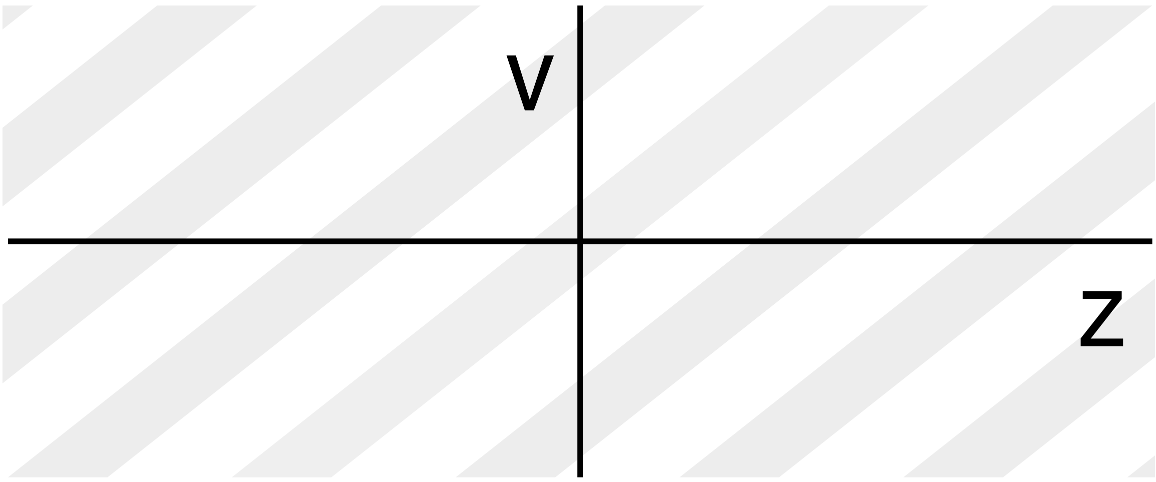

Advected perturbation at time $t = 1$.

Figure 4.1: Illustration of the Plasma Echo. An initial density perturbation is shown in the first picture with spatial structure having wave number $k = 3$. After some time, the perturbation has tilted in phase space, so the perturbation averaged over velocities has decayed.

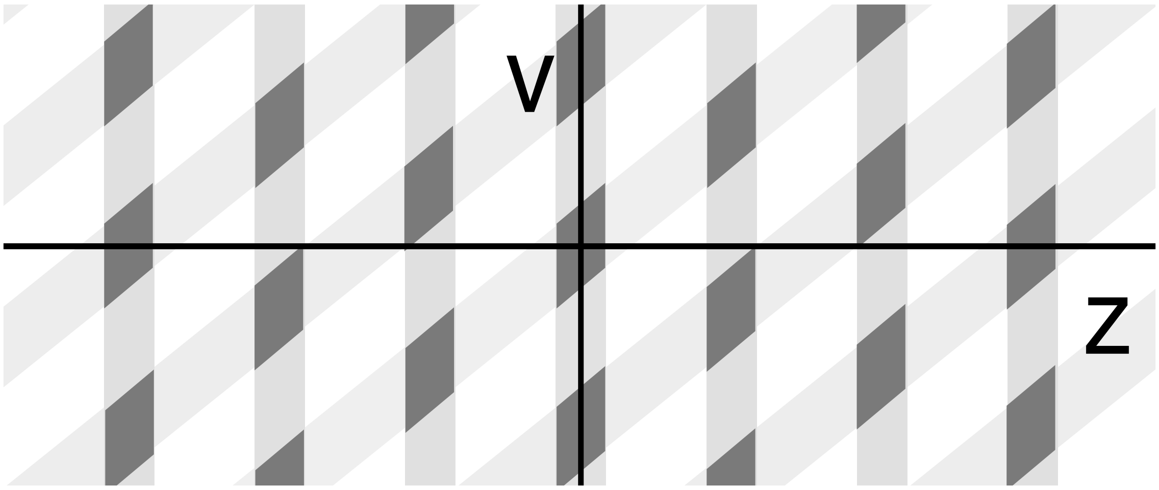

Second perturbation with $k = 2$.

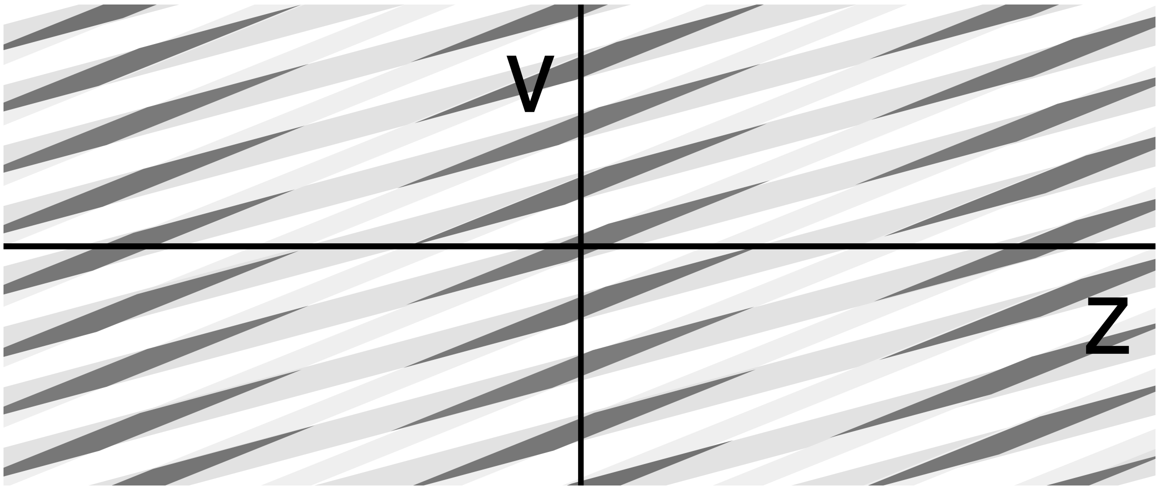

Echo appears at time $t = 3$.

Figure 4.2: Continuation of the plasma echo illustration. A second perturbation with longer wavelength ($k = 2$) is superimposed on the initial perturbation in the first picture. The second-order perturbation is indicated by the dark grey regions. The second picture shows a later time, at which both first-order perturbations have been stretched out in phase space, but the second-order perturbation has reconstituted with a spatial structure with wave number $k = 1$. This reconstituted perturbation at a later time is called *the plasma echo*.

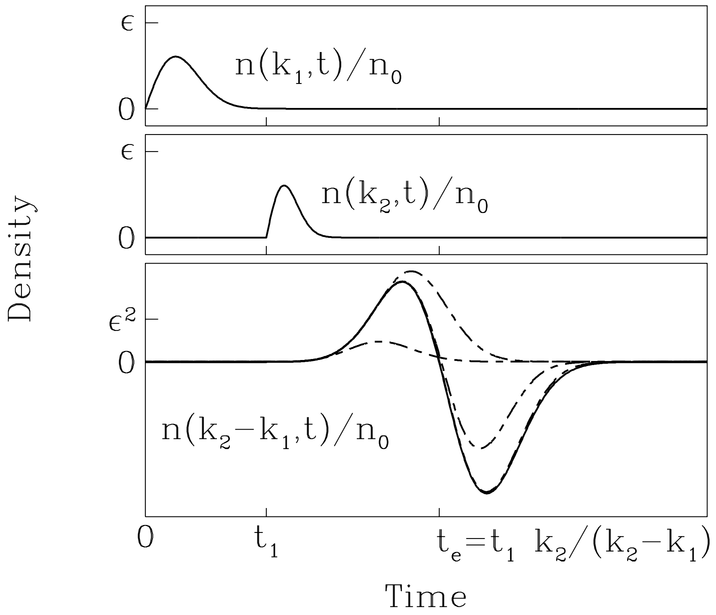

Figure 4.3: The plasma echo response. The density response to two pulses in the potential at wave numbers k_1 and k_2 is plotted here. (For this graph, $\epsilon = 0.01$, $t_1 k_1 v_t = 4$, and $k_2 = 1.7k_1$.) The solid lines denote the exact response for the first-order density components at k_1 and k_2 and the second-order "echo" component at $k_2 - k_1$. The dashed lines indicate the approximate second-order response obtained when 10, 20, 30, and 40 moment equations are used.

Landau damping. The perturbation has not disappeared, however, it has just become convoluted in phase space (phase mixing). If the plasma is then perturbed at a shorter wavelength, a density perturbation will be excited at that wavelength and die away as well. The second perturbation will also interact with the initial perturbation, though, generating a perturbation at the difference wave number that "un-phase-mixes" to appear as a density perturbation at a later time, *the plasma echo*.

Figs. 4.1 and 4.2 present a rough cartoon of the physics of the plasma echo. In Fig. 4.1, an initial perturbation is represented by shaded areas. The streaming of the plasma leads to the usual phase mixing, so the real-space density decays even though the perturbation continues to exist. In Fig. 4.2, a second perturbation is added, which is assumed to interact with the first to produce the second-order contribution indicated by the dark grey regions. At a later time, the second-order contributions line up to produce a spatial density variation at a lower wave number equal to the difference of the two original wave numbers. Note that in the second picture of

Fig. 4.2 the second-order contributions have remained sufficiently localized to produce a perturbation at the low wave number. The criterion for an echo to occur is that the second perturbation occur at a higher wave number than the first. The second-order parts will still line up at a later time if this criterion is not satisfied, but in that case they will have become extremely elongated and produce a small response.

This picture should be only be view as an intuitive guide to the plasma echo, however. In reality, plasmas rarely experience density perturbations of this sort. A more interesting problem, therefore, is to consider the response of the plasma to potential perturbations. The model problem to be considered here is the evolution of a distribution of electrons in one dimension governed by the Vlasov equation (3.5), assuming an externally applied potential of the form

$$\phi(z,t) = -\epsilon_1 \frac{m v_t}{e k_1} \sin(k_1 z)\delta(t-t_1) - \epsilon_2 \frac{m v_t}{e k_2} \sin(k_2 z)\delta(t-t_2), \tag{4.1}$$

and given an initially Maxwellian distribution

$$f(z,v,t=0) = \frac{n_0}{\sqrt{2\pi v_t{}^2}} \exp(-v^2/2v_t{}^2). \tag{4.2}$$

Assuming fixed background ions, and considering the unphysical limit where all of the wavelengths are much shorter than the Debye length, the plasma contribution to the potential may be ignored. Electron fluid equations in this limit are of little physical interest, but this problem contains second-order nonlinearities that can be solved for exactly, and therefore serves as a useful test for the nonlinear performance of fluid moment closures. (Including the self-consistent potential leads to wave propagation that complicates the analysis. The basic second-order effect is the phase de-mixing of second-order perturbations.) O'Neil and Gould (1968) derived the density evolution

$$\begin{aligned} n(z,t) =& n_0 \sum_{l,m} (-i)^{l+m} e^{i k_{lm} z} J_l(\epsilon_1 k_{lm} v_t (t-t_e)) \\ & \times J_m(\epsilon_2 k_{lm} v_t (t-t_2)) \exp(-k_{lm}{}^2 v_t{}^2 (t-t_e)^2/2) \qquad (t > t_2), \end{aligned} \tag{4.3}$$

$$k_{lm} = -\, l k_1 + m k_2, \tag{4.4}$$

$$t_e = \frac{m k_2 t_2 - l k_1 t_1}{m k_2 - l k_1}, \tag{4.5}$$

where J_n is the usual nth Bessel function and the echo time t_e has been defined for each wave number k_{lm} that enters the response.

Upon expanding the Bessel functions in the echo response (4.3) for small arguments, one notes that the contribution at each wave number scales as $\epsilon_1{}^l \epsilon_2{}^m$. As expected, the contributions at the initially excited wave numbers k_1 and k_2 constitute the first-order contributions to the response. There is a second-order contribution at the sum and difference wave numbers. At the sum wave number $k_1 + k_2$, however,

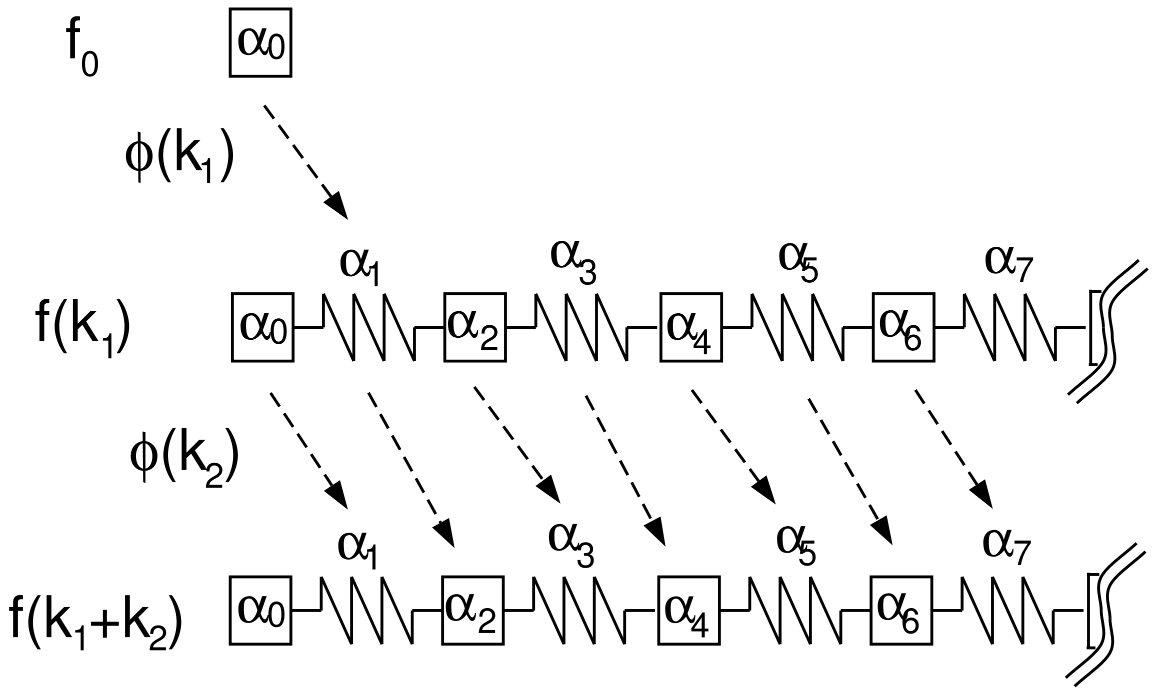

Figure 4.4: The mass–spring system view of the plasma echo. From Section 2.7.2, there is a correspondence between the orthogonal-polynomial moment system and the semi-infinite mass–spring system. Even Hermite moments correspond to the velocities of the masses and odd Hermite moments correspond to the contractions of the springs between them. [See the mass–spring variables in Eq. (2.109).] The initial potential pulse $\phi(k_1)$ couples the background distribution, which has only one nonzero moment a_0, to the wave number k_1 component of the moments (the mass–spring system in the middle of the picture). The perturbation travels as a wave to higher-order moments. The second pulse $\phi(k_2)$ couples the k_1 component of the moments to the $k_1 + k_2$ component of the moments (the mass–spring system at the bottom of the picture). If the echo criterion is satisfied, the perturbation can travel back to lower moments, producing a density echo.

the echo time occurs before the second pulse ($t_e < t_2$), so the exponential term in the response in Eq. (4.3) is very small and the response is negligible. The difference wave number $k_2 - k_1$, on the other hand, has an echo time after the second pulse (possibly much later). Higher-order echoes can appear as well, but this second-order response in the difference wave number is what will be called the *echo response*, and will calculated for closed fluid moment systems in the following section. A typical echo response is plotted in Fig. 4.3 along with the initial density perturbation responsible for the generation of the echo. Note that the echo can occur after both initial perturbations have completely phase-mixed away.

One can also understand the plasma echo in terms of the mass–spring analogy from Chapter 2. Each wave number k has a set of equations in Hermite moments of the form

$$\frac{\partial a_j(k,t)}{\partial t} + ikv_t\left[\sqrt{j}a_{j-1}(k,t) + \sqrt{j+1}a_{j+1}(k,t)\right] = -\sum_{k'}\frac{q\sqrt{j}}{v_t m}a_{j-1}(k-k',t)ik'\phi(k',t), \quad (4.6)$$

which can be mapped to a one-dimensional mass–spring system if the potential interaction is ignored. The zeroth-order distribution only has one nonzero Hermite moment, a_0, so an initial potential pulse excites the first mass in the mass–spring system at wave number k_1. The density perturbation $a_0(k,t)$ dies away in time as the original excitation propagates along the mass–spring chain to higher-order moments. The potential term in the Hermite moment equation (4.6) couples the mass–spring system for wave number k' to that for wave number k through the potential at wave number $k-k'$. [The moment $a_{j-1}(k',t)$ enters the equation for $a_j(k,t)$, so the coupling shifts to the next higher-order moment.] Thus the second potential pulse at wave number k_2 effectively copies that propagated wave in the mass–spring system for wave number k_1 to the mass–spring system for wave number k_1+k_2. If the echo condition is satisfied, then k_1+k_2 has sign opposite to that of k_1 and the new mass–spring wave travels in the opposite sense of the original, transferring energy back to lower moments and eventually to the density $a_0(k_1+k_2,t)$. The mass–spring wave then bounces off the free boundary condition at the first mass a_0, which is attached to nothing on the left, and the echo decays as the wave travels back to higher-order moments. This picture is illustrated in Fig. 4.4.

4.2 The Echo in Closed Moment Systems

The potential failing of a system that evolves a finite number of moments is clear from the picture in Fig. 4.4. If one attempts to model a pair of pulses such as those in Eq. (4.1) for an interaction time t_2-t_1 that is too long, then the the first-order perturbation wave will have hit the end of the chain of moments and been dissipated by the closure model. The closed moment system will therefore fail to produce the predicted second-order response in this case. Studies of series solutions of the Vlasov equation (Armstrong et al. 1970) noted that simulations could only capture the complete nonlinear physics for times $t < \sqrt{m}/(kv_t)$, where m is the number of coefficients in the series used. After that time, the effect of the truncated coefficients is no longer negligible. Since the Hermite moment equations are equivalent to the Hermite series approach, one expects the same limitation for fluid equations.

Solution of the application of the potential pulses in Eq. (4.1) to the closed Hermite moment system discussed in Section 3.3 is very straightforward. The pulses will produce nonzero Fourier components for wave numbers 0, k_1, k_2, and $\pm k_1 \pm k_2$ only. The n-moment system solution for the echo can therefore be found by evolving the

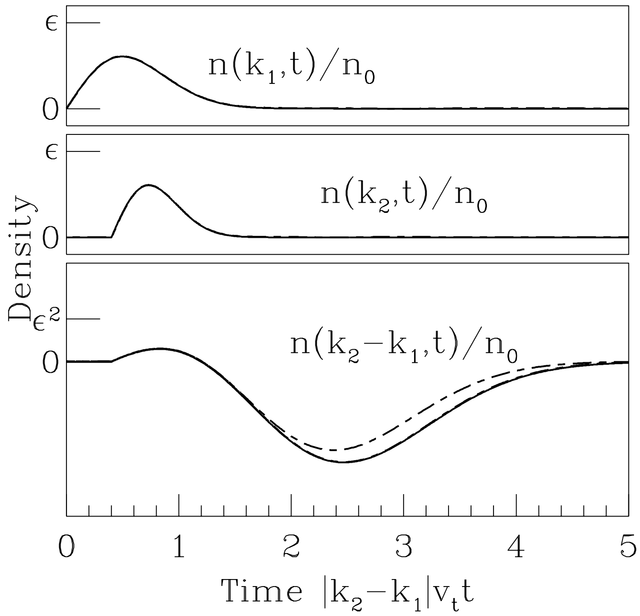

Figure 4.5: The plasma echo density response for short interaction time $(t_2-t_1)k_1v_t = 0.8$. The exact density responses are plotted with solid lines and there are two sets of dotted lines indicating the responses for the 10 Hermite moment system with the $q = 3$ closure and $q = 9$ closure. Both choices of closure give the correct first-order response. The $q = 3$ closure matches the second-order response almost exactly, however, while the $q = 9$ closure departs slightly from the correct answer.

equations

$$\frac{\partial}{\partial t}a_0(k_1,t)+ik_1v_ta_1(k_1,t) = 0, \tag{4.7}$$

$$\frac{\partial}{\partial t}a_1(k_1,t)+ik_1v_t\left[a_0(k_1,t)+\sqrt{2}a_2(k_1,t)\right] = n_0\frac{\epsilon_1}{2}\delta(t-t_1), \tag{4.8}$$

$$\frac{\partial}{\partial t}a_j(k_1,t)+ik_1v_t\left[\sqrt{j}a_{j-1}(k_1,t)+\sqrt{j+1}a_{j+1}(k_1,t)\right] = 0 \quad (2\le j<n), \tag{4.9}$$

$$\begin{aligned}\frac{\partial}{\partial t}a_j(k_1-k_2,t)+i(k_1-k_2)v_t&\left[\sqrt{j}a_{j-1}(k_1-k_2,t)+\sqrt{j+1}a_{j+1}(k_1-k_2,t)\right]\\ &= \sqrt{j}a_{j-1}(k_1,t)\frac{\epsilon_2}{2}\delta(t-t_2) \qquad (0\le j<n),\end{aligned} \tag{4.10}$$

along with the closure condition discussed in Section 3.2 for the unresolved moments $a_n(k_1,t)$ and $a_n(k_1-k_2,t)$. The results can then be compared to the k_1-k_2 component of the exact solution (4.3).

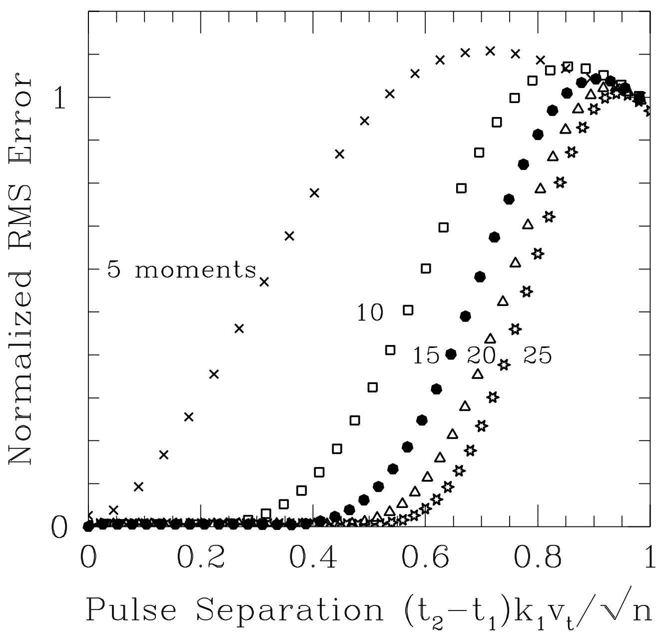

Figure 4.6: The normalized root-mean-squared error of the second order response $\int_0^\infty [n^a(k_2-k_1,t) - n(k_2-k_1,t)]^2\,dt / \int_0^\infty n(k_2-k_1,t)^2\,dt$ is plotted against the normalized interaction time $(t_2-t_1)k_1v_t/\sqrt{n}$ for closed Hermite moment systems with $n = 5$, 10, 15, 20 and 25 moment equations.

Some results are displayed for a fairly long interaction time $[k_1v_t(t_2-t_1) = 4]$ in Fig. 4.3. With 40 Hermite moments the echo is reproduced almost exactly in that case, but for 10 moments the system produces almost no echo. The 10-moment system fails for this example because the initial perturbation has become sufficiently convoluted after this interaction time that it is no longer represented by the first 10 Hermite moments. In Fig. 4.5, the results for a shorter interaction time $(k_1v_t[t_2-t_1] = 0.8)$ are displayed for the 10 Hermite moment system, which is successful in this case. Two choices of q, the number of times the linear response is matched in the $\omega \to 0$ limit, are illustrated in this figure. For $q = 3$, the dotted line for the second-order response is indistinguishable from the exact response. For $q = 9$ there is some error, although the simulation still gives a reasonable response. Both choices of q give an excellent fit to the linear theory, so for large numbers of moments it is probably best to take a small value of q. (The linear theory converges very slowly for $q = 1$, however, so the choices $q = 2$ or $q = 3$ are better.)

The mean-squared error in the second-order response was calculated for a number of closed moment systems with $q = 3$ for various interaction times. The results are plotted in Fig. 4.6. For a sufficiently large number of moments, there is almost no error in modeling the second-order response for interaction times $(t_2-t_1)k_1v_t < \sqrt{n}/2$, and there is a transition of increasing error until $(t_2-t_1)k_1v_t > \sqrt{n}$, at which point the closed moment system gives virtually no second-order response, so the error is 1. These results indicate, however, that a small number of moment equations can model the second-order response for very short interaction times only.

4.3 Relation to Perturbation Expansions

It is instructive to derive the response for this model problem perturbatively. Assume the potential is small, $\phi(z,t) = \epsilon\psi(z,t)$, and expand the distribution formally in a perturbation series

$$f(z,v,t) = f_0(z,v,t) + \epsilon f_1(z,v,t) + \epsilon^2 f_2(z,v,t) + \cdots . \tag{4.11}$$

Solving the Vlasov equation (3.5) term by term with the potential given by Eq. (4.1) yields the hierarchy of equations

$$\frac{\partial f_0}{\partial t} + v\frac{\partial f_0}{\partial z} = 0 \tag{4.12}$$

$$\frac{\partial f_1}{\partial t} + v\frac{\partial f_1}{\partial z} = \frac{q}{m}\frac{\partial\psi}{\partial z}\frac{\partial f_0}{\partial v}, \tag{4.13}$$

$$\frac{\partial f_2}{\partial t} + v\frac{\partial f_2}{\partial z} = \frac{q}{m}\frac{\partial\psi}{\partial z}\frac{\partial f_1}{\partial v}, \tag{4.14}$$

$$\vdots$$

Assuming a Fourier decomposition with periodic boundary conditions, $\psi(z,t) = \sum_k \exp(ikz)\psi_k(t)$ and $f_i(z,v,t) = \sum_k \exp(ikz) f_i(k,v,t)$, these equations are easily solved to give the evolution of each term in the expansion,

$$f_0(z,v,t) = \frac{n_0}{\sqrt{2\pi v_t{}^2}}\exp(-v^2/2v_t{}^2), \tag{4.15}$$

$$f_1(k,v,t) = \frac{q}{m}\int_0^t e^{-ikvt_1} ik\psi(k,t-t_1)\frac{\partial}{\partial v}f_0(v)\,dt_1, \tag{4.16}$$

$$\begin{aligned} f_2(k,v,t) =& \frac{q}{m}\int_0^t \sum_{k'} e^{-ikvt_1} i(k-k')\psi(k-k',t-t_1) \\ &\times \frac{\partial}{\partial v}f_1(k',v,t-t_1)\,dt_1. \end{aligned} \tag{4.17}$$

The density response therefore expands as $n(z,t) = n_0 + \epsilon n_1(z,t) + \epsilon^2 n_2(z,t) + \cdots$, and one finds that the second component is

$$\begin{aligned} \epsilon^2 n_2(k,t) =& n_0\int_0^t\int_0^{t-t_2}\sum_{k'}\frac{q^2}{m^2 v_t{}^2}(k-k')\phi(k-k',t-t_2) \\ &\times k'\phi(k',t-t_2-t_1)\mathsf{R}_2(kv_tt_2,k'v_tt_1)\,dt_1\,dt_2, \end{aligned} \tag{4.18}$$

where the second-order response function is

$$\mathsf{R}_2(\tau_2, \tau_1) = \tau_2(\tau_1 + \tau_2)\exp(-(\tau_1 + \tau_2)^2/2). \tag{4.19}$$

This second-order response gives the density at time t caused by the potential at times $t - t_2$ and $t - t_2 - t_1$. The response is typically exponentially small unless the argument $\tau_1 + \tau_2$ vanishes, which will occur if k and k' have opposite signs. (This is equivalent to the echo criterion that the wave number $k - k'$ of the second pulse is larger than that of the first pulse, k'.)

Note that the echo response increases linearly with the delay t_1 between the two potential pulses. The exact nonlinear response in Eq. (4.3), on the other hand, replaces $\epsilon^2 \mathsf{R}_2(\tau_1, \tau_2)$ with $J_1(2\epsilon\tau_1)J_1(2\epsilon(\tau_1 + \tau_2))\exp(-(\tau_1 + \tau_2)^2/2)$. Thus, the second-order expansion is only valid for analyzing delay times such that $\epsilon k v_t t_1 \ll 1$. The second-order perturbation is a function of the velocity derivative of the first-order perturbation. Even when the first-order perturbation is rigorously small, the derivatives increase with time as the perturbation becomes convoluted in phase space. One should be careful, therefore, in interpreting the long-time behavior of any second-order perturbation theory.

The difference between kinetic theory and Landau-fluid theory that was demonstrated by Mattor (1992) can be understood by looking at the Hermite moment expansion. From the picture in the previous section illustrated in Fig. 4.4, one can see that the second-order density response can be decomposed as the linear density response to initial conditions in higher-order moments that are in turn linear responses to an initial perturbation in the first moment $a_1(k_1)$. In terms of the general orthogonal-polynomial responses defined in Eq. (2.62), the second-order echo response can be decomposed as

$$\mathsf{R}_2(\tau_2, \tau_1) \propto \sum_{j=0}^{\infty} \mathsf{R}_{0,j+1}(\tau_2)\sqrt{j}\,\mathsf{R}_{j,1}(\tau_1). \tag{4.20}$$

The errors introduced in the second-order response for a truncated moment system with closure are fairly complicated then, since we must consider the errors introduced in all the linear responses of the form $\mathsf{R}_{0,j+1}$ and $\mathsf{R}_{j,1}$. The theory from Chapter 2 indicates that the Laplace transform of all the components of the linear response matrix will eventually converge, given enough moments. From Result 3, if the first p closure coefficients are set to zero for $p \geq 1$, then the errors in $\mathsf{R}_{0,j+1}$ for $j + 1 \leq p$ and all $\mathsf{R}_{j,1}$ are all related to one another by factors of Hermite polynomials. For the Maxwellian (Gaussian) case, the response functions converge with increasing numbers of moments for any fixed choice of q, the number of times the response is matched in the $\omega \to 0$ limit. Thus a set of closures exists for which $n \to \infty$ and $p \to \infty$, so that all the response functions eventually converge.

For a given closed moment system with a sufficiently large number of moments n, therefore, the main source of error in the second-order response will come from the truncation of the decomposition (4.20) due to the fact that moments with $j > n$ are not modeled. (The responses that are modeled are modeled very well with large numbers of moments.) Assume that the linear time response of each moment could be modeled exactly. The Hermite moments are expanded in the formal series $a_j(z,t) = a_j^0(z,t) + \epsilon a_j^1(z,t) + \epsilon^2 a_j^2(z,t) + \cdots$, where $a_j^0(z,t)$ is the jth Hermite moment of $f_0(z,v,t)$ and so on. Expanding the first-order response (4.16) in terms of the first n Hermite moments yields an approximation to the first-order part of the density:

$$\begin{aligned} f_1(k,v,t) &\sim \sum_{j=0}^{n-1} a_j^1(k,t) \frac{1}{\sqrt{2^j j!}} H_j(v/\sqrt{2}v_t) \frac{1}{\sqrt{2\pi v_t{}^2}} \exp(-v^2/2v_t{}^2) \\ &= \sum_{j=0}^{n-1} \frac{1}{\sqrt{2^j j!}} H_j(v/\sqrt{2}v_t) \frac{n_0}{\sqrt{2\pi v_t{}^2}} \exp(-v^2/2v_t{}^2) \\ &\quad \times \frac{q}{m} ik \int_0^t \psi(k,t-t_1) \frac{-1}{v_t\sqrt{j!}} \left[(-ikv_t t_1)^{j+1}\right. \\ &\qquad \left. + j\,(-ikv_t t_1)^{j-1}\right] e^{-(kv_t t_1)^2/2}\, dt_1. \end{aligned} \tag{4.21}$$

By inserting this approximation into the equation for the second-order component of the density equation (4.17), one obtains an approximation to the density response,

$$\begin{aligned} \mathsf{R}_2^{\mathrm{a},n}(\tau_2,\tau_1) \sim \tau_2\,(\tau_2+\tau_1) \exp(-(\tau_1{}^2+\tau_2{}^2)/2) \\ \times \left[\sum_{l=0}^{n-1} \frac{1}{l!} (-\tau_2\tau_1)^l - \frac{\tau_2(-\tau_2\tau_1)^{n-1}}{\tau_2+\tau_1} \right]. \end{aligned} \tag{4.22}$$

Using a finite set of moments effectively replaces the term $\exp(-\tau_2\tau_1)$ in the second-order response (4.19) with a Taylor series in $\tau_2\tau_1$. For small τ_1 and small τ_2, the Taylor series is a good approximation. For large τ_1 and τ_2, the exponential terms in the approximate echo response (4.22) dominate to give an exponentially small response. This result is a good approximation to the true response (4.19) except near the line $\tau_1 = -\tau_2$ where the combined exponential terms are $\mathcal{O}(1)$. [When the argument of $\exp(-\tau_2\tau_1)$ is positive it can balance the other exponential terms.] Since the n-term Taylor series of $\exp(x)$ is a good approximation out to $|x| \sim n$, this approximate second-order response is valid for interaction times $|\tau_1\tau_2| < n$. The response is exponentially small except where $\tau_1 \sim -\tau_2$, so this condition corresponds to $(kv_t t_1)^2 < n$, which is essentially the recurrence-time condition discussed in the previous section.

This response is very similar to that obtained for second-order perturbations in weak-turbulence theory (Mattor 1992). The Laplace transform of the second-order response in Eq. (4.18) can be written as

$$\begin{aligned} \epsilon^2 n_2(k,\omega) =& \frac{n_0}{2\pi} \int_{-\infty}^{\infty} \sum_{k'} \frac{q^2}{m^2 v_t{}^2} (k-k')\phi(k-k',\omega_1) k'\phi(k',\omega-\omega_1) \\ &\times \frac{1}{4|k||k'|v_t{}^2} \widehat{\mathsf{R}}_2\left(\frac{\omega}{\sqrt{2}|k|v_t}, \frac{\omega-\omega_1}{\sqrt{2}|k'|v_t}\right)\, d\omega_1, \end{aligned} \tag{4.23}$$

where the transformed second-order response is given by

$$
\begin{aligned}
\widehat{\mathsf{R}}_2(\zeta_2,\zeta_1) &= \int_0^\infty \int_0^\infty e^{i\zeta_2\tau_2} e^{i\zeta_1\tau_1} \mathsf{R}_2\left(s\frac{\tau_2}{\sqrt{2}}, s'\frac{\tau_1}{\sqrt{2}}\right) d\tau_1\, d\tau_2 \\
&= s\frac{\partial}{\partial\zeta_2}\left(s'\frac{\partial}{\partial\zeta_1} + s\frac{\partial}{\partial\zeta_2}\right)\frac{sZ(\zeta_2) - s'Z(\zeta_1)}{s\zeta_2 - s'\zeta_1}.
\end{aligned}
\tag{4.24}
$$

(To simplify the expression, the sign variables $s = k/|k|$ and $s' = k'/|k'|$ have been introduced.) The series expansion from Eq. (4.22), on the other hand, gives approximately the response

$$
\widehat{\mathsf{R}}_2(\zeta_2,\zeta_1) \approx s\frac{\partial}{\partial\zeta_2}\left(s'\frac{\partial}{\partial\zeta_1} + s\frac{\partial}{\partial\zeta_2}\right)\left[\sum_{j=0}^{n-1}\frac{1}{j!}\left(\frac{1}{2}s\frac{\partial}{\partial\zeta_2}s'\frac{\partial}{\partial\zeta_1}\right)^j\right] sZ(\zeta_2)s'Z(\zeta_1).
\tag{4.25}
$$

Mattor (1992) pointed out that the Landau-fluid approximation to the response remains finite for all ζ_1 and ζ_2 and therefore misses the resonant behavior in Eq. (4.23) when $ss' = -1$ and $\zeta_1 \to -\zeta_2$. It is worth pointing out, however, that this approximation converges with increasing numbers of moments. Near the resonance, however, this expression (4.25) converges extremely slowly with increasing n, the number of moments.

4.4 Limitations of Moment Equations

The time response for the linear Vlasov equation is modeled extremely well by Landau-fluid equations with as few as four moment (Hammett et al. 1992). The echo phenomenon, however, reconstructs information from the entire velocity-dependent part of the distribution function. Hence, although a plasma echo is essentially a linear response to the perturbation of a linear response, simply getting the linear response correct is not sufficient to model the echo. The ability of any set of moment equations to model a plasma echo is limited by the amount of velocity-dependent distribution information that is contained in the finite number of moments kept.

Previous studies using truncated Hermite series expansions noted this time limit as well. For example, Armstrong et al. (1970) were forced to terminate their simulations at a time $t < \sqrt{N}/kv_t$. Part of this time restriction arose from their choice of closure $\alpha_N(x,t) = 0$, which effectively reflects information back to lower moments, causing recurrence. With the linear closure used here, perturbations will decay correctly according to the linear theory without recurring. What is missed, however, is the interaction between waves separated by times larger than $\sim \sqrt{n}/kv_t$. In reality, however, a second interaction cannot occur for arbitrarily large separation times. Echoes can only occur in an almost collisionless plasma, since they depend on delicate convolutions in velocity space that are easily destroyed by collisions.

By considering the simple collision model in equation 3.5, Su and Oberman (1968) found that a free-streaming perturbation of wave number k is damped by an exponential term of the form $\exp(-\nu k^2 {v_t}^2 t^3/3)$. This decay implies that for separation times of the order

$$t_2 - t_1 \sim \left(\frac{1}{\nu {k_1}^2 {v_t}^2}\right)^{1/3}, \tag{4.26}$$

there will be no second-order response when the effect of collisions is taken into account. The number of moments required to model this separation time scales as $N \sim (t_2 - t_1) v_t k_1$, so a rough estimate of the number of moments N needed to model all second-order effects that can occur is given by

$$N \sim \left(\frac{k v_t}{\nu}\right)^{2/3}. \tag{4.27}$$

4.5 Summary

The dissipative Landau-fluid closure has a significant impact on the linear physics of closed moment systems. A model nonlinear problem, the plasma echo, was considered as a simple nonlinear test of the closure. The plasma echo is essentially the second-order component of the nonlinear response expanded in the limit of small perturbations. The second-order response has an exact solution (4.3) in the limit where the self-consistent potential is dropped. This exact solution was used to gauge the weakly nonlinear performance of moment systems with closure.

In contrast to the linear picture, the choice of linear closure does not have a large impact on the second-order response. (See Fig. 4.5.) The number of moments simulated, however, is an essential factor in resolving second-order effects. The results summarized in Fig. 4.6 that modeling the second-order response for interaction time $t_2 - t_1$ requires $n \sim [(t_2 - t_1) k_1 v_t]^2$ moments. A simple model of the rate of decay of perturbations due to a finite collision rate ν indicates that $n \sim (k v_t/\nu)^{2/3}$ moments are sufficient to resolve all second-order effects.

Clearly this second-order streaming nonlinearity cannot be accurately modeled with small numbers of moments. This effect is second-order, however, so for perturbations that are small with respect to the background, the unresolved density perturbations should be a small correction.

Chapter 5

2D Drift-Wave Model

The turbulent cascade of fluctuation energy to small scales is analogous in some ways to the transfer of fluctuation energy to fine velocity scales through phase-space mixing. The transfer of energy in turbulence can be very nonlinear in character in some situations (the inverse energy cascade in 2D, for example). There are limits, however, where the stretching of small-scale eddies by long wavelengths is similar in character to the passive phase mixing of the Vlasov equation. The basic physical scaling of damping to transfer of fluctuation energy to small scales that is discussed in Chapter 3 will be used in Chapter 6 to develop nonlinear viscosity models that model the transfer of fluctuation energy in drift turbulence due to flow shear.

The chief goal of developing subgrid turbulence models for drift-wave turbulence is to improve the accuracy of comprehensive 3D turbulence simulations. In order to effectively study the physics of fluctuation transfer in a simplified situation, however, the initial research of this thesis focuses on a 2D model problem. The model equation for this study was chosen to be as simple as possible while retaining the basic physics relevant to subgrid turbulence processes in fluid simulations of drift wave turbulence.

Saturation in toroidal gyrofluid turbulence simulations (Beer 1995) involves a balance between the source of fluctuations in linearly unstable modes and the dissipation in modes that are stabilized by terms that model Landau damping. Fluctuation energy is transferred from unstable to stable modes through the advection nonlinearity. A useful 2D model will at least contain the $\mathbf{E}\times\mathbf{B}$ drift advection nonlinearity, a linear instability, and dissipation to model Landau damping, which is primarily a function of the parallel wavelength and should therefore be present at long perpendicular wavelengths. The system presented here includes models of these three essential effects; however, it is a relatively simple one-field 2D equation resulting from major approximations. For example, it does not model bad curvature and ion temperature dynamics, which are important instability mechanisms in the core region of many tokamaks. As a 2D model, it is missing a special constraint on the adiabatic electron response, which enhances the role of the $k_y = k_z = 0$ component of the electrostatic potential (Dorland 1993), leading to turbulence-generated sheared flows that are important in toroidal simulations (Hammett et al. 1993; Beer 1995; Dimits et al. 1994; Waltz et al. 1994). Nevertheless, the system used in this study is a useful paradigm for studying certain effects important in plasma turbulence where the $\mathbf{E}\times\mathbf{B}$ nonlinearity is important, and some of the lessons learned in this simple model can then be applied in more complicated 3D multi-field simulations.

5.1 Model Equation

There is a significant literature on 2D models for drift-wave turbulence. The prototypical model of Hasegawa and Mima (1978) captures the basic physics of the $\mathbf{E}\times\mathbf{B}$ nonlinearity in a one-field 2D equation, but contains no linear drive to produce fluctuations. A model of linear drive is introduced in so-called "$i\delta$" equations (Terry and Horton 1982; Liang et al. 1993) through a simple model for the non-adiabatic part of the electron response. The model equation derived here is a simplified $i\delta$ model, with an additional term added to model Landau damping at long wavelengths.

There are a number of derivations in the literature of this model starting from standard fluid equations. Here the derivation is sketched from a gyrokinetic/gyrofluid perspective. The starting point is just a conservation equation for the ion-guiding-center density n_{gc},

$$\frac{\partial n_{gc}}{\partial t} + \boldsymbol{\nabla}\cdot[n_{gc}(\mathbf{V}_{\mathbf{E}\times\mathbf{B}} + u_{\|}\hat{\mathbf{z}})] = 0, \tag{5.1}$$

where

$$\mathbf{V}_{\mathbf{E}\times\mathbf{B}} = \frac{c}{B}\hat{\mathbf{z}}\times\boldsymbol{\nabla}\phi \tag{5.2}$$

is the $\mathbf{E}\times\mathbf{B}$ drift velocity, ϕ is the potential, and $u_{\|}$ is the parallel ion flow. The ion FLR effects are ignored (via the assumption $T_i \ll T_e$) while the ion polarization effects are retained by including the ion polarization density in addition to the guiding-center density in determining the actual ion density

$$n_i = n_{gc} + n_0\frac{\rho_s^2 e}{T_e}\boldsymbol{\nabla}_{\perp}{}^2\phi, \tag{5.3}$$

where $\rho_s = c_s/\Omega_{ci}$ is the gyroradius using the ion gyrofrequency $\Omega_{ci} = eB/m_i c$, and the sound speed is $c_s = \sqrt{T_e/m_i}$. (This approach is the standard method used in the gyrokinetic Poisson equation (Lee 1983; Dubin et al. 1983; Lee 1987).) For the ion parallel flow velocity, the "1-moment" model of Landau damping,

$$n_0\frac{d}{dz}u_{\|} \approx C_1 v_t|k_{\|}|(n+\phi) \approx C_2 v_t|k_{\|}|n, \tag{5.4}$$

of Dorland and Hammett (1993) is used, where C_1 and C_2 are constants of order unity. Making use of the standard two-scale approximations to expand n_{gc} in Eq. (5.1) via

$$n_{gc} = n_0\left(1 + \frac{x - x_0}{L_n}\right) + \tilde{n}_i \tag{5.5}$$

into a long-scale equilibrium part with density gradient scale length, L_n, and a short-scale fluctuating component $\tilde{n}_i$, leads to

$$\frac{\partial \tilde{n}_i}{\partial t} + \mathbf{V}_{\mathbf{E}\times\mathbf{B}} \cdot \boldsymbol{\nabla} \tilde{n}_i + n_0 V_d \frac{\partial}{\partial y}\left(\frac{e\phi}{T_e}\right) = -\alpha \frac{c_s}{L_n} \tilde{n}_i + \mu \frac{c_s {\rho_s}^2}{L_n} {\boldsymbol{\nabla}_\perp}^2 \tilde{n}_i, \tag{5.6}$$

where the diamagnetic drift velocity, $V_d = c_s \rho_s / L_n$, has been introduced. The density gradient in the long-scale equilibrium is responsible for the introduction of the diamagnetic drift term. The viscosity-like term containing μ is included to provide a sink for fluctuation energy at high k. The Landau damping model introduces the dissipative term $-\alpha c_s \tilde{n}_i / L_n$, where α is set to $C_2 v_t |k_{||}| L_n / c_s$ for a typical small but finite $k_{||}$ [$\sim (qR)^{-1}$ in a tokamak]. Three-dimensional simulations of drift-wave turbulence have found that the bulk of the dissipation comes from Landau damping (Beer 1995), so it is necessary to include a model for this process in 2D simulations where $k_{||}$ has been ignored.

To close the model system, the fluctuation density must be related to the potential. The real-space ion density δn_i is just the sum of the guiding space density $\tilde{n}_i$ and the ion polarization density ${\rho_s}^2 {\boldsymbol{\nabla}_\perp}^2 e\phi / T_e$. As a crude model for the electron response that will provide linear drive, we set $\delta n_e = (1 - \delta_0 \rho_s \partial / \partial y) e\phi / T_e$ (Terry and Horton 1982). Quasineutrality therefore gives us

$$\tilde{n}_i = \frac{n_0 e}{T_e}\left(1 - {\rho_s}^2 {\boldsymbol{\nabla}_\perp}^2 - \delta_0 \rho_s \frac{\partial}{\partial y}\right)\phi. \tag{5.7}$$

Upon using the normalized variables

$$\tau = \frac{c_s}{L_n} t, \quad x' = x \rho_s, \quad y' = y \rho_s, \quad \psi = \frac{L_n}{\rho_s} \frac{e}{T_e} \phi, \tag{5.8}$$

and then dropping the primes, we obtain the evolution equation

$$\left(\frac{\partial}{\partial \tau} + \alpha - \mu {\boldsymbol{\nabla}_\perp}^2\right)\left(1 - {\boldsymbol{\nabla}_\perp}^2 - \delta_0 \frac{\partial}{\partial y}\right)\psi$$
$$+ \hat{\mathbf{z}} \times \boldsymbol{\nabla} \psi \cdot \boldsymbol{\nabla}\left(-{\boldsymbol{\nabla}_\perp}^2 - \delta_0 \frac{\partial}{\partial y}\right)\psi + \frac{\partial \psi}{\partial y} = 0. \tag{5.9}$$

Expressing the potential as a sum of Fourier modes, $\psi = \sum_{\mathbf{k}} \exp(i\mathbf{k} \cdot \mathbf{x}) \psi_{\mathbf{k}}$, gives the mode coupling equation

$$\left(\frac{\partial}{\partial \tau} + i\omega_{\mathbf{k}} - \gamma_{\mathbf{k}} - \gamma_{\mathbf{k}}^d\right)\psi_{\mathbf{k}} = N_{\mathbf{k}}, \tag{5.10}$$

where the nonlinear term is defined as

$$N_{\mathbf{k}} = \sum_{\mathbf{k}'} \frac{\hat{\mathbf{z}} \times \mathbf{k}' \cdot \mathbf{k}\left[|\mathbf{k} - \mathbf{k}'|^2 - i\delta_0 (k_y - k'_y)\right]}{1 + |\mathbf{k}|^2 - i\delta_0 k_y} \psi_{\mathbf{k}'} \psi_{\mathbf{k}-\mathbf{k}'} \tag{5.11}$$

and the linear frequency and growth rate are given by

$$\omega_{\mathbf{k}} = \frac{k_y(1+|\mathbf{k}|^2)}{(1+|\mathbf{k}|^2)^2 + {\delta_0}^2 {k_y}^2}, \tag{5.12}$$

$$\gamma_{\mathbf{k}} = \frac{\delta_0 {k_y}^2}{(1+|\mathbf{k}|^2)^2 + {\delta_0}^2 {k_y}^2} - \alpha - \mu|\mathbf{k}|^2. \tag{5.13}$$

An additional growth rate $\gamma_{\mathbf{k}}^d$ has been introduced to contain one of the numerical dissipation models discussed in the following chapter. The true system that is being studied has $\gamma_{\mathbf{k}}^d = 0$, and with sufficiently high resolution the turbulent saturated state can be numerically simulated. Other dissipation models, to be defined later, can be used to improve the accuracy of simulations with insufficient resolution. [The dissipation models that will be considered are regular hyperviscosity (6.16), parameterized hyperviscosity (6.19), and the Smagorinsky eddy viscosity (6.5).] The linear physics of this model agrees with a model for dissipative trapped-electron drift waves derived by Liang et al. (1993) to first order in δ_0 (D_0 in their notation) and second order in $k\rho_s$. Setting $\alpha = 0$, $\mu = 0$, and $\delta_0 = 0$ gives the equation of Hasegawa and Mima (1978).

The model equation used here was chosen for simplicity and only contains the gross features of drift-wave turbulence. To be of practical use, in fact, the results concerning eddy viscosity should not depend on the precise nature of Eq. (5.9), since we are interested in applications to more sophisticated models of drift-wave turbulence. The toroidal gyrofluid equations (Beer 1995; Waltz et al. 1992), which evolve multiple fields and contain significantly more complicated (hence more accurate) linear physics, share the same basic nonlinear advection term contained in this model. Hence the eddy viscosity calculated in this study is parameterized as a function of the advecting velocity without reference to the linear physics.

5.2 Physics of the Saturated State

Before considering the effects of the subgrid scales, we examine the results of simulating the model, Eq. (5.9), for a typical set of parameters. Simulations were performed with periodic boundary conditions using the standard dealiased pseudospectral approach. A hyperviscous damping term of the form discussed in the next section was used for the results considered here. Initially we consider a box of size $50\rho_s \times 50\rho_s$, using a 128×128 grid in real space, for parameters $\delta_0 = 0.35$, $\alpha = 0.035$, and $\mu = 0.0001$, with a hyperviscosity defined by Eq. (6.16) with power $p = 16$ and coefficient set to the average rate of shear, $\nu_h = S(t)$. [See Eq. (6.17).] This choice of δ_0 gives growth rates large enough that the saturated state is in the strong-turbulence regime. [For this model equation, the wave frequencies are fixed, and the growth rates are proportional to the parameter δ_0. For low growth rates, the total energy saturates at a level proportional to δ_0. For large growth rates, the total energy in the saturated state

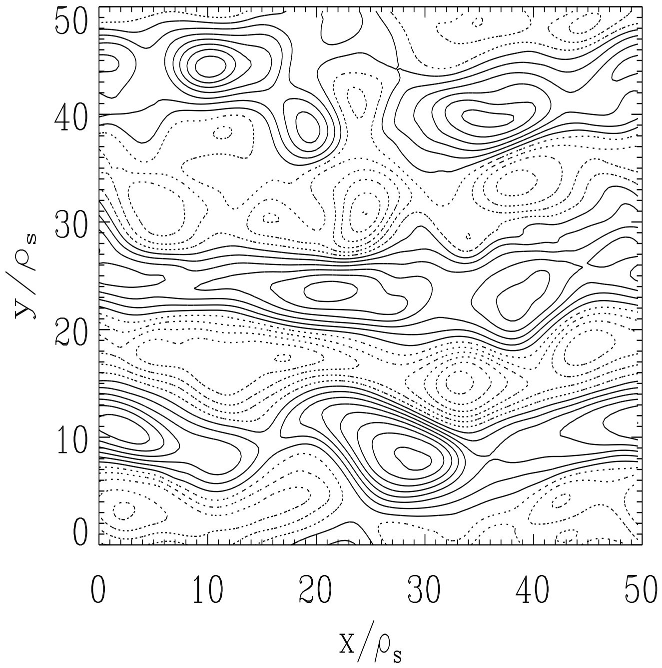

Figure 5.1: Contours of potential for saturated turbulence at one instant.

scales as ${\delta_0}^2$. For the purposes of this study, when the drive δ_0 lies in the transition between these two scalings the simulations will be said to take place in the moderate-turbulence regime. The strong- and weak-turbulence regimes are defined respectively for larger and smaller values of the drive δ_0. [Krommes and Hu (1994) discuss saturation levels for some simple drift-wave models.] The instantaneous potential late in the simulation is shown in Fig. 5.1.

One useful macroscopic parameter that can be expressed in this model is the volume-averaged particle flux

$$\begin{aligned}\Gamma &= \frac{1}{L_x L_y}\int_0^{L_x}\int_0^{L_y} \hat{\mathbf{x}}\cdot\mathbf{V}_{\mathbf{E}\times\mathbf{B}}\tilde{n}_i\,dy\,dx \\ &= \delta_0\left(\frac{\rho_s}{L_n}D_{\mathrm{B}}\right)\frac{n_0}{L_n}\sum_{\mathbf{k}}{k_y}^2|\psi_{\mathbf{k}}|^2.\end{aligned} \tag{5.14}$$

(The Bohm diffusivity, $D_{\mathrm{B}} = cT_e/eB$, has been introduced here.) The gyro-Bohm scaling of the flux is the natural scaling for this system, since the use of periodic boundary conditions and a constant background gradient prevents the system scale from directly entering the analysis. (The system scale could in principle enter through the size of the simulation domain $L_x \times L_y$, implying a Bohm scaling. The fact that "flux-tube" simulations saturate (Beer et al. 1995; Dimits et al. 1996) and that the

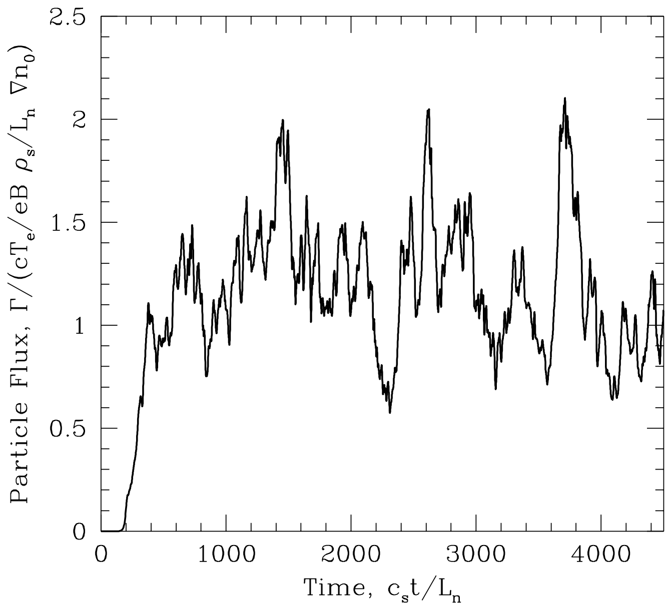

Figure 5.2: Particle flux from simulation of the model equation in a periodic box ($50\rho_s \times 50\rho_s$) in the strong-turbulence regime, $\delta_0 = 0.35$, $\alpha = 0.035$, $\mu = 0.0001$.

saturation amplitude is independent of the size of the simulation domain indicates that a gyro-Bohm scaling regime exists for sufficiently small ρ_s/L.) The time history of the flux for a typical set of parameters is shown in Fig. 5.2.

Since observable physical quantities such as the particle flux and mean-square density fluctuations can be expressed as quadratic functions of the potential, one is led to study the evolution and saturation of the squared magnitude of the modes. There is only one quadratic quantity that is conserved by the nonlinear term of the model equation (5.9) corresponding to the fact that the volume-integrated square density, $\int \tilde{n}_i(\mathbf{x})^2\, d\mathbf{x}$, is conserved by divergence-free advection. This conserved quantity is denoted by Ω. A normalized modal contribution to the conserved quantity is defined by

$$\Omega_{\mathbf{k}} = \frac{1}{2}\left[(1+|\mathbf{k}|^2)^2 + {\delta_0}^2 {k_y}^2\right] |\psi_{\mathbf{k}}|^2. \tag{5.15}$$

Fig. 5.3 displays the saturated spectrum for the initial set of parameters, where the standard 2D spectral density is defined by $\Omega(k) = 2\pi k\langle\Omega_{\mathbf{k}}\rangle$, where the average is taken over the band of $\mathbf{k}$'s at radius k. (The growth rates for this simulation are displayed in Fig. 5.4.) An attempt to infer an inertial-range power law scaling from

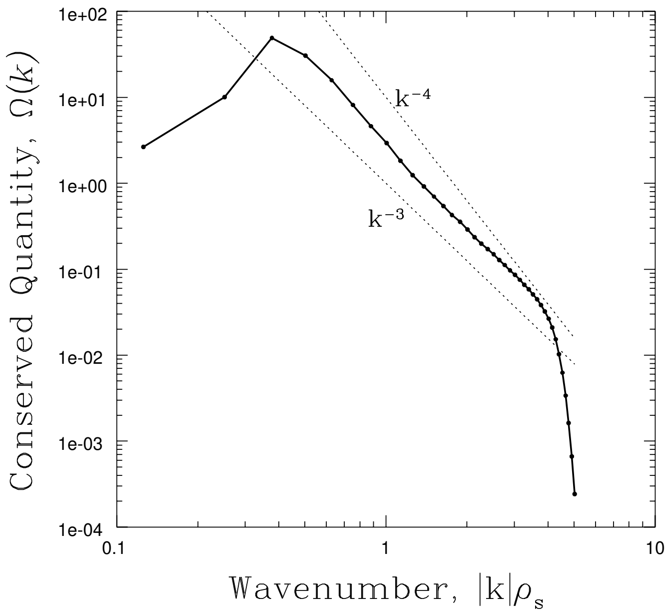

Figure 5.3: Time averaged spectrum of density fluctuations for the simulation of Fig. 5.2.

this spectrum would give $\Omega(k) \sim k^p$ with $-4 < p < -3$, which is very different from the 2D Navier–Stokes high-k inertial range where enstrophy scales as k^{-1} (Kraichnan 1967; Batchelor 1969). In fact, simulations of 2D Navier–Stokes turbulence have typically observed inertial ranges significantly steeper than theoretically predicted. The k^{-1} enstrophy range is an asymptotic limit that can only be observed when the dissipation scales are separated from the forcing scales by at least two orders of magnitude (Borue 1993). The separation of scales required to observe inertial-range scaling is particularly large in 2D turbulence, where the enstrophy transfer is very nonlocal. Such a scenario is highly unlikely for plasma-turbulence problems where significantly damped modes exist at wave numbers very close to the unstable modes driving the turbulence. Therefore, one should not expect to find universal exponents in drift-wave simulations.

The evolution equation for this quadratic invariant is

$$\left(\frac{\partial}{\partial \tau} - 2\gamma_{\mathbf{k}}\right)\Omega_{\mathbf{k}} = T_{\mathbf{k}}, \tag{5.16}$$

where the nonlinear transfer $T_{\mathbf{k}}$ is given by

$$T_{\mathbf{k}} = \left[(1+|\mathbf{k}|^2)^2 + {\delta_0}^2 {k_y}^2\right] 2\mathrm{Re}(\psi^*_{\mathbf{k}} N_{\mathbf{k}}). \tag{5.17}$$

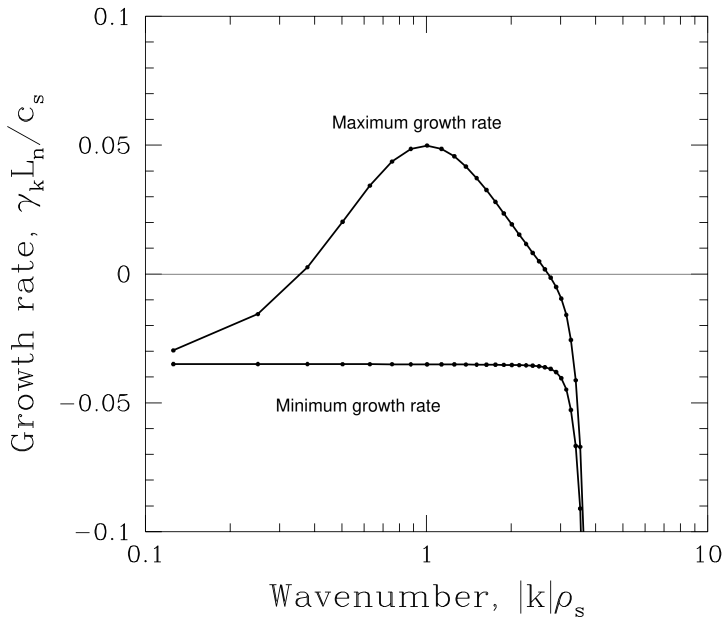

Figure 5.4: Growth rates for the simulation of Fig. 5.2. A k^{16} hyperviscosity damping term has been used to improve the resolution of the inertial range.

In steady state, the nonlinear transfer balances the production and dissipation of fluctuations due to linear growth or damping. (See Fig. 5.5 for a typical example of the linear production.) For 2D equations of this form, with only one quadratic invariant, it has been noted that arguments from statistical mechanics imply transfer to small scales (Diamond and Biglari 1990), in contrast to the dual cascade picture from 2D Navier–Stokes turbulence. With moderate dissipation due to Landau damping at all scales, there is no clearly defined inertial range or cascade. The production of the conserved quantity for a typical run is plotted in Fig. 5.5. Note that the dominant source and the major sink for fluctuation energy both lie near the peak of the spectrum. The major transfer in $\mathbf{k}$ space of fluctuation energy is in fact not a cascade, and takes energy from unstable modes near the $k_x = 0$ axis to Landau-damped modes of nearly the same magnitude near the $k_y = 0$ axis. (Realistic simulations of transport therefore require accurate models of Landau damping.) The dissipation near the cutoff indicates a small cascade of fluctuation energy to high k. This picture of energy production in k space is qualitatively similar to that observed in toroidal gyrofluid simulations. [See Fig. 5.9 of Beer (1995).] The small amount of transfer to high k is dynamically insignificant, leading to the conclusion that the level of turbulence is set primarily by eddy turnover at long wavelengths. Simulations of just

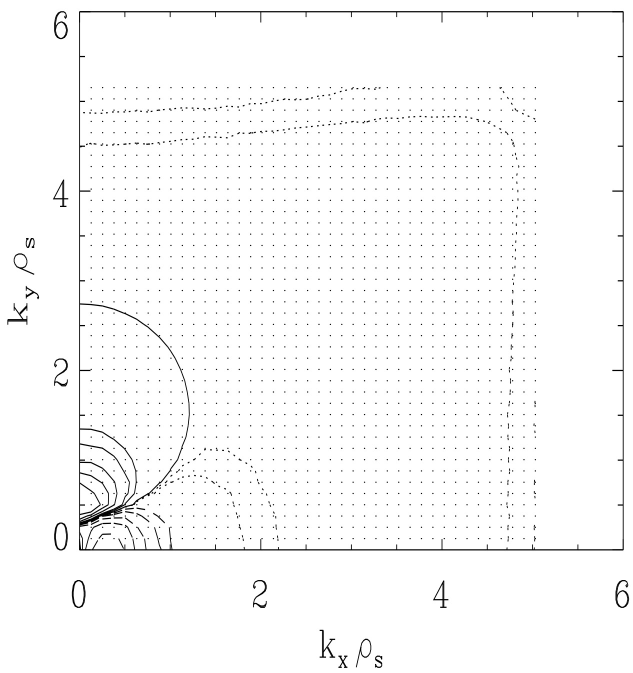

Figure 5.5: Time averaged production and dissipation of density fluctuations for the simulation of Fig. 5.2 (contours of $\langle \gamma_{\mathbf{k}} \Omega_{\mathbf{k}} \rangle$). Each point is a resolved mode. Solid lines are contours of the production region at $0, 1, 2, 5, 10$, and 20 (dimensionless units). Dashed lines are contours of the dissipation region at $-1, -2, -5, -10$, and -20. The dotted lines are contours at -0.05 and -0.1.

the long wavelengths are therefore theoretically feasible. Simply eliminating modes that lie beyond the bulk of the spectrum can give catastrophic results, however, as the small transfer of fluctuation energy 'piles up' secularly at the cutoff.

Chapter 6

Eddy Viscosity and Hyperviscosity

Models for the subgrid-scale dissipation in numerical simulations of turbulence have long been necessary in the study of atmospheric and oceanographic turbulence, for which the direct numerical simulation of the full range of scales is infeasible. 'Large Eddy Simulations' (LES) (Galperin and Orszag 1993) evolve the largest scales of a problem and model the average interaction with the unresolved small scales through dissipative terms called eddy viscosity. Our goal is to apply these techniques to simulations of drift-wave turbulence in tokamaks. This preliminary study tests some basic dissipative terms in a simple 2D drift-wave model. By restricting the problem to two dimensions, a large number of simulations can be performed with sufficient time histories for the statistics necessary to compute the eddy viscosity. In Chapter 7 extensions to three dimensions are discussed and applied to gyrofluid turbulence simulations.

When it is computationally impossible to resolve the dissipation scales in homogeneous isotropic turbulence, the standard tool used in numerical simulations is hyperviscosity, a damping rate of the form $M|\mathbf{k}|^p$ where the power p is larger than 2; $p = 2$ gives ordinary viscosity. Hyperviscosity introduces an artificial dissipation range into the problem that is narrower than the usual dissipation range and therefore requires less resolution. The choice of power and magnitude is somewhat arbitrary. Numerical studies of 2D Navier–Stokes turbulence have found that a moderately high power ($p = 8$ or $p = 16$) allows the hyperviscosity to effectively remove energy from small scales with a minimum of unphysical dissipation at the large scales (Basdevant and Sadourny 1983). While the dissipation range introduced by hyperviscosity acts as a model for the true dissipation range, the damping provided by hyperviscosity has not been systematically compared with the nonlinear transfer rates to unresolved scales.

Eddy viscosities attempt to model the sink of energy at small scales by introducing dissipation into the resolved scales. The nonlinear viscosity of Smagorinsky (1963), for example, is a simple model with a long history of applications in fluid turbulence. The damping given by the Smagorinsky viscosity is proportional to $|\mathbf{k}|^2$, which is rigorously correct only in the limit where the separation of scales between resolved and unresolved modes is asymptotically large. When there is significant transfer of energy that is local in k space, as in Navier–Stokes turbulence, the contribution to the eddy viscosity from local transfer to unresolved modes near the cutoff is poorly represented by a k^2 damping rate (Kraichnan 1976). This theoretical eddy viscosity has been tested for the inverse cascade range in large eddy simulations of 2D Navier–Stokes turbulence (Chekhlov 1995).

The ideas of hyperviscosity and eddy viscosity are combined here to create a nonlinear filter for use in simulations of drift-wave turbulence. Theoretical predictions of the nonlinear transfer do not yet exist for comprehensive models of drift-wave turbulence. For simple drift-wave models, predictions of the nonlinear transfer from closure theories have only been made very recently (Hu et al. 1997). Therefore, the approach taken here is to choose the form of the hyperviscosity model by comparison with direct numerical simulations. The eddy viscosity is calculated for a given set of parameters and resolution from a higher-resolution simulation by calculating the transfer from modes that are contained in the low-resolution simulation to all other modes. The eddy viscosity was calculated in this fashion for a wide range of parameters and various resolutions. The hyperviscosity was fit to the calculated damping rate by adjusting the power and magnitude. The power p and magnitude M were then parameterized as functions of the resolved modes based on insights from Kraichnan's eddy viscosity for the 2D enstrophy range.

The resulting parameterized hyperviscosity has several advantages over traditional approaches. The choice of power and magnitude are calculated from functions of the resolved scales, eliminating what are arguably free parameters in the standard application of hyperviscosity. The damping rate comes closer to modeling the actual eddy damping rate than do eddy viscosities like Smagorinsky's that have damping rates proportional to k^2. For problems of interest, the actual eddy damping rate has not been predicted theoretically and can only be calculated from high resolution simulations. This method is straightforward to implement in spectral simulations of homogeneous turbulence, where k-dependent damping rates are trivial to incorporate.

The parameterization is based on the general physical processes of nonlinear advection and 2D enstrophy cascade. This model should therefore be useful for more general drift-wave calculations that resolve the main energy injection scales and are using this hyperviscosity only to reduce the resolution needed for modes at scales smaller than the injection scales. This model may also be useful for passive-scalar advection problems. Situations with inverse cascade and significant energy production at unresolved scales, such as may be found in magneto-hydrodynamic turbulence or 2D Navier–Stokes turbulence, result in negative eddy viscosities and are therefore clearly beyond the scope of this model, but have been studied with other models (Chekhlov 1995).

6.1 Large Eddy Simulation

The model equation (5.9) can be written symbolically as

$$\frac{\partial}{\partial \tau}\psi = N(\psi) + L\psi, \tag{6.1}$$

where L is a linear operator and N is the quadratic nonlinearity defined by Eq. (5.11). Numerical simulations cannot follow the detailed behavior of the continuous field ψ. Pseudospectral simulations on a periodic box of size $l \times l$ with a finite number of modes are considered. The resolved modes (those that are evolved in a simulation) can be defined through a filter function, $f \to \overline{f}$, such that in Fourier space

$$\overline{f}_{\mathbf{k}} = G_{\mathbf{k}} f_{\mathbf{k}}, \tag{6.2}$$

where $G_{\mathbf{k}} = 1$ for $|k_x| < k_x^c$ and $|k_y| < k_y^c$, and $G_{\mathbf{k}} = 0$ otherwise. (The boundary wave numbers k_x^c and k_y^c are called the cutoff wave numbers. For theoretical studies of isotropic turbulence, a spherical region in k space, $|\mathbf{k}| \leq k_c$, is typically used.) Fields such as the potential ψ can then be decomposed into a resolved part $\overline{\psi}$ and a subgrid contribution $\psi^s = \psi - \overline{\psi}$. The filtered evolution equation can be written as

$$\frac{\partial}{\partial \tau}\overline{\psi} = \overline{N(\overline{\psi})} + N^s + L\overline{\psi}, \tag{6.3}$$

where the subgrid contribution to the nonlinear term is defined by

$$N^s = \overline{N(\psi)} - \overline{N(\overline{\psi})}. \tag{6.4}$$

Given the resolved field $\overline{\psi}$, pseudospectral evaluation of the nonlinear term gives precisely $\overline{N(\overline{\psi})}$, so the only term in the evolution equation (6.3) that is not calculated in a simulation of the resolved field is the subgrid contribution N^s.

The field of Large Eddy Simulation is concerned with deriving approximate models for the effect of the subgrid term N^s that can expressed in terms of the resolved field $\overline{\psi}$. Traditionally it is argued that the average contribution of the subgrid term N^s can be viewed as an eddy viscosity, draining energy from the resolved scales.

If there were a true separation of scales and the subgrid field ψ^s had asymptotically short wavelengths and short time scales compared to the resolved field $\overline{\psi}$, then the subgrid term would truly act like a viscosity (Kraichnan 1987). Upon averaging over a time that is short for the resolved modes but long compared to the turnover time for the subgrid modes, we would find that $\langle N^s \rangle = \nu_{\text{eddy}} \boldsymbol{\nabla}^2 \overline{\psi}$, where the eddy viscosity ν_{eddy} is a function of the statistics of the small scales. In reality, however, the length and time scales of the subgrid modes are nearly identical to those of barely resolved modes.

Various approaches to estimating the subgrid contribution have been proposed. We will examine two simple estimates: a k-space-dependent eddy viscosity, and the eddy viscosity of Smagorinsky (1963). In numerical simulations, application of these approaches corresponds to introducing a simple dissipative term [$N^s_{\mathbf{k}} \approx \nu_k k^2 \psi_{\mathbf{k}}$ or $N^s \approx \mathbf{\nabla} \cdot \nu(\mathbf{x}) \mathbf{\nabla} \psi$ respectively] where the damping [ν_k or $\nu(\mathbf{x})$] is predicted either theoretically or empirically as a function of the resolved scales. Several authors have pointed out that in a turbulent state subgrid scales do not act in a purely dissipative fashion and that a more complete model would contain terms to simulate noise and backscatter of energy from the subgrid scales (Rose 1977). Simple damping terms, however, are extremely efficient to calculate. It is not clear which approach, adding higher-order terms to the subgrid model or increasing grid resolution with a simple subgrid model, is more efficient at improving the statistics of the long-wavelength modes for a given increase in computational complexity. For the current study, simple dissipative terms are considered.

6.1.1 Smagorinsky Eddy Viscosity

A traditional view of eddy viscosity is that the short-wavelength modes act in some sense like a thermal noise on the resolved scales and hence serve to enhance the regular viscosity. Estimating the subgrid contribution by a spatially varying eddy viscosity yields

$$N^s \approx \mathbf{\nabla} \cdot \nu_{\text{eddy}}(\mathbf{x}) \mathbf{\nabla} \psi(\mathbf{x}). \tag{6.5}$$

Smagorinsky (1963) gave heuristic arguments for the scaling of this eddy viscosity in the context of simulations of quasi-geostrophic turbulence; he concluded that

$$\nu_{\text{eddy}}(\mathbf{x}) = (C_s d)^2 S(\mathbf{x}, t), \tag{6.6}$$

where C_s is a non-dimensional constant, d is an estimate of the subgrid length scale, and $S(\mathbf{x}, t)$ is the local strain rate of the velocity field defined by

$$S(\mathbf{x}, t) = \sqrt{\left(\frac{\partial V_x}{\partial x}\right)^2 + \left(\frac{\partial V_y}{\partial y}\right)^2 + \frac{1}{2}\left(\frac{\partial V_x}{\partial y} + \frac{\partial V_y}{\partial x}\right)^2}. \tag{6.7}$$

Note that $S = 0$ for rigid rotation as well as for uniform flows.

The Smagorinsky model has been applied in computations of flows far outside the realm of its original derivation, with success in many cases. This model was used in simulations in this study for the purpose of comparison, to illustrate the behavior of the standard eddy viscosity with k^2 damping. Different choices of length scale and constant have been found to give optimal results in different situations in fluid turbulence. We therefore arbitrarily set d to the physical-space grid spacing, and used $C_s = 0.1$ based on initial tests for one choice of parameters with moderate resolution.

6.1.2 Kraichnan's Eddy Viscosity

One approach to defining a damping term originating from the subgrid modes is by comparing the nonlinear transfer term with the viscous term in a two-point closure theory (Kraichnan 1976). By splitting the modes into resolved modes and subgrid modes, the quadratic invariant evolution equation (5.16) can be written as

$$\left(\frac{\partial}{\partial \tau} - 2\gamma_{\mathbf{k}}\right)\Omega_{\mathbf{k}} = T^r_{\mathbf{k}} + T^s_{\mathbf{k}}, \tag{6.8}$$

where the transfer defined in Eq. (5.17) has been decomposed into a resolved piece $T^r_{\mathbf{k}}$ and the subgrid piece $T^s_{\mathbf{k}}$. In the context of this equation, the analog to Kraichnan's *effective eddy viscosity* would be defined as

$$\nu_{\text{eddy}}(\mathbf{k}) = \frac{-\langle T^s_{\mathbf{k}}\rangle}{2k^2\langle\Omega_{\mathbf{k}}\rangle}, \tag{6.9}$$

for some appropriately defined ensemble average. The motivation for this definition of an eddy viscosity comes from introducing a damping term of the form $-\nu_{\text{eddy}}(\mathbf{k})k^2\psi_{\mathbf{k}}$ on the right-hand side of the primitive equation (5.10). This damping term would introduce the term $-\langle T^s_{\mathbf{k}}\rangle\Omega_{\mathbf{k}}/\langle\Omega_{\mathbf{k}}\rangle$ to the right-hand side of Eq. (6.8) above, which, on average, will balance the subgrid transfer term $T^s_{\mathbf{k}}$.

Kraichnan derives predictions of this eddy viscosity (Kraichnan 1976) in 2D and 3D Navier-Stokes inertial ranges using the Test Field Model (Kraichnan 1971). While plasma turbulence is not expected to exhibit inertial-range behavior, there are several generic conclusions about eddy viscosity worth noting. The primary discovery was that the eddy viscosity does not give a damping rate proportional to k^2 that is traditionally associated with an eddy viscosity. The eddy viscosity does asymptote to a constant value at long wavelengths. This constant, however, is negative for 2D turbulence. The major contribution to the subgrid energy transfer comes from coherent straining of the short-wavelength modes by long-wavelength velocity shear, which causes the eddy viscosity to become large and positive near the high-wave-number cutoff k_c. The simulations considered here correspond most closely to the 2D case where the cutoff k_c lies in the enstrophy range. For this case, the significant positive contribution to the eddy viscosity lies in a region near the cutoff wave number k_c of width k_0, where the straining field is dominated by wave numbers of size k_0 and smaller. The shape of the eddy-viscosity function in this region depends on the nature of the spectrum at long wavelengths. For an artificial spectrum that allowed for a simpler calculation, the eddy viscosity in the near-cutoff region was found to be

$$\nu_{\text{eddy}}(k) \approx (\theta k_c k_0)^{-1} f\left(\frac{k_c - k}{k_0}\right) \qquad [(k_c - k) \ll k_c], \tag{6.10}$$

where θ is the eddy circulation time of the long wavelengths. See Eq. (6.5) of Kraichnan (1976).

6.1.3 Numerical Eddy Viscosity

In the original work on this eddy viscosity (Kraichnan 1976), the subgrid transfer $\langle T^s \rangle$ was viewed as a theoretically derived quantity containing contributions from all three-mode couplings that cross the cutoff in k space. The standard approach to calculating eddy viscosity in numerical simulations (Maltrud and Vallis 1993; Chekhlov et al. 1994) defines the subgrid transfer based on the subgrid contribution to the nonlinear term as defined in Eq. (6.4). For our model the subgrid transfer is defined by

$$T_{\mathbf{k}}^s = \left[(1 + |\mathbf{k}|^2)^2 + {\delta_0}^2 {k_y}^2\right] 2\mathrm{Re}(\psi_{\mathbf{k}}^* N_{\mathbf{k}}^s). \tag{6.11}$$

Substituting this definition for T^s into the definition of eddy viscosity in Eq. (6.9) yields

$$\nu_{\mathrm{eddy}}(\mathbf{k}) = -\frac{\mathrm{Re}\left(\langle \psi_{\mathbf{k}}^* N_{\mathbf{k}}^s \rangle\right)}{k^2 \left\langle |\psi_{\mathbf{k}}|^2 \right\rangle}. \tag{6.12}$$

With this definition, the eddy-viscosity approximation for the subgrid term,

$$N_{\mathbf{k}}^s \approx -\nu_{\mathrm{eddy}}(\mathbf{k}) k^2 \psi_{\mathbf{k}}, \tag{6.13}$$

can be viewed as the linear (in $\psi_{\mathbf{k}}$) approximation that minimizes the mean-squared residual error.

To calculate the eddy viscosity for a given low-resolution simulation with cutoff wave number k_c, a simulation is performed at much higher resolution containing a large number of higher-k modes ($|\mathbf{k}| > k_c$) along with all the modes resolved by the low-resolution simulation. The 'unresolved' component of the nonlinear term N^s defined in Eq. (6.4), is calculated for the low-resolution simulation from modes resolved in the higher-resolution simulation. Calculating the eddy viscosity from high-resolution simulations to apply to low-resolution simulations cannot by itself reduce the computational cost of a particular problem since presumably the high-resolution simulations yield accurate results already. It is hoped that by parameterizing the eddy viscosity calculated for a number of runs, a model for the eddy viscosity can be obtained that extrapolates to drift-wave problems for a larger range of parameters.

The sample simulation mentioned in Sec. 5.2 was used to calculate the eddy viscosity for a simulation with half of its resolution. The resulting eddy viscosity $\nu_{\mathrm{eddy}}(\mathbf{k})$ is plotted in Fig. 6.1 with the linear drive and damping for lines of modes out to the cutoff wave number in two directions in k space. As noted in Sec. 5.2, inertial-range behavior should not be expected in simulations of this kind of plasma turbulence, and there is no inverse cascade of energy from very short wavelengths. While there is a small negative eddy viscosity at long wavelengths for this simulation, it is dynamically insignificant compared to the linear drive and dissipation at long wavelengths. The dominant effect of the eddy viscosity lies in a narrow region near the cutoff where it becomes positive and large compared to the linear drive. The mechanism for this

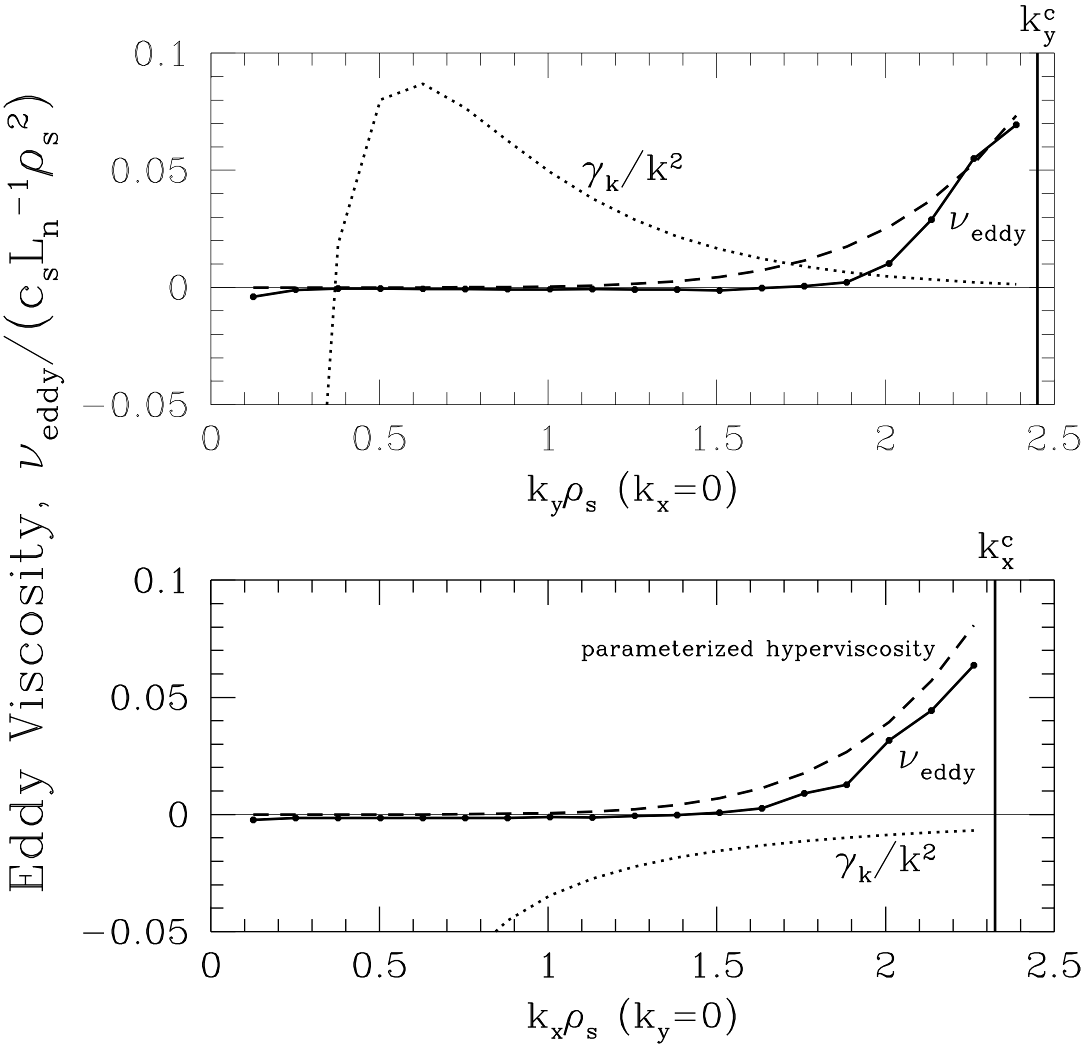

Figure 6.1: Eddy viscosity calculated for the simulation of Fig. 5.2. The transfer was calculated for a box of 37×39 modes (representing a simulation with half the actual resolution) to modes outside the box, but resolved by the simulation. The dotted line is the linear growth rate, expressed as a viscosity by dividing by k^2. The eddy viscosity has a small negative component as $k \to 0$, but it is negligible compared to the linear driving term. The eddy viscosity becomes important in a small region near the cutoff. The dashed line is the parameterized hyperviscosity derived in Sec. (6.2). For these parameters and cutoff wave number, the parameterization provides a good fit to the actual eddy viscosity.

damping near the cutoff is the loss of fluctuation energy from resolved modes by the coherent straining due to long-wavelength modes (Kraichnan 1976). This damping mechanism is probably the dominant physical effect of subgrid modes in drift-wave turbulence simulations, so the focus of this study is to effectively model the positive eddy viscosity in the region near the cutoff.

6.1.4 Heuristic Scaling of the Eddy Damping Rate

Consider a fictitious wave packet of short-wavelength fluctuations, localized in k space and real space so that the long-wavelength advecting velocity field looks locally like a shear flow. Without loss of generality, consider the action of the local shear flow, $\mathbf{V}_{\mathbf{E}\times\mathbf{B}}(x,y) = -\theta^{-1} y\hat{\mathbf{x}}$, where the shearing time is denoted by θ. The advection part of the continuity equation then has the form of a shear flow in Fourier space as well,

$$\frac{\partial}{\partial t}\tilde{n}_i(\mathbf{k}) + \theta^{-1}\frac{\partial}{\partial k_y} k_x \tilde{n}_i(\mathbf{k}). \tag{6.14}$$

Fig. 6.2 illustrates this process. The wave packet will be advected in k space in a particular direction depending on the local shear. The random variations of the local shear will thus lead to a random-walk diffusion of this wave packet in k space, with a net transfer of fluctuation energy to high k (Leith 1968).

In the numerical simulation, however, the absence of the nonlinear interactions with unresolved modes and the conservative nature of the nonlinearity cause the cutoff in k space to act as a reflecting boundary. Thus, in Fig. 6.2 the wave packet, represented by the dark circle, would be reflected back to long wavelengths instead of leaving the system. A reasonable estimate of the amount of eddy damping required by an eddy viscosity, therefore, would be given by the inverse of the time that a wave-packet spends in the near-cutoff region of width Δk_{eddy} where the eddy viscosity operates. (In reality a wave packet may enter and leave this region of k space several times as it random walks to the dissipation range, so the eddy viscosity may be reduced from this estimate.) For this example, the velocity of the packet in k space is $\theta^{-1}k_x$ so the time it spends in the edge region is $\theta {k_x}^{-1}\Delta k_{\text{eddy}}$. An eddy-damping rate of the form

$$\gamma_{\text{eddy}}(k) \sim -\theta^{-1} k_c {\Delta k_{\text{eddy}}}^{-1} f\left(\frac{k_c - k}{\Delta k_{\text{eddy}}}\right) \tag{6.15}$$

would therefore effectively damp fluctuations being sheared to high wave number. The maximum damping rate given by the theoretical enstrophy-range eddy viscosity defined in Eq. (6.10) scales as $\nu_{\text{eddy}}(k_c){k_c}^2 \approx \theta^{-1}k_c {k_0}^{-1}$ while $-\gamma_{\text{eddy}}(k_c){k_c}^2 \sim \theta^{-1}k_c{\Delta k_{\text{eddy}}}^{-1}$, so the same basic scaling is obtained if k_0 is identified with Δk_{eddy}.

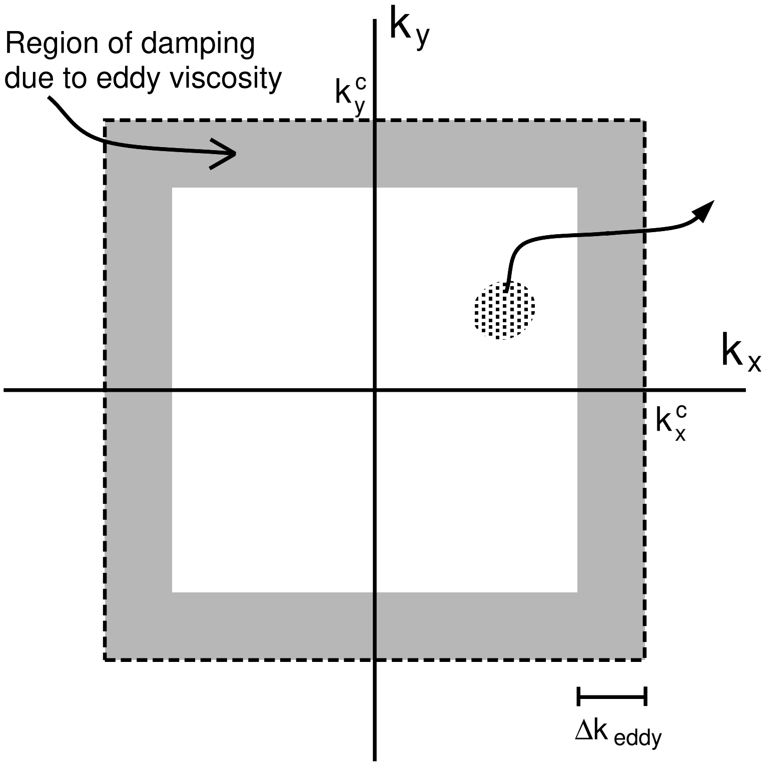

Figure 6.2: Heuristic picture of a fluctuation wave packet undergoing shear. As discussed in Sec. (6.1.4), the region of significant eddy viscosity near the cutoff (the grey region), acts as an absorbing buffer for fluctuation energy that would leave the system unaided if the system were truly unbounded.

6.1.5 Hyperviscosity

Hyperviscosity is defined as a damping term of the form

$$\gamma^d_{\mathbf{k}} = -\nu_h(|\mathbf{k}|/k_c)^p, \tag{6.16}$$

where p is larger than two. Hyperviscosity has been used as a numerical tool for simulating high-Reynolds-number turbulence in order to provide an artificially narrow dissipation range in the resolved modes, effectively increasing the extent of the inertial range simulated for a given resolution (Borue and Orszag 1995). Hyperviscosity has been regarded as an artificial damping term that does not attempt to estimate the subgrid interaction. Authors have, however, viewed hyperviscosity as a kind of subgrid model in the way that it serves as a sink for small-scale fluctuation energy (Basdevant and Sadourny 1983).

The choice of power p and size of the hyperviscosity ν_h is rarely discussed in the literature. Typically the size of the damping is set experimentally so that a dissipation range appears within the resolved modes. Studies of 2D Navier–Stokes turbulence (Basdevant and Sadourny 1983) have found that large powers ($p \sim 16$) work well, but that the optimal choice depends on the resolution of the simulation. With insufficient damping at the cutoff, fluctuation energy will tend towards equipartition in the Fourier modes leading to a spectrum $\Omega(k) \propto k$ towards the cutoff, which disagrees with the converged dissipative result. If the power used is too small, then damping that is sufficient to prevent unphysical behavior at the cutoff will introduce significant damping at long wavelengths and strongly affect the results. On the other hand, there must clearly be an upper limit to the power used. For a very high power there would be virtually no damping for almost all the modes except for a few modes near the cutoff that would be extremely damped. The results would be similar to performing a simulation with those modes removed and no damping on the remaining modes. This behavior may be considered analogous to impedance matching at the end of an electrical cable, where strong reflections occur if the load impedance is either too small or too large.

The constant ν_h is typically chosen so that modes near the cutoff experience damping that is large compared to the eddy turnover rate. An artificial dissipation region is introduced into the resolved modes that is much narrower in k space than the dissipation region given by the usual k^2 damping term. If the precise form of the dissipation does not affect the large-scale dynamics, then the use of artificial damping terms like hyperviscosity can yield significant savings in computation by greatly reducing the required resolution.

6.2 Hyperviscosity as a Model for Eddy Viscosity

The exact form of the eddy damping depends on the detailed nature of the saturated spectrum and the mode-mode coupling to unresolved modes. If one could accurately predict the eddy viscosity from theory, then there would be no point in performing numerical simulations. There are a large number of models for drift-wave turbulence, each of which will saturate with a different spectrum, so in general one should expect a different eddy viscosity from that predicted for Navier–Stokes turbulence by Kraichnan (Kraichnan 1976). Hence we are motivated to parameterize the basic features of the eddy viscosity in terms of the large-scale flow.

Hyperviscosity provides significant damping in a narrow region near the cutoff wave number, just as the calculated eddy damping for this model does (Fig. 6.1). An obvious method of fixing the two hyperviscosity parameters, the power p and magnitude M in Eq. (6.19), is to match the width and overall damping rate with the calculated eddy-damping term. The width and the damping are functions of the large-scale flow, so to apply the results to simulations, quantities corresponding to the long-wavelength scale k_0 and eddy circulation time θ must be defined. A surrogate for the long-wavelength eddy turnover time is the volume-averaged shearing rate

$$S(t) = \left[\frac{1}{L_x L_y} \int_0^{L_x} \int_0^{L_y} S(x,y,t)^2 \, dy \, dx \right]^{1/2} . \tag{6.17}$$

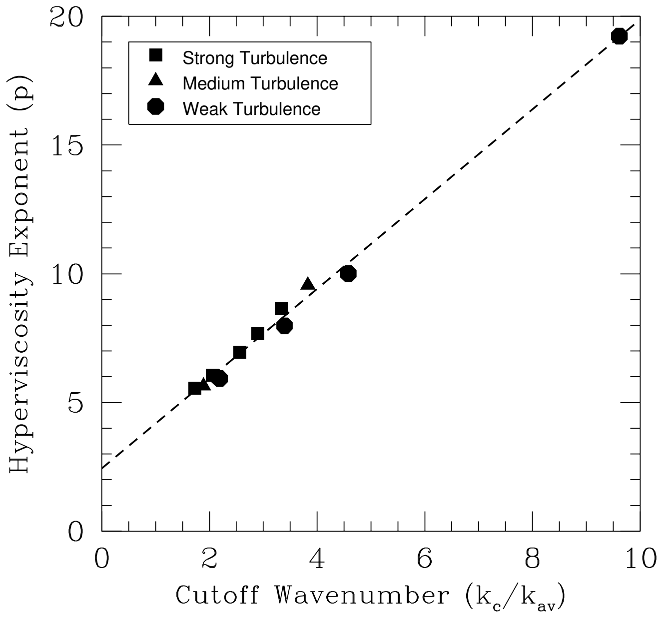

Figure 6.3: Hyperviscosity power predicted from direct numerical simulations.

An average wave number of the large scales is given by dividing the rate of shear by the root mean square of the velocity field,

$$k_{\rm av} = S\left(\frac{1}{L_x L_y}\int_0^{L_x}\int_0^{L_y} {V_x}^2 + {V_y}^2\, dy\, dx\right)^{-1/2}. \tag{6.18}$$

We will use the average wave number $k_{\rm av}$ as an estimate for the long-wavelength scale k_0 and the inverse rate of shear $S(t)^{-1}$ as an estimate for the eddy circulation time θ.

The hyperviscosity used for the simulations considered here introduces a damping term of the form

$$\gamma_h = -M\left[\left(\frac{k_x}{k_{xc}}\right)^p + \left(\frac{k_y}{k_{yc}}\right)^p\right] \tag{6.19}$$

into the model, Eq. (5.10), by setting $\gamma^d_{\mathbf{k}} = \gamma_h$. This hyperviscous damping term γ_h can be compared to the damping rate $\nu_{\rm eddy}(\mathbf{k})k^2$ given by the theoretical eddy viscosity of Eq. (6.10), and to the heuristic eddy damping rate defined in Eq. (6.15). The width of the theoretical eddy viscosity scales with the long-wavelength scale k_0 while the width of this hyperviscosity scales as k_c/p, so the power should scale as $p \propto k_c/k_{\rm av}$.

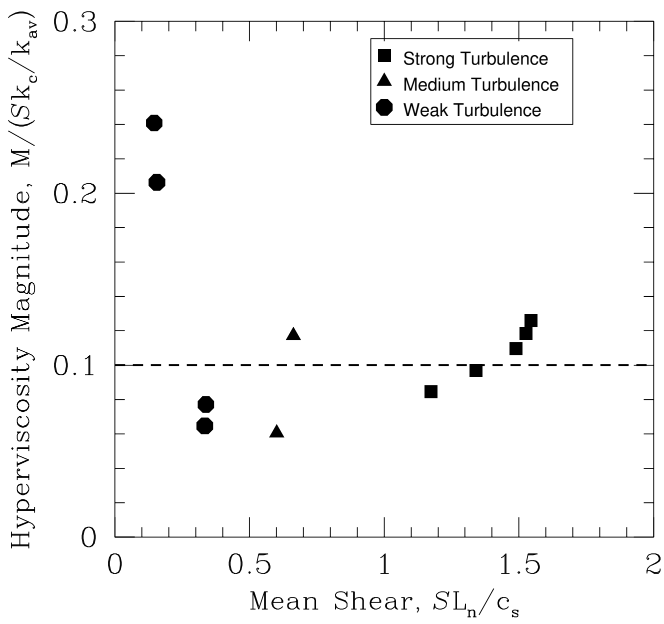

Figure 6.4: Hyperviscosity magnitude predicted from direct numerical simulation.

Comparing the magnitude of the three damping rates at the cutoff wave number k_c gives the scaling for the magnitude, $M \propto Sk_c/k_{\rm av}$.

An estimate for the power p and magnitude M was obtained from the numerically calculated eddy viscosity by setting two moments in k space to zero by

$$\begin{aligned} 0 &= \sum_{\mathbf{k}} \left[-\nu_{\rm eddy}(\mathbf{k}) k^2 - \gamma_h \right], \\ 0 &= \sum_{\mathbf{k}} \left[-\nu_{\rm eddy}(\mathbf{k}) k^2 - \gamma_h \right] \min(k_{xc} - |k_x|, k_{yc} - |k_y|). \end{aligned} \tag{6.20}$$

This estimate matches the width and magnitude of the damping region given by the hyperviscosity to that of the eddy viscosity. The estimates for the power and magnitude from simulations with a range of parameters and resolutions are summarized in Figures 6.3 and 6.4. The scaling of the power (and hence the width of the damping region), seems very robust. The estimate from these simulations gives

$$\begin{aligned} p &\sim 1.7 k_c/k_{\rm av} + 2.4, \\ M &\sim 0.1 S k_c/k_{\rm av}. \end{aligned} \tag{6.21}$$

The scaling of the magnitude (Fig. 6.4) is less robust than the scaling of the power (Fig. 6.3). There may be other macroscopic quantities that can be used to refine the estimate for the size of the damping.

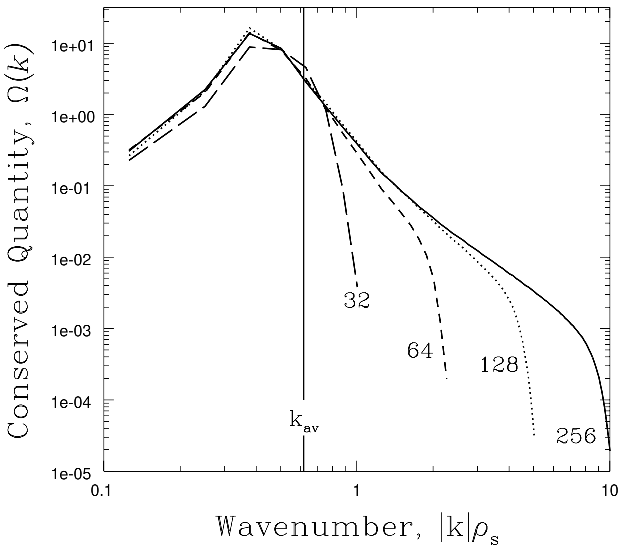

Figure 6.5: Convergence of simulations using hyperviscosity at moderate turbulence levels. (The parameters $\delta_0 = 0.15$, $\alpha = 0.015$, and $\mu = 0.0001$ were used with periodic box size $50\rho_s \times 50\rho_s$.) A hyperviscosity with an *a priori* fixed power $p = 16$ was used as is typically done in simulations of isotropic turbulence. The damping was set to the rate of shear ($\nu_h = S$) to insure that resolved high-k modes were sufficiently damped. The large-scale average wave number k_{av} calculated from the highest-resolution simulation is included for reference.

Note in Fig. 6.4 that the largest variation in estimates for the magnitude of the hyperviscosity (hence the overall eddy damping rate) occurs for low mean shear. In the weak-turbulence regime, the effects of wave dispersion are comparable to or larger than those from the nonlinear mode coupling. The magnitude scaling proposed here is based on the nature of 2D neutral-fluid turbulence where there is no wave physics. Some measure of the wave dispersion could prove useful in improving the parameterization. (On the other hand, it will be shown in the next section that the dissipation model has less impact on the accuracy of simulations in the weak-turbulence regime.)

6.3 Tests of Damping Models

Simulations were performed for a range of parameters, and grid sizes ranging from 32×32 to 256×256 to test the performance of three dissipation models against each other and against the use of no dissipation model. An ordinary hyperviscosity was

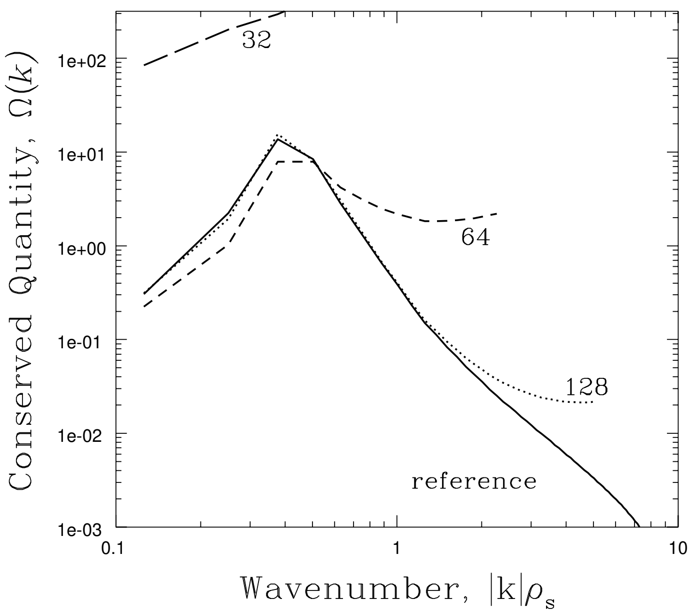

Figure 6.6: Convergence of simulations using no added dissipative terms for the same choice of parameters used in Fig. 6.5. The lower-resolution results failed to give reasonable results in this case.

tested with power $p = 16$ and coefficient set based on the rate of shear, $\nu_h = S$. The Smagorinsky eddy viscosity was tested with the constant $C_s = 0.1$ chosen arbitrarily. Based on the results from the previous section, the parameterized hyperviscosity was tested with power $p = 1.7k_c/k_{\rm av} + 2.4$ and magnitude $M = 0.1S(t)k_c/k_{\rm av}$.

Typically simulations of isotropic turbulence will use an *a priori* fixed-power hyperviscosity to provide the necessary damping. Resulting spectra for simulations using the fixed-power hyperviscosity are shown in Fig. 6.5 for the parameter choice that gave moderate levels of turbulence. The rate of transfer of fluctuations to short wavelengths scales with the rate of shear S, so the choice of a hyperviscous damping of the form $S(k/k_c)^p$ corresponds to setting the dissipation wave number to a fixed fraction of the cutoff wave number k_c. (The dissipation wave number is the scale at which the damping of the conserved quantity becomes dynamically significant.) The spectrum at long wavelengths observed in simulations (Borue 1993) is a slowly changing function of Reynolds number for the 2D Navier–Stokes enstrophy cascade where hyperviscosity is the primary source of dissipation. Since the physics of this drift-wave model is dominated by production and dissipation of fluctuations at long wavelengths (see Fig. 5.5), there should be an even weaker dependence of the

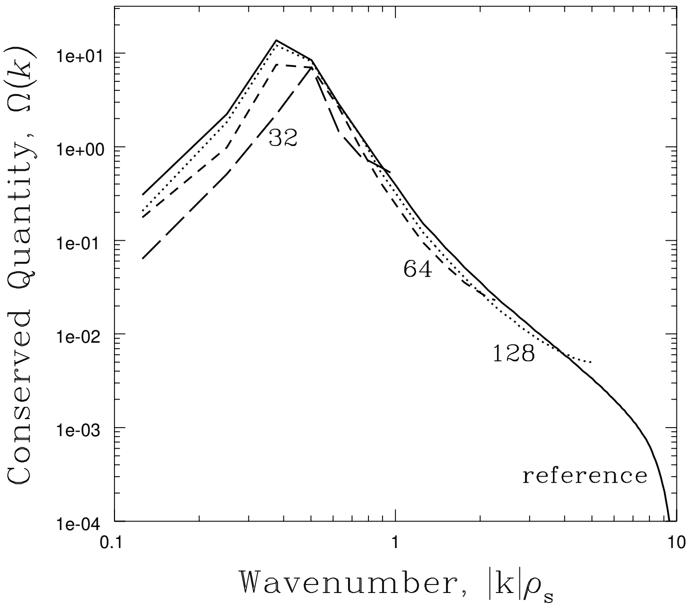

Figure 6.7: Convergence of simulations using the Smagorinsky eddy viscosity with $C_s = 0.1$, for the same choice of parameters used in Fig. 6.5.

long-wavelength saturation on the precise details of the dissipation range. Moving the hyperviscous dissipation scale with the cutoff allows us to resolve more of the small-scale dynamics with increased resolution. The spectra are almost identical at long wavelengths for grid sizes 128×128 and 256×256, so we are confident that the 256×256 case well represents the converged solution.

The results of simulations using no eddy viscosity or hyperviscosity term are shown in Fig. 6.6 for comparison. It is well known that lack of an eddy viscosity leads to unphysical results in Navier–Stokes turbulence when the small-scale dissipation wave number exceeds the cutoff. One might think that since dissipation from terms that model Landau damping at long wavelengths is the dominant drain of energy, then the transfer to small spatial scales can be completely ignored. From the results, this hypothesis is clearly only partially true. Given sufficient resolution, the spectrum converges to the reference spectrum obtained from the highest-resolution hyperviscosity run. The lower resolution runs, however, give wildly inaccurate results despite the fact that the lowest resolution considered here (32×32) resolves the primary production and dissipation wave numbers in Fig. 5.5. Drift-wave turbulence will typically exhibit only a moderate separation of scales between the spectral peak and the dissipative range, so it is practical to perform 2D simulations with sufficient resolution

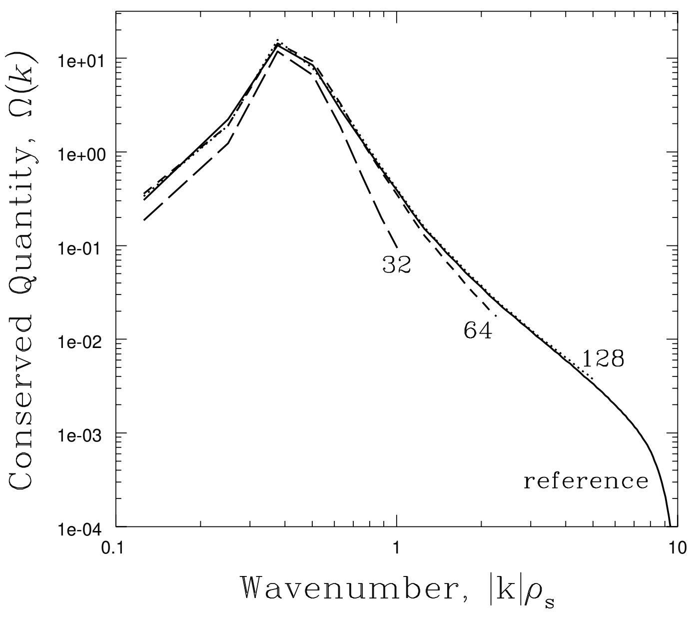

Figure 6.8: Convergence of simulations using the parameterized hyperviscosity ($p = 1.7k_c/k_{\rm av} + 2.4$, $M = 0.1Sk_c/k_{\rm av}$) for the same choice of parameters used in Fig. 6.5.

that an eddy viscosity or hyperviscosity term is unnecessary. On the other hand, for 3D simulations of drift-wave turbulence, the reduction in required resolution can be significant.

Performance of the Smagorinsky eddy viscosity with constant $C_s = 0.1$ for the same parameter choice is shown in Fig. 6.7. Again, given sufficient resolution, the spectrum converges to the reference spectrum. Results at long wavelengths ($k\rho_s \sim 0.4$) for lower-resolution runs are better than those obtained using no additional dissipation terms but not as good as those obtained using a hyperviscosity. Choosing a larger value of the constant C_s will improve the results somewhat at lower resolution but degrades the results for the 128×128 case. The constant C_s is probably not universal for the kind of turbulence studied here, in contrast to the case of the inertial range in Navier–Stokes turbulence. A fundamental problem with applying any eddy viscosity that gives damping scaling as k^2, however, is that providing sufficient damping for modes near the cutoff forces one to introduce a significant artificial damping into the long-wavelength modes that dominate the nonlinear physics.

Simulation results using the parameterized hyperviscosity are shown in Fig. 6.8. In this case, results at low resolution are obtained that are superior to those from all

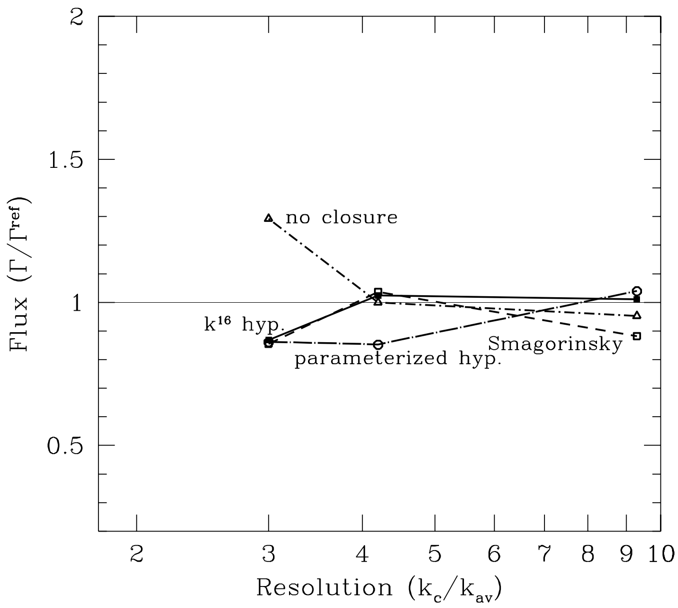

Figure 6.9: Convergence of the measured flux as a function of resolution for the case of weakly driven turbulence. (The parameters $\delta_0 = 0.20$, $\alpha = 0.03$, and $\mu = 0.0001$ were used with periodic box size $40\rho_s \times 40\rho_s$.) The flux is normalized to the flux measured by a reference simulation where $k_c/k_{\rm av} \approx 13$. In this case the nonlinear transfer to shorter wavelengths is a small effect, so the use of a subgrid damping term is unnecessary.

other approaches considered in this study. The performance of the parameterized hyperviscosity indicates that it provides a reasonable model of the actual eddy-damping process. Note that in the lowest-resolution run here a significant portion of driven modes lies beyond the cutoff wave number, so the spectrum falls below the reference spectrum. It is possible that even better results may be obtained for low-resolution simulations by modeling the transfer of energy from unresolved small scales to resolved long wavelengths by adding a negative term to the eddy viscosity to model this backscatter.

To summarize the convergence properties with various dissipation models, we need to define a measure of the resolution. The cutoff wavenumber k_c is a natural measure of the simulation resolution, but there are several choices of wavenumbers that the cutoff can be normalized to. The long-wavelength scale $k_{\rm av}$ defined in this study is a natural choice, which gives $k_c/k_{\rm av}$ as a measure of resolution. This definition seems unnatural to those used to dealing with fluid turbulence simulations. One could argue that the cutoff wavenumber should be normalized to some dissipation wavenumber.

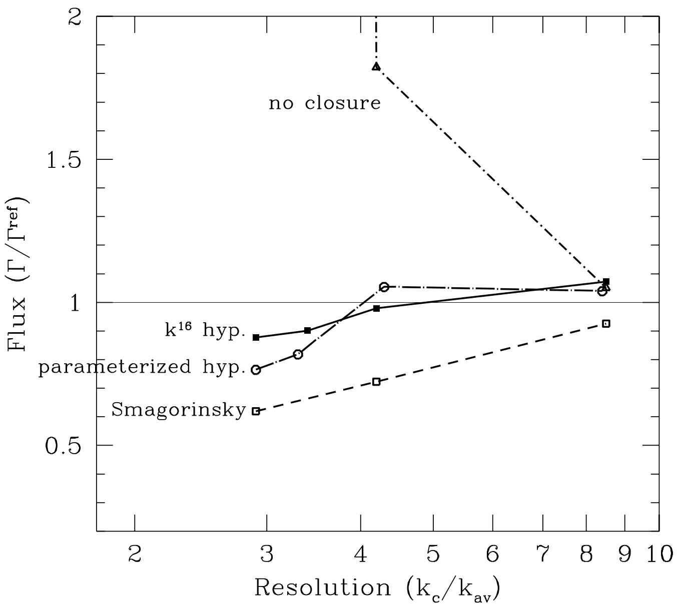

Figure 6.10: Convergence of the measured flux as a function of resolution for the cases of moderately driven turbulence. (See Fig. 6.5 for the parameters.) The flux is normalized to the flux measured by a reference simulation where $k_c/k_{\rm av} \approx 15$. In this case the nonlinear transfer is sufficiently strong that the simulations will blow up with no damping term for lower-resolution runs. A hyperviscosity with large exponent outperforms the Smagorinsky viscosity.

For these simulations, the bulk of the dissipation occurs at long wavelengths, so a dissipation wavenumber defined for the Landau damping term would be $\sim k_{\rm av}$. One could define a dissipation wavenumber in terms of the hyperviscous dissipation only. With the parameterized hyperviscosity, however, this dissipation wavenumber is forced to lie near the cutoff wavenumber. For lack of a better definition of resolution, we therefore use the quantity $k_c/k_{\rm av}$, which can be viewed as a kind of 'Reynolds' number for the inertial range part of the simulation. The true solution can be viewed as the infinite 'Reynolds' number limit. Since the dynamics of the turbulence in these simulations seems to be dominated by the long wavelength production and dissipation, we expect the results to be insensitive to any measure of the scale range of the short-wavelength 'inertial range'.

Convergence of the measured flux is summarized for simulations of weakly driven, moderately driven, and strongly driven turbulence (Figures 6.9, 6.10, and 6.11 respectively). In each case, the measured flux is normalized to a reference value obtained

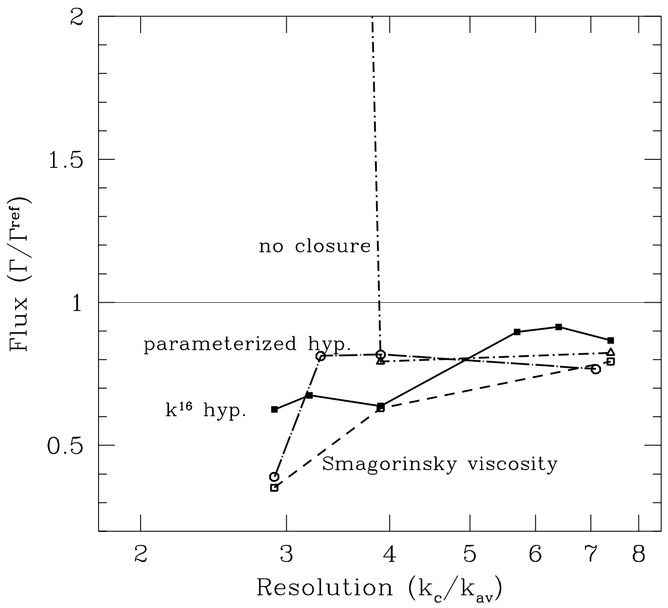

Figure 6.11: Convergence of the measured flux as a function of resolution for the cases of strongly driven turbulence. (See Fig. 5.2 for the parameters.) The flux is normalized to the flux measured by a reference simulation where $k_c/k_{\rm av} \approx 13$. The results are similar to those obtained for the case of moderately driven turbulence (Fig. 6.10).

from a high-resolution (grid size 256×256) simulation using hyperviscosity. In all cases, the most reasonable results obtained at lower resolution were obtained using the parameterized hyperviscosity or the k^{16} hyperviscosity. For the moderate- and strong-turbulence cases, one obtains reasonable results at resolutions at least a factor of 2 smaller than those necessary for simulations with no added dissipation. For the case of weakly driven turbulence, however, the nonlinear coupling to unresolved modes is less important and there is little difference between any of the models used. In summary, a hyperviscous damping term works effectively in drift-wave simulations at low resolutions (working down to $k_c/k_{\rm av} \sim 4$) and moderate to strong levels of turbulence.

6.4 Resolution Requirements

The simulations performed in this study indicate that if the cutoff wave number is at least a factor of 3 or so greater than the long-wavelength scale $k_{\rm av}$ (or roughly a factor of 6 larger than the spectral-peak wave number), then reasonable results can

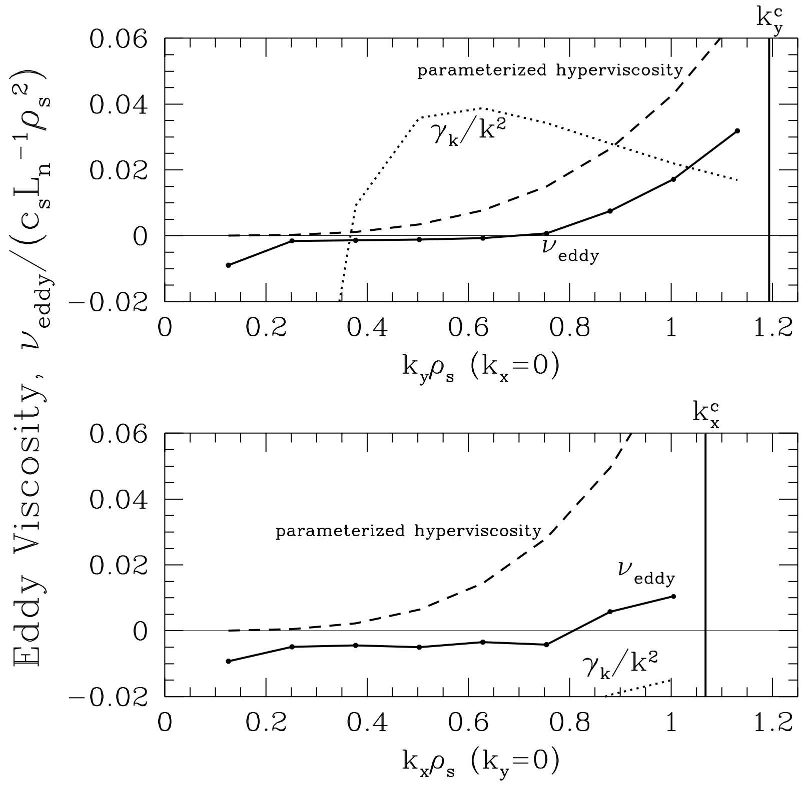

Figure 6.12: Eddy viscosity calculated for a low-resolution simulation at moderate turbulence levels of turbulence. (See Fig. 6.5 for the parameters.) In this case, the parameterized hyperviscosity grossly overestimates the damping. Note that the calculated eddy viscosity is anisotropic in this case and has a significant negative component at long wavelengths. Simulations at this resolution estimated $k_c/k_{\rm av} \approx 3$.

be obtained with the use of a hyperviscosity. There are several sources of error in calculating macroscopic quantities such as the flux from lower-resolution simulations. Contributions to the flux from unresolved modes may be significant or the resolved modes may fail to saturate at the correct level. Incorrect saturation levels may be due to the failure of our parameterization to model the eddy viscosity or from the failure of eddy viscosity to model the physics of unresolved modes.

For the lowest resolution simulations considered in this study, the contribution to the flux from unresolved modes is too small (5% or less) to explain the discrepancy between the calculated flux at low and high resolution. As is clear from the spectra in Figures 6.5 and 6.8, the error in the calculated flux at the lowest resolution comes from the failure of resolved modes to saturate at the correct level. The eddy viscosity calculated for grid size 32×32 for moderate levels of turbulence is plotted in Fig. 6.12. The parameterization overestimates the eddy viscosity significantly in

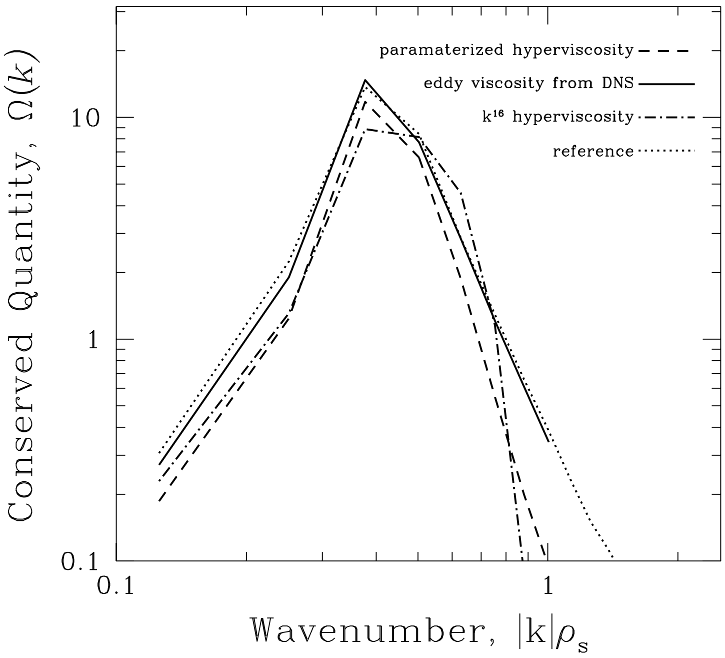

Figure 6.13: Comparison of simulations at low resolution using hyperviscosity and the calculated eddy viscosity in Fig. 6.12. (At this resolution, the Smagorinsky eddy viscosity gives very poor results, and simulations with no added dissipative term blow up.)

this case. As well, the calculated eddy viscosity is significantly anisotropic and the negative viscosity at long wavelengths is of size comparable to the positive portion that the parameterization models. For comparison, the calculated eddy viscosity was used in a simulation at this resolution. The resulting spectrum is shown compared to the hyperviscosity simulations and the high-resolution reference spectrum in Fig. 6.13. Using the calculated eddy viscosity gives very accurate results in this case. The flux calculated from this simulation is within 5% of the flux calculated from the highest-resolution run.

The current limits of the parameterized hyperviscosity are therefore clearly due to its failure to model accurately the eddy viscosity at low resolution. Future work will attempt to improve the parameterization of the magnitude of the hyperviscosity, generalize the parameterization to provide anisotropic damping, and possibly to incorporate a model for the negative viscosity at long wavelengths. Also, it may be useful to examine the effects of wave dispersion on the eddy viscosity. It is not clear from this work which of these improvements will have the greatest effect on improving the accuracy of low-resolution simulations.

6.5 Summary

A new parameterized hyperviscosity, Eqs. (6.19) and (6.21), was derived by analyzing the eddy viscosity calculated from simulations with a range of parameters and resolutions. Simulations using the parameterized hyperviscosity perform somewhat better than those using hyperviscosity with fixed power, and significantly better than those using no extra damping term or a Smagorinsky-type eddy viscosity. Accurate results are obtained provided the cutoff wave number, k_c, is approximately four or more times greater than the characteristic wave number k_{av} of the advecting velocity. At lower resolutions, the parameterization fails to accurately model the eddy viscosity.

Because this hyperviscosity is based on physics generic to most drift-wave turbulence, application to more complete models is straightforward. This hyperviscosity is very useful computationally, since reducing resolution requirements by even a factor of 2 reduces the computational requirements by a factor of 8 in two dimensions, or 16 in three dimensions.

Chapter 7

Extensions to Three Dimensions

The 2D drift-wave model introduced in Chapter 5 gave insight into the basic physics of energy transfer to subgrid-scale modes due to the shearing action of the **E**×**B** velocity. That model does not even attempt to capture the linear physics of ITG-driven instabilities, however, and is therefore of no use for predicting experimental results. A generalization to three dimensions of the parameterized hyperviscosity described in Section 6.2 is proposed here. The hyperviscosity model was inserted into the toroidal gyrofluid code developed by Beer, Dorland and Hammett (Beer et al. 1992; Hammett et al. 1994; Beer 1995), a comprehensive fluid moment code in flux-tube coordinates (Beer et al. 1995), which accurately models the linear physics of ITG-driven instabilities for a wide range of parameters.

The generalized 3D hyperviscosity proposed here correctly accounts for the modification of the effective eddy turnover time due to the fact that eddies in ITG turbulence tend to be highly elongated along the field line. Due to the computational cost of 3D turbulence simulations, a comprehensive study of the performance of this hyperviscosity has yet to be performed. Several simulations are presented here using Numerical Tokamak Project (NTP) test-case parameters that demonstrate that use of this hyperviscosity is capable in this one case of reducing the required resolution for a given accuracy by a factor of 2.

Finally, simulations of a particular high-gradient regime are presented with a saturated spectrum that peaks at an unusually long wavelength ($k_\perp \rho_i \sim 0.03$). This simulation could not be performed on the system currently being used for gyrofluid simulations (a Cray YMP) without the hyperviscosity model. Dorland discovered a shift in the linear ITG physics to longer-wavelength instabilities for high-gradient regimes (private communication), and suggests that this shift may be useful in explaining the experimental results concerning longer-wavelength modes in the near-edge region of the tokamak (Durst et al. 1993).

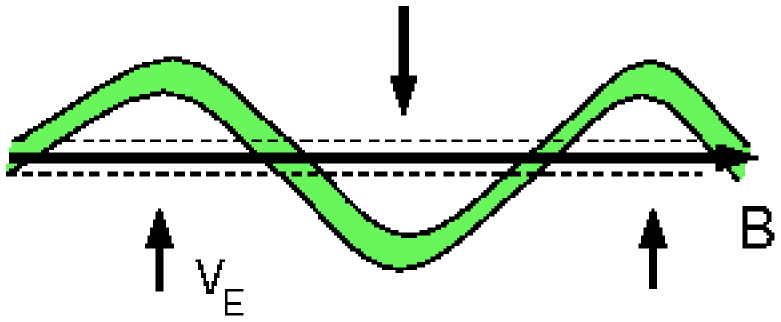

Figure 7.1: The shearing of an eddy in 3D ITG turbulence is illustrated. The dotted lines represent an initial perturbation lined up in the direction of the magnetic field. A small parallel gradient in the **E**×**B** velocity quickly results in an eddy with a large parallel wave number.

7.1 3D Hyperviscosity

In 3D ITG turbulence, eddies tend to be highly elongated along the magnetic field lines, so the perpendicular wave number $k_\perp$ is much larger than the parallel wave number $k_{||}$. As the picture in Fig. 7.1 demonstrates, a small deflection due to differences in the **E**×**B** velocity at different points along the field line can quickly lead to large parallel wave number. (In the discussion to follow, the variables x and y will be used to represent coordinates perpendicular to the magnetic field and z will be used to represent the coordinate along the field line.) Since the **E**×**B** velocity only has perpendicular components, the velocity shear tensor takes the form

$$\boldsymbol{\nabla}\mathbf{V}_{\mathbf{E}\times\mathbf{B}} = \left(\begin{array}{cc|c} \multicolumn{2}{c|}{\multirow{2}{*}{$\boldsymbol{\nabla}_\perp \mathbf{V}_{\mathbf{E}\times\mathbf{B}}$}} & \nabla_{||}\mathbf{V}_{\mathbf{E}\times\mathbf{B}_x} \\ & & \nabla_{||}\mathbf{V}_{\mathbf{E}\times\mathbf{B}_y} \\ \hline 0 & 0 & 0 \end{array}\right). \tag{7.1}$$

Note that some of the components of this tensor are zero, and the parallel gradients are much smaller than the perpendicular ones. One can see from the picture in Fig. 7.1, however, that the elongation of the modes enhances the effect of the parallel shear in the advecting velocity.

A strain rate defined analogously to the one in Eq. (6.7) would effectively ignore any contribution from the parallel gradient terms in taking the mean square of the components of the shear tensor displayed in Eq. (7.1). Splitting the problem into perpendicular and parallel components yields a simple approach for estimating the appropriate damping term for this situation. The perpendicular strain rate $S_\perp$ is given by applying the strain-rate definition (6.7) to the perpendicular component

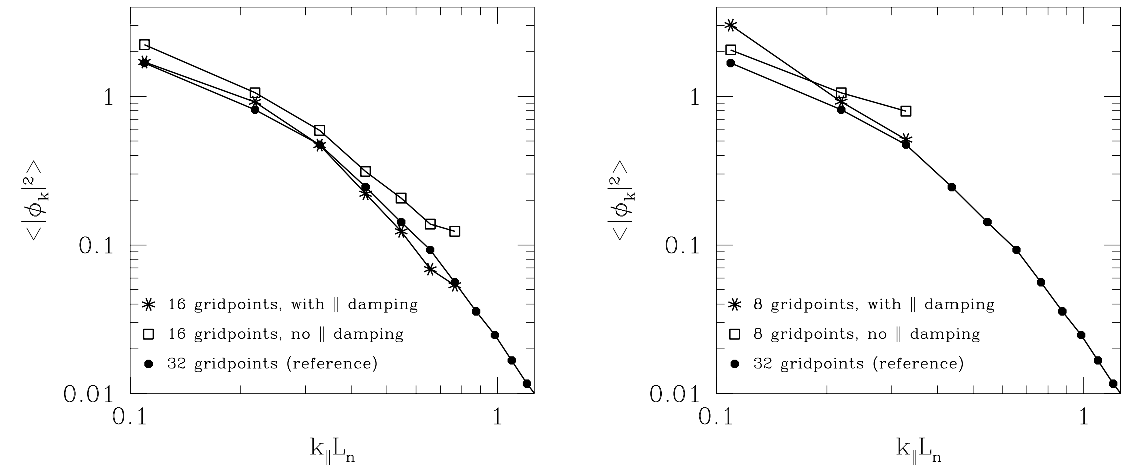

Figure 7.2: Convergence in the number of parallel grid points for the NTP test case with and without the parallel hyperviscosity term.

of the strain tensor $\boldsymbol{\nabla}_\perp \mathbf{V}_\perp$. The average perpendicular wave number is defined by $k_{\perp\mathrm{av}} = S_\perp / V_{\mathrm{RMS}}$ as in two dimensions [Eq. (6.18)]. A parallel strain rate is defined analogously by

$$S_{||}(x, y, z, t) = \sqrt{\left(\nabla_{||} V_x\right)^2 + \left(\nabla_{||} V_y\right)^2}, \tag{7.2}$$

and so therefore is the average parallel wavenumber $k_{||\mathrm{av}} = S_{||}/V_{\mathrm{RMS}}$. The shearing velocity in k space of a typical eddy due to the parallel gradients scales roughly as $|\mathbf{k}_\perp| \langle S_{||} \rangle$, so the heuristic arguments of Section 6.1.4 suggest that the damping near the cutoff in parallel wave-number space should be of the order $|\mathbf{k}_\perp| \langle S_{||} \rangle / k_{||\mathrm{av}}$. Hence, the form of the subgrid dissipation term for 3D used here is

$$k^2 \nu_{\mathrm{eddy}}(k) = C_{||} \frac{\langle S_{||} \rangle |\mathbf{k}_\perp|}{k_{||\mathrm{av}}} \left(\frac{k_{||}}{k_{||c}} \right)^{p_z} + C_\perp \frac{\langle S_\perp \rangle k_{\perp c}}{k_{\perp\mathrm{av}}} \left[\left(\frac{k_x}{k_{xc}} \right)^{p_x} + \left(\frac{k_y}{k_{yc}} \right)^{p_y} \right]. \tag{7.3}$$

As in the 2D case, the powers should scale with the cutoff wave numbers, $p_x \sim k_{xc}/k_{\perp\mathrm{av}}$, $p_y \sim k_{yc}/k_{\perp\mathrm{av}}$, and $p_z \sim k_{||c}/k_{||\mathrm{av}}$. (For simplicity, the initial study in 3D takes the constant $C_{||} = C_\perp = 0.1$ based on the 2D results and fixes all the powers $p_x = p_y = p_z = 6$ for convenient implementation. Allowing the power to vary may improve the results, but the simulations were performed at fairly low resolutions where the power predicted from the 2D study should be close to 6 anyway, so fixing the powers is a reasonable approximation.)

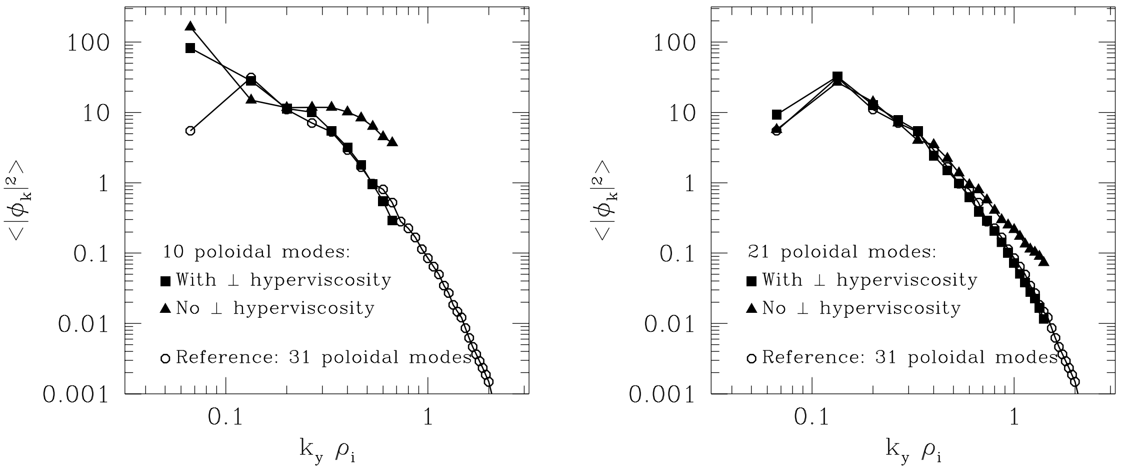

Figure 7.3: Convergence in the number of poloidal modes for the NTP test case with and without the perpendicular hyperviscosity term.

7.2 Numerical Tokamak Project Test Case

The hyperviscosity model was first benchmarked in the toroidal gyrofluid code Griffin on the Numerical Tokamak Project (NTP) Test Case set of parameters taken from TFTR L-mode shot #41309, $\hat{s} = 1.5$, $q = 2.4$, $L_n/R = 0.4$, $\eta_i = 4$, and $T_i = T_e$. Convergence with respect to the physical box size was considered by Beer (1995). Convergence with the number of modes for a fixed box size is examined here.

To test the parallel damping term $C_{||}$, the code was run with 21 poloidal mode numbers, for 8, 16, and 32 points along the field line, with ($C_{||} = 0.1$) and without ($C_{||} = 0$) the parallel damping term. The parallel wave-number spectra for these simulations are shown in Fig. 7.2. Neither of the low-resolution runs with 8 points along the field line have spectra that match the highest-resolution simulation. When the parallel damping term $C_{||}$ is included, the parallel spectrum with 16 grid points is virtually identical to that obtained with 32 points, whereas there are errors at this resolution with no parallel damping. These results indicate that it is possible to save a factor of 2 in resolution in this case while maintaining the same accuracy (provided the largest simulation represents the converged solution).

The code was also run with 10, 21, and 31 poloidal mode numbers, with 16 points along the field line, with and without the perpendicular damping term $C_{\perp}$. The perpendicular spectra for these simulations are shown in Fig. 7.3. The longest wavelengths in the lowest-resolution simulations show large deviations from the high-resolution simulation, both with and without the damping term. In the medium-resolution simulations, the spectra match the high-resolution spectrum very well both

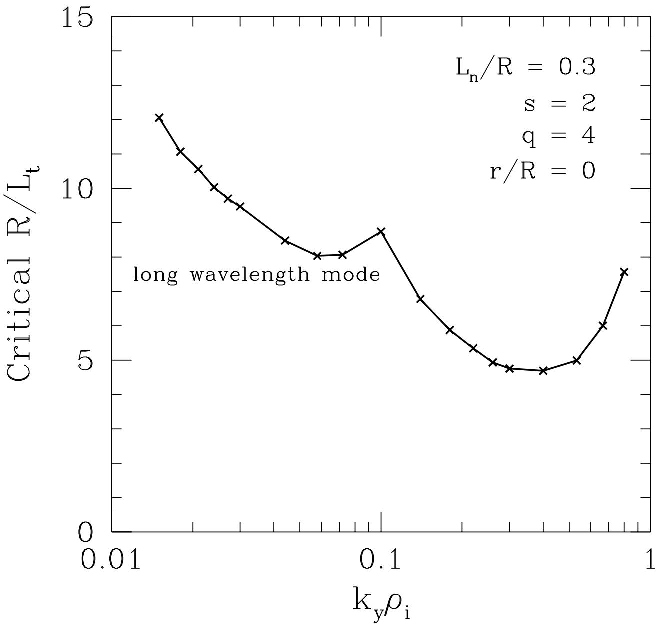

Figure 7.4: Critical temperature gradient of the ITG mode as a function of wave number for a regime with large density gradient. There is a sudden transition at temperature gradients around $R/L_T \sim 8$, at which point significantly longer wavelengths are driven unstable.

with and without the damping term. The perpendicular damping term appears to improve the behavior at short wavelengths, but if one is only interested in accurately modeling the long-wavelength modes responsible for transport, then the new perpendicular hyperviscosity term does not seem to provide any benefit in this case.

7.3 Long-Wavelength Instability

Near the edge of a tokamak, trapped ion effects and large temperature gradients may be a source of drive for long-wavelength instabilities. Calculating the nonlinear evolution of such modes becomes difficult if simulations are required to resolve the peak of the linear growth rate (typically around $|\mathbf{k}_\perp|\rho_i \sim 1/2$). To obtain convergence of simulations without added dissipation, it is often necessary to resolve modes with wavenumbers out to $|\mathbf{k}_\perp|\rho_i \sim 1$ due to unstable modes in this range. This situation is precisely where the hyperviscosity model has the greatest potential for use. It is necessary to eliminate small-scale modes to perform the simulations, but in this case there may not be a sufficient number of resolved damped modes to allow the simulation to saturate.

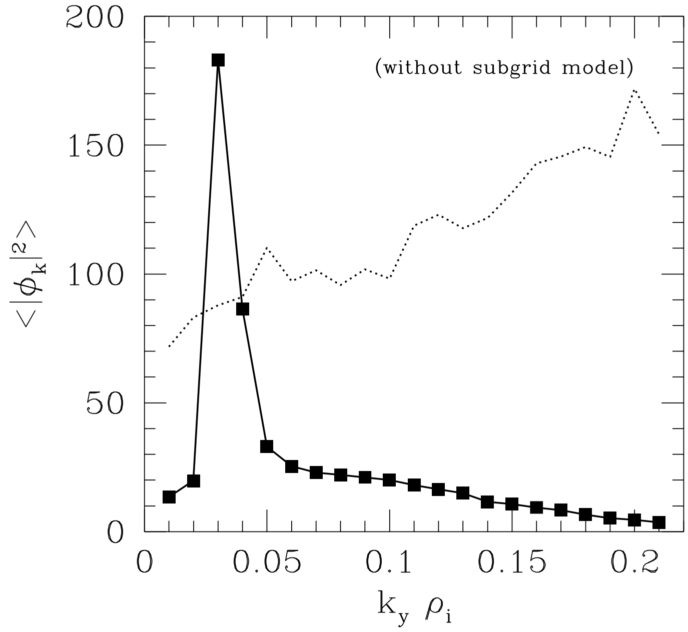

Figure 7.5: Plot of the saturated poloidal spectrum for the simulation discussed in this section. The dotted line indicates the spectrum obtained in a simulation with no subgrid model.

In Fig. 7.4, the critical temperature gradient of the ITG mode is plotted as a function of the poloidal wave number for the parameters $\hat{s} = 2$, $q = 4$, $L_n/R = 0.4$, and $r/R = 0.3$. As the temperature gradient is increased, there is a sudden transition around $R/L_T \sim 8$, at which point significantly longer wavelengths are driven unstable. For most typical parameters (such as the NTP test case in the previous section), the saturated poloidal wave-number spectrum peaks for $k_y\rho_i > 0.1$. In the near-edge region of a tokamak, gradients as large as those considered here are typical, and there is experimental evidence that fluctuations at significantly longer wavelengths $k_y\rho_i \sim 0.05$ are present (Durst et al. 1993).

The edge-like parameters $\hat{s} = 2$, $q = 4$, $L_n/R = 0.1$, $r/R = 0$, $\eta_i = 2$, and $T_i/T_e = 1$ were chosen to test hyperviscosity in this regard. The simulation box had 54 grid points along the field line by 64 points toroidally by 48 points in the radial direction and the $4 + 2$ moment gyrofluid equations were used. Although the fastest growing linear modes are not resolved, the turbulence saturates and is dominated by long-wavelength modes. The saturated spectrum is shown in Fig. 7.5. Without using any subgrid model in this case, the spectrum tends towards a non-physical equipartition results (the dotted line in the figure). This result can be contrasted

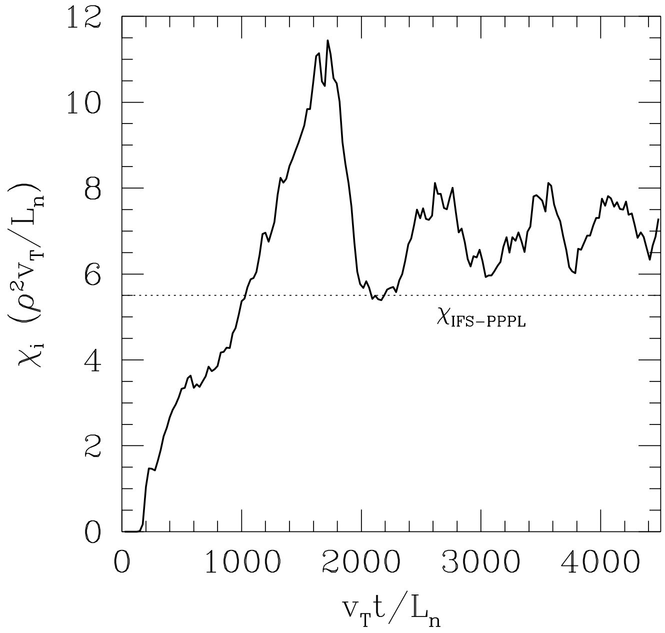

Figure 7.6: Calculated thermal diffusivity for the long-wavelength ITG simulation considered in this section. The dotted line indicates the heat flux predicted by the IFS–PPPL model (Kotschenreuther et al. 1995) for these parameters.

to the NTP test case discussed in the previous section, where a comparable number of modes is capable of resolving enough unstable modes that a subgrid model is unnecessary.

The thermal diffusivity calculated from this simulation is plotted in Fig. 7.6. The dotted line gives a reference diffusivity predicted by the IFS–PPPL model, a mixing-length-based parameterization of the thermal diffusivity that has had significant success in explaining the transport near the core of tokamak discharges. [The value of $\chi_{IFS--PPPL}$ displayed here is calculated from the formula of Dorland et al. (1994), which differs slightly in the treatment of trapped electron physics from the final "IFS–PPPL" model as reported by Kotschenreuther et al. (1995).] While this simulation has saturated at significantly longer wavelengths than is typical, the predicted heat flux is not significantly higher. (Experimentally measured heat fluxes in the near-edge region are typically much larger than the parameterization. This simulation indicates that the shift to longer-wavelength turbulence may not be responsible for the increased heat flux. More work is necessary to answer this question conclusively, however.)

The actual damping rate produced by the perpendicular part of the hyperviscosity

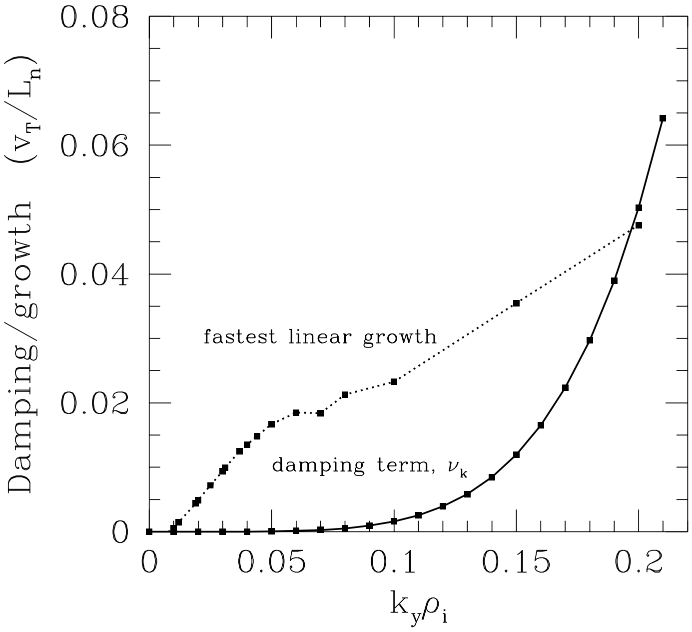

Figure 7.7: Plot of the damping from the hyperviscosity for a given poloidal wave number (with $k_x = 0$) compared with the fastest linear growth rate.

is plotted in Fig. 7.7 against the linear growth rate of the most unstable mode at a given poloidal wave number. The subgrid damping rate is insignificant in comparison to the linear growth rate for most of the resolved modes, including those that form the peak of the saturated spectrum. The damping rate becomes significant only for modes near the cutoff. This comparison serves as a useful check on the consistency of the model. One could question the use of a damping term that has a significant effect on the dominant modes in the saturated spectrum.

7.4 Summary

Heuristic arguments concerning the effect of velocity shear on elongated eddies were used to extend the 2D parameterized hyperviscosity of Eqs. (6.19) and (6.21) to applications in three dimensions where eddies are highly elongated along the additional dimension. This new 3D hyperviscosity [Eq. (7.3)] is essentially the 2D hyperviscosity with the addition of a parallel damping term that scales with parallel velocity shear enhanced by a factor of $|\mathbf{k}_\perp|/k_\|$.

The 3D hyperviscosity was tested in a comprehensive toroidal gyrofluid turbulence code (Beer 1995). Simulations of the Numerical Tokamak Project Test Case set of parameters indicates that the new heuristically derived parallel damping term can reduce the required parallel resolution by a factor of 2 in some cases. A set of high gradient edge-like parameters were simulated to demonstrate that there are conditions under which the saturated spectrum shifts to significantly longer wavelengths ($k_\theta \rho_i \sim 0.03$). These nonlinear simulations could not be performed without the use of the subgrid damping term proposed here.

To rigorously test the hyperviscosity, one must of course go to higher-resolution simulations. Where higher-resolution simulations are possible, the results considered so far indicate that use of hyperviscosity improves the accuracy of the predicted saturation levels. This model is computationally useful in three ways: it can provide plausible results in situations where a fully resolved simulation is impossible due to time or memory constraints; it can improve the accuracy of resolved simulations; and it can enable one to perform larger numbers of low-resolution simulations for the purpose of parameterizing the heat flux as a function of parameters.

Chapter 8

Conclusions

8.1 Moment Closures in One Dimension

A general linear closure for the hierarchy of moment equations of the stochastic oscillator problem is introduced here, based on the Landau-fluid approach to obtaining fluid moment closures for collisionless plasmas (Hammett and Perkins 1990). The n closure coefficients for the n-moment system are computed using conditions obtained by matching the response function for the closed moment system to the exact response function q times in the $\omega \to 0$ limit and $n - q$ times in the $\omega \to \infty$ limit. Results concerning the form of this closure are easily expressed for closures written in terms of polynomial moments where the polynomials are orthogonal with respect to the underlying distribution.

There is strong numerical evidence that the linear response of the closed moment system converges to the exact response for any choice of closure with increasing numbers of moments n, as long as there is some dissipation in the closure for the highest moment and the underlying distribution function is sufficiently smooth (i.e., can be represented as a Gaussian times a few low order Hermite polynomials). Convergence can be accelerated with a judicious choice of the closure dissipation, and is faster if q scales with n. However, if the underlying distribution function contains small scale features or sharp discontinuities (so its expansion in terms of Hermite polynomials requires high order polynomials), then convergence may be very slow, and a very large number of moments would be required. In some examples with sharp features in the distribution function, there was no convergence with n unless q also increased proportional to n. The poles of the approximate response functions were found to lie in the lower-half complex plane for a large number of choices of n and q.

The linear response to a potential perturbation given by the one-dimensional Vlasov equation has been shown to be equivalent to the stochastic oscillator problem. The fluid moment closure problem in this case is therefore equivalent to a statistical moment closure problem. It has also been shown that the fluid moments of the Vlasov equation are equivalent to Hermite polynomial moments, which in turn are equivalent to coefficients in the Hermite series that has traditionally been used in simulations of the Vlasov equation (Armstrong et al. 1970).

A model nonlinear problem, the plasma echo, was considered as a simple nonlinear test of the closure. The plasma echo is essentially the second-order component of the nonlinear response expanded in the limit of small perturbations. The second-order response has a simple exact solution (4.3) in the limit where the self-consistent potential is dropped. This exact solution was used to gauge the weakly nonlinear performance of moment systems with closure.

An essential factor in resolving the echo is having a large enough number of moments. (See Figs. 4.4 and 4.6.) The results, summarized in Fig. 4.6, show that modeling the second-order response for interaction time $t_2 - t_1$ requires $n \sim [(t_2 - t_1)k_1 v_t]^2$ moments. A very large number of moments would therefore be required to model a large time separation $t_2 - t_1$. Physically the large number of moments are required because the echo involves nonlinear interactions that un-phase-mix very fine scales in velocity space, which require many moments or Hermite polynomials to be fully represented. In the plasma echo problem, a simple model of the rate of decay of perturbations due to a finite collision rate ν indicates that $n \sim (kv_t/\nu)^{2/3}$ moments are sufficient to resolve all second-order effects.

This physics of the echo problem appears to be related to the problem pointed out by Mattor (1992) that the Landau-fluid equations miss certain nonlinear effects in some weak-turbulence regimes (or at least would require a very large number of moments to accurately represent them). However, we believe it reasonable that the Landau-fluid approximations will usually be adequate in strong turbulence regimes where the decorrelation times τ_c are relatively short, i.e., if the effective $t_2 - t_1 \sim \tau_c$ is relatively small or the effective $\nu \sim 1/\tau_c$ is relatively large. [Hammett et al. (1993) and Dorland (1993) discuss these issues in greater detail.] This picture is supported by comparisons between Landau-fluid simulations and particle simulations of nonlinear slab 3D ITG turbulence (Parker et al. 1994), which found fairly good agreement in the turbulent heat diffusivity χ_i, though there were $\sim 40\%$ differences in the fluctuation level of $|\phi|$. More work on this would be useful, and detailed Landau-fluid/particle comparisons in toroidal geometry have recently begun but the results are not yet clear.

In summary, the picture which emerges from our work is that, while the Landau-fluid closure approximations might be expected to work well in strong-turbulence regimes where decorrelation rates are short and the dominant saturation mechanisms are $\mathbf{E}\times\mathbf{B}$ transfers from unstable modes to Landau-damped modes at high k, one should be aware that the approximations break down (or require a large number of moments to converge) in cases such as the plasma echo or certain weak-turbulence regimes (Mattor 1992), where fine-scale structures in velocity space are important in the nonlinear physics.

8.2 Subgrid-Scale Closures

A new parameterized hyperviscosity, Eqs. (6.19) and (6.21), was derived by analyzing the eddy viscosity calculated from simulations with a range of parameters and resolutions. Simulations using the parameterized hyperviscosity perform somewhat better than those using hyperviscosity with fixed power, and significantly better than those using no extra damping term or a Smagorinsky-type eddy viscosity. Accurate results are obtained provided the cutoff wave number k_c is approximately four or more times greater than the characteristic wave number k_{av} of the advecting velocity. At lower resolutions, the parameterization fails to accurately model the eddy viscosity.

Because this hyperviscosity is based on physics generic to most drift-wave turbulence, application to more complete models is straightforward. This hyperviscosity is very useful computationally, since reducing resolution requirements by even a factor of 2 reduces the computational requirements by a factor of 8 in two dimensions, or 16 in three dimensions.

Heuristic arguments concerning the effect of velocity shear on elongated eddies were used to extend the 2D parameterized hyperviscosity of Eqs. (6.19) and (6.21) to applications in three dimensions where eddies are highly elongated along the additional dimension. The 3D hyperviscosity was tested in a comprehensive toroidal gyrofluid turbulence code (Beer 1995). Simulations of the Numerical Tokamak Project Test Case set of parameters indicates that the new heuristically derived parallel damping term can reduced the required parallel resolution by a factor of 2 in some cases. A set of high-gradient edge-like parameters were simulated to demonstrate that there are conditions under which the saturated spectrum shifts to significantly longer wavelengths ($k_\theta \rho_i \sim 0.03$). These nonlinear simulations could not have been performed without the use of the subgrid damping term proposed here.

8.3 Future Directions

The results in three dimensions are still somewhat preliminary in nature. Ideally one would like to compute the transfer rates in the 3D simulation to see if the magnitude of the transfer in parallel wave-number space compared to the perpendicular transfer corresponds to the heuristic predictions made in Section 7.1. The NTP test case results seem to indicate that the transfer of fluctuation energy to high parallel wave number may be more important physically than the transfers in perpendicular wave-number space. Measurements of the eddy damping due to transfer in both directions could provide useful insights into the nature of drift-wave turbulence saturation.

It would be interesting to apply the techniques of Chapter 2 to the more general problem of toroidal-drift phase mixing that has been successfully modeled with 6 fluid moment equations (Beer and Hammett 1996). One could imagine writing down the general toroidal Landau-fluid equations for the arbitrary ${v_\parallel}^n {v_\perp}^m$ moment (or in the appropriate orthogonal polynomials in $v_\parallel$ and $v_\perp$) and modifying a code to solve these equations for general n and m. Such a direct nonlinear turbulent test of the convergence with the number of moments evolved would add to the justification of the Landau-fluid approach to simulating drift-wave turbulence. This could compliment related work of ongoing comparisons of particle and Landau-fluid simulations (Parker et al. 1994).

Our approximations for both Landau damping fluid closures and sub-grid turbulence closures focus on the net transfer from resolved scales (in velocity or space) to unresolved scales. There are cases however where inverse-transfers can occur from unresolved scales to resolved scales. One might wonder if the closure approximations could be extended in some way to to represent such inverse-transfers, perhaps as noise source terms in resolved scales.

A fairly simple parameterization of the subgrid dissipation was constructed in this thesis. As it stands, the parameterized hyperviscosity yields significant improvements for numerical simulations of drift-wave turbulence. Recently, renormalization-group techniques have been successfully used to predict the subgrid transfer in the inverse cascade range of 2D turbulence (Chekhlov et al. 1994) and improved closure models have successfully predicted the nonlinear transfer rates for anisotropic 2D drift-wave turbulence (Bowman and Krommes 1997; Hu et al. 1997). It is possible that use of one of these theories may lead to more accurate estimates of the subgrid dissipation.

Bibliography

Armstrong, T., R. Harding, G. Knorr, and D. Montgomery (1970). Solution of Vlasov's equation by transform methods. In *Methods in Computational Physics*. New York: Academic Press.

Armstrong, T. P. (1967). Numerical studies of the nonlinear Vlasov equation. *Phys. Fluids* **10**, 1269.

Baker, G. A. (1975). *Essentials of Padé Approximants*. London: Academic Press.

Baker, G. A. and P. Graves-Morris (1996). *Padé Approximants*. Cambridge: Cambridge University Press.

Basdevant, C. and R. Sadourny (1983). Modélisation des Échelles virtuelles dans la simulation numérique des Écoulements turbulents bidimensionnels. *Journal de Méchanique théorique et Appliquée Numéro Spécial*, 243.

Batchelor, G. K. (1969). Computation of the energy spectrum in homogeneous two-dimensional turbulence. *Phys. Fluids Suppl.* **II**, 233.

Beer, M. A. (1995). *Gyrofluid Models of Turbulent Transport in Tokamaks*. Ph. D. thesis, Princeton University.

Beer, M. A., S. C. Cowley, and G. W. Hammett (1995). Field-aligned coordinates for nonlinear simulations of tokamak turbulence. *Phys. Plasmas* **2**, 2687.

Beer, M. A. and G. W. Hammett (1996). Toroidal gyrofluid equations for simulations of tokamak turbulence. *Phys. Plasmas* **3**, 4046.

Beer, M. A., G. W. Hammett, W. D. Dorland, and S. C. Cowley (1992). Nonlinear ballooning gyrofluid simulations of toroidal ITG turbulence. *Bull. Am. Phys. Soc.* **37**, 1478.

Bender, C. M. and S. A. Orszag (1978). *Advanced Mathematical Methods for Scientists and Engineers*. McGraw-Hill Publishing Co.

Borue, V. (1993). Spectral exponents of enstrophy cascade in stationary two-dimensional homogeneous turbulence. *Phys. Rev. Lett.* **71**, 3967.

Borue, V. and S. A. Orszag (1995). Self-similar decay of three-dimensional homogeneous turbulence with hyperviscosity. *Phys. Rev. E* **51**, R856.

Bowman, J. C. and J. A. Krommes (1997). The realizable Markovian closure and realizable test-field model. II. Application to anisotropic drift-wave dynamics. (in press).

Braginskii, S. I. (1965). Transport processes in a plasma. In M. A. Leontovich (Ed.), *Reviews of Plasma Physics*, Volume 1, pp. 205–311. New York: Consultants Bureau.

Brook, D. L. (1987). NRL plasma formulary. Naval Research Laboratory Publication 0084-4040.

Carrier, G. F., M. Krook, and C. E. Pearson (1983). *Functions of a Complex Variable: Theory and Technique.* Ithaca, New York: Hod Books.

Chang, Z. and J. D. Callen (1992). Unified fluid/kinetic description of plasma microinstabilities. part I: Basic equations in a sheared slab geometry. *Phys. Fluids B* **5**, 1167.

Chekhlov, A. (1995). *Studies of Forced-Dissipative Turbulence in Model Hydrodynamics.* Ph. D. thesis, Princeton University.

Chekhlov, A., S. Orszag, S. Sukoriansky, B. Galperin, and I. Staroselsky (1994). Direct numerical simulation tests of eddy viscosity in two dimensions. *Phys. Fluids* **6**, 2548.

Conway, J. B. (1990). *A Course in Functional Analysis.* New York: Springer-Verlag.

Diamond, P. H. and H. Biglari (1990). Theory of dissipative trapped-ion convective-cell turbulence. *Phys. Rev. Lett.* **65**, 2865.

Dimits, A. M., J. A. Byers, T. J. Williams, B. I. Cohen, X. Q. Xu, R. H. Cohen, J. A. Crotinger, and A. E. Shestakov (1994). Gyrokinetic and global fluid simulations of tokamak microturbulence and transport. In *Plasma Physics and Controlled Nuclear Fusion Research, 1994*, Volume 2, Vienna, pp. 457–462. International Atomic Energy Agency.

Dimits, A. M., T. J. Williams, J. A. Byers, and B. I. Cohen (1996). Scalings of ion-temperature-gradient-driven anomalous transport in tokamaks. *Phys. Rev. Lett.* **77**, 71.

Dorland, W. (1993). *Gyrofluid Models of Plasma Turbulence.* Ph. D. thesis, Princeton University.

Dorland, W. and G. W. Hammett (1993). Gyrofluid turbulence models with kinetic effects. *Phys. Fluids B* **5**, 812.

Dorland, W., M. Kotschenreuther, M. A. Beer, G. W. Hammett, R. E. Waltz, R. R. Dominguez, P. M. Valanju, W. H. M. Jr., J. Q. Dong, W. Horton, F. L. Waelbroeck, T. Tajima, and M. J. LeBrun (1994). Comparison of nonlinear toroidal turbulence simulations with experiment. In *1994 IAEA Conference (Seville, Spain).*

Dubin, D. H. E., J. A. Krommes, C. Oberman, and W. W. Lee (1983). Nonlinear gyrokinetic equation. *Phys. Fluids* **26**, 3524.

Durst, R., R. Fonck, J. Kim, S. Paul, N. Bretz, C. Bush, Z. Chang, and R. Hulse (1993). Observation of a localized transition from edge to core density turbulence in the TFTR tokamak. *Phys. Rev. Lett.* **71**, 3135.

Engelmann, F., M. Feix, E. Minardi, and J. Oxenius (1963). Nonlinear effects form Vlasov's equation. *Phys. Fluids* **6**, 266.

Fried, B. D. and S. D. Conte (1961). *The Plasma Dispersion Function.* New York: Academic Press.

Galperin, B. and S. A. Orszag (Eds.) (1993). *Large Eddy Simultation of Complex Engineering and Geophysical Flows.* Cambridge: Cambridge University Press.

Gould, R. W., T. M. O'Neil, and J. H. Malmberg (1967). Plasma wave echo. *Phys. Rev. Lett.* **19**, 219.

Gradshteyn, I. S. and I. M. Ryzhik (1980). *Table of Integrals, Series, and Products.* Academic Press, Inc.

Grant, F. C. and M. R. Feix (1967). Fourier-Hermite solutions of the Vlasov equations in the linearized limit. *Phys. Fluids* **10**, 696.

Hammett, G., W. Dorland, and F. Perkins (1992). Fluid models of phase mixing, Landau damping, and nonlinear gyrokinetic dynamics. *Phys. Fluids B* **4**, 2052.

Hammett, G. and F. Perkins (1990). Fluid moment models for Landau damping with application to the ion temperature gradient instability. *Phys. Rev. Lett.* **64**, 3019.

Hammett, G. W., M. A. Beer, W. Dorland, S. C. Cowley, and S. A. Smith (1993). Developments in the gyrofluid approach to tokamak turbulence simulations. *Plasma Phys. Controlled Fusion* **35**, 973.

Hammett, G. W., W. Dorland, M. Beer, and F. W. Perkins (1994). The gyrofluid approach to simulating tokamak turbulence. In M. N. Rosenbluth (Ed.), *New Ideas in Tokamak Confinement.* New York: American Institute of Physics.

Hasegawa, A. and K. Mima (1978). Pseudo-three-dimensional turbulence in magnetized nonuniform plasma. *Phys. Fluids* **21**, 87.

Hedrick, C. L. and J.-N. Leboeuf (1992). Landau fluid equaitons for electromagnetic and electrostatic fluctuations. *Phys. Fluids B* **4**, 3915.

Hu, G., J. A. Krommes, and J. C. Bowman (1997). Statistical theory of resistive drift-wave turbulence and transport. (in press).

Knorr, G. (1973). Plasma simulation with few particles. *J. Comp. Phys.* **13**, 165.

Kotschenreuther, M., W. Dorland, M. Beer, and G. Hammett (1995). Quantitative predictions of tokamak energy confinement from first-principles simulations with kinetic effects. *Phys. Plasmas* *2*(6), 2381.

Kraichnan, R. H. (1961). Dynamics of nonlinear stochastic systems. *Journal of Mathematical Physics* **2**, 124.

Kraichnan, R. H. (1967). Inertial ranges in two-dimensional turbulence. *Phys. Fluids* **10**, 1417.

Kraichnan, R. H. (1968). Convergents to infinite series in turbulence theory. *Physical Review* **174**, 240.

Kraichnan, R. H. (1970). Convergents to turbulence functions. *J. Fluid Mech.* **41**, 180.

Kraichnan, R. H. (1971). An almost-Markovian Galilean-invariant turbulence model. *J. Fluid Mech.* **47**, 513.

Kraichnan, R. H. (1976). Eddy viscosity in two and three dimensions. *Journal of the Atmospheric Sciences* **33**, 1521.

Kraichnan, R. H. (1980). Realizability inequalities and closed moment equations. In R. H. G. Helleman (Ed.), *Nonlinear Dynamics*, pp. 37. New York: New York Academy of Sciences.

Kraichnan, R. H. (1985). Decimated amplitude equations in turbulence dynamics. In D. L. Dwoyer, M. Y. Hussaini, and R. G. Voight (Eds.), *Theoretical Approaches to Turbulence*, pp. 91. New York: Springer Verlag.

Kraichnan, R. H. (1987). Eddy viscosity and diffusivity: Exact formulas and approximations. *Complex Systems* **1**, 805.

Krommes, J. A. and G. Hu (1994). The role of dissipation in the the theory and simulations of homogeneous plasma turbulence, and resolution of the entropy paradox. *Phys. Plasmas* **1**, 3211.

Kubo, R. (1963). Stochastic Liouville equations. *Journal of Mathematical Physics* **4**, 174.

Lee, W. W. (1983). Gyrokinetic approach in particle simulation. *Phys. Fluids* **26**, 556.

Lee, W. W. (1987). Gyrokinetic particle simulation model. *J. Comput. Phys.* **72**, 243.

Leith, C. E. (1968). Diffusion approximation for two-dimensional turbulence. *Phys. Fluids* **11**, 671.

Lenard, A. and I. B. Bernstein (1958). Plasma oscillations with diffusion in velocity space. *Phys. Rev.* **112**, 1456.

Liang, Y.-M., P. Diamond, X.-H. Wang, D. Newman, and P. Terry (1993). A two-nonlinearity model of dissipative drift wave turbulence. *Phys. Fluids* **5**, 1128.

Maltrud, M. E. and G. K. Vallis (1993). Energy and enstrophy transfer in numerical simulations of two-dimensional turbulence. *Phys. Fluids A* **5**, 1760.

Mattor, N. (1992). Can Landau-fluid models describe nonlinear Landau damping? *Phys. Fluids B* **4**, 3952.

O'Neil, T. M. and R. W. Gould (1968). Temporal and spatial plasma wave echoes. *Phys. Fluids* **11**, 134.

Parker, S. E. and D. Carati (1995). Renormalized dissipation in plasmas with finite collisionality. *Phys. Rev. Lett.* **75**, 441.

Parker, S. E., W. Dorland, R. A. Santoro, M. A. Beer, Q. P. Liu, W. W. Lee, and G. W. Hammett (1994). Comparisons of gyrofluid and gyrokinetic simulations. *Phys. Plasmas* **1**, 1461.

Rose, H. A. (1977). Eddy diffusivity, eddy noise and subgrid-scale modelling. *J. Fluid Mech.* **81**, 719.

Smagorinsky, J. (1963). General circulation experiments with the primitive equations. *Monthly Weather Review* **91**, 99.

Smith, S. A. and G. W. Hammett (1997). Eddy viscosity and hyperviscosity in spectral simulations of 2D drift wave turbulence. *Phys. Plasmas* **4**, 978.

Su, C. H. and C. Oberman (1968). Collisional damping of a plasma echo. *Phys. Rev. Lett.* **20**, 427.

Terry, P. W. and W. Horton (1982). Stochasticity and the random phase approximation for three electron drift waves. *Phys. Fluids* **25**, 491.

Wall, H. S. (1967). *Analytic Theory of Continued Fractions*. New York: Chelsea Publishing Co.

Waltz, R. E., R. R. Dominguez, and G. W. Hammett (1992). Gyro-Landau fluid models for toroidal geometry. *Phys. Fluids B* **4**, 3138.

Waltz, R. E., G. D. Kerbel, and J. Milovich (1994). Toroidal gyro-Landau fluid model turbulence simulations in a nonlinear ballooning mode representation with radial modes. *Phys. Plasmas* **1**, 2229.

Weissglas, P. (1962). Longitudinal plasma oscillations. *Plasma Phys. (Journal of Nuclear Energy Part C)* **4**, 329.